THE UNIVERSITY OF QUEENSLAND

SCHOOL OF CIVIL ENGINEERING

REPORT CH89/12

FIELD MEASUREMENTS IN THE TIDAL BORE OF THE GARONNE RIVER AT ARCINS (JUNE 2012)

AUTHORS: David REUNGOAT, Hubert CHANSON and Bastien CAPLAIN

HYDRAULIC MODEL REPORTS

This report is published by the School of Civil Engineering at the University of Queensland. Lists of recently-published titles of this series and of other publications are provided at the end of this report. Requests for copies of any of these documents should be addressed to the Civil Engineering Secretary.

School of Civil Engineering
The University of Queensland
Brisbane QLD 4072
AUSTRALIA

Telephone: (61 7) 3365 4163
Fax: (61 7) 3365 4599

URL: http://www.eng.uq.edu.au/civil/

First published in 2012 by
School of Civil Engineering
The University of Queensland, Brisbane QLD 4072, Australia

ISBN No. 9781742720616

The University of Queensland, St Lucia QLD, Australia

Field Measurements in the Tidal Bore of the Garonne River at Arcins (June 2012)

by
David REUNGOAT
Université de Bordeaux, I2M, Laboratoire TREFLE, 16 avenue Pey-Berland, Pessac, France, CNRS UMR 5295, Pessac, France, E-mail: reungoat@enscbp.fr

Hubert CHANSON
Professor, The University of Queensland, School of Civil Engineering, Brisbane QLD 4072, Australia, Email: h.chanson@uq.edu.au
Université de Bordeaux, I2M, Laboratoire TREFLE, 16 avenue Pey-Berland, Pessac, France, CNRS UMR 5295, Pessac, France

and
Bastien CAPLAIN
Université de Bordeaux, I2M, Laboratoire TREFLE, 16 avenue Pey-Berland, Pessac, France, CNRS UMR 5295, Pessac, France, Email: caplainbastien@gmail.com

REPORT No. CH89/12

ISBN 9781742720616

School of Civil Engineering, The University of Queensland
July 2012

Tidal bore of the Garonne River at Arcins on 7 June 2012

ABSTRACT

A tidal bore is a series of waves propagating upstream in an estuarine zone as the tidal flow turns to rising during spring tide conditions when the tidal range exceeds 4 to 6 m and the tidal flow is confined into a narrow funnelled estuary. A well-known macro-tidal environment is the Gironde estuary connected to the Garonne and Dordogne Rivers in south-western France. Some detailed field measurements were conducted in the tidal bore of the Garonne River on 7 July 2012. The velocity components were sampled in the Arcins channel with an acoustic Doppler velocimeter (ADV) at a relatively high-frequency (50 Hz) prior to, during and after the tidal bore. The sediment material was tested: it consisted of a cohesive mud with a typical particle size of about 13 μm, exhibiting a non-Newtonian behaviour. A series of experiments under controlled conditions were performed to use the acoustic backscatter amplitude of the ADV as a surrogate estimate of the suspended sediment concentration (SSC). On 7 June 2012, the tidal bore was a flat undular bore with a bore Froude number close to unity: Fr_1 = 1.02 and 1.19 in the morning and afternoon respectively. A feature of the field data set was some effect of recent floods (April-May 2012) of the Garonne River. At the end of ebb tide, the current was strong, the water level was relatively high and the water was predominantly some freshwater. Despite the high initial water level, the bore front exhibited a sharp discontinuity in terms of water elevation: i.e., 0.45 m and 0.52 m on 7 June 2012 morning and afternoon respectively. The field observations highlighted a number of unusual features on the morning of 7 June 2012. These included (1) a slight rise in water elevation starting about 70 s prior to the front, (2) a flow reversal about 50 s after the bore front, (3) some large fluctuations in suspended sediment concentration (SSC) about 100 s after the bore front and (4) a transient water elevation lowering about 10 minutes after the bore front passage. The measurements of water temperature and salinity showed nearly identical results before and after the tidal bore: there was no evidence of saline or thermal front. The turbulent velocity data showed a marked impact of the tidal bore. The longitudinal velocity component highlighted some rapid flow deceleration with the passage of the tidal bore, although the flow reversal took place about 50 s after the bore front passage. While unusual, such a delayed flow reversal as previously documented in another system. It is hypothesised that the flow reversal delay was caused by the significant freshwater flow prior to the bore passage. During the flood flow, the turbulent stress magnitudes were larger than during the ebb tide, and some large fluctuations in all stresses were observed. The suspended sediment flux data indicated a downstream positive suspended sediment flux during the end of the ebb tide prior to the tidal bore. After the passage of the bore, the net sediment mass transfer per unit area was negative (i.e. upriver) and its magnitude was 1.5 to 2 times larger than the ebb tide net flux. Overall the sediment concentration and data highlighted some very significant suspended sediment load and it is likely that the flood flow had some non-Newtonian behaviour.

Keywords: Undular tidal bore, Garonne River, Field measurements, Granulometry, Rheology, Suspended sediment concentration, Suspended sediment flux and load, Acoustic Doppler velocimetry, Experimental works, Flow reversal delay, Salinity, Temperature, Equipment damage.

TABLE OF CONTENTS

	Page
Abstract	ii
Keywords	ii
Table of contents	iii
List of symbols	v
1. Introduction	1
2. Field investigation and instrumentation	7
3. Sediment properties and suspended sediment concentration measurements	17
4. General observations	24
5. Turbulent velocity characteristics	37
6. Conclusion	55
7. Acknowledgments	57

APPENDICES

Appendix A - List of field work participants (Field study G12, 7 June2012)	58
Appendix B - Photographs of the field study G12 (7 June 2012)	62
Appendix C - Acoustic Doppler velocimeter configurations (Field study G12, 7 June 2012)	75
Appendix D - Appendix D - Granulometry of Garonne River Sediment samples	79
Appendix E - Rheometry of Garonne River Sediment samples	84
Appendix F - Experimental data: acoustic backscatter intensity versus suspended sediment concentration	90
Appendix G - Unsteady turbulent Reynolds stresses during the tidal bore (Field study G12, 7 June 2012)	98

REFERENCES 103
Bibliography
Internet bibliography
Open Access Repositories
Bibliographic reference of the Report CH89/12

LIST OF SYMBOLS

The following symbols are used in this report:

A channel cross-section area (m^2);

A_1 initial channel cross-section area (m^2) immediately prior to the tidal bore passage;

A_2 channel cross-section area (m^2) immediately after to the tidal bore passage;

Ampl ADV signal amplitude (counts);

B 1- free-surface width (m);
2- characteristic free-surface width (m) defined by Equation (1-5);

B' characteristic free-surface width (m) defined by Equation (1-6)

B_1 initial free-surface width (m) immediately prior to the tidal bore passage;

B_2 initial free-surface width (m) immediately after the tidal bore passage;

d water depth (m);

d_1 initial water depth (m) immediately prior to the tidal bore passage;

d_2 conjugate water depth (m) immediately after the tidal bore passage;

Fr Froude number;

Fr_1 tidal bore Froude number defined as:

$$Fr_1 = \frac{V_1 + U}{\sqrt{g \times \frac{A_1}{B_1}}}$$

g gravity acceleration (m/s^2);

N number of data points;

m dimensionless exponent;

q_s instantaneous advective suspended sediment flux per unit area ($kg/m^2/s$) defined as:

$$q_s = SSC \times V_x$$

R_{xx} normalised auto-correlation coefficient;

SSC suspended sediment concentration (kg/m^3);

s relative density of wet sediment;

t time (s);

T integration period (s);

T_{qs} integral time scale (s) of the longitudinal velocity component;

T_{SSC} integral time scale (s) of the suspended sediment concentration;

T_{Vx} integral time scale (s) of the sediment flux;

U tidal bore celerity (m/s) for an observer standing on the bank, positive upstream;

V flow velocity (m/s);

V_1 initial flow velocity (m/s) immediately prior to the tidal bore passage;

V_1 conjugate flow velocity (m/s) immediately after the tidal bore passage;

V_x instantaneous longitudinal velocity component (m/s);

V_y instantaneous transverse velocity component (m/s);

V_z instantaneous vertical velocity component (m/s);

$\overline{V}$	variable interval time-averaged velocity (m/s)
v	instantaneous velocity fluctuation (m/s) : $v = V - \overline{V}$;
v_x	instantaneous fluctuation (m/s) of V_x;
v_y	instantaneous fluctuation (m/s) of V_y;
v_z	instantaneous fluctuation (m/s) of V_z;
x	longitudinal distance (m) positive downstream;
y	transverse distance (m) positive towards the Arcins island;
z	vertical distance (m) positive upwards;
μ	effective viscosity (Pa.s);
ρ	water density (kg/m^3);
τ	1- shear stress (Pa);
	2- time lag (s);
τ_c	apparent yield stress (Pa);
τ_o	boundary shear stress (Pa);
$(\tau_o)_c$	critical boundary shear stress (Pa) for bed load motion;

Subscript

x	longitudinal direction positive downstream;
y	transverse direction positive towards the Arcins island;
z	vertical direction positive upwards;
1	flow property immediately prior to the tidal bore passage;
2	flow property immediately after the tidal bore passage;

Abbreviations

ADV	acoustic Doppler velocimeter;
h	hour;
IGN	Institut National Géographique;
min	minute;
Nb	number;
ppm	parts per million;
SSC	suspended sediment concentration;
Std	standard deviation;
s	second
VITA	variable-interval time average.

Note

All times are expressed in local French times (GMT + 1).

1. INTRODUCTION

1.1 PRESENTATION

A tidal bore is a series of waves propagating upstream as the tidal flow turns to rising (Fig. 1-1). The bore forms during spring tide conditions when the tidal range exceeds 4 to 6 m and the flood tide flow is restrained into a narrow funnelled estuary. Figure 1-1 illustrates a variety of tidal bores. The word 'bore' is believed to derive from the Icelandic '*bara*' indicating a potentially dangerous phenomenon such as a breaking tidal bore (COATES 2007). The French name '*mascaret*' is said to derive from the Gascony word '*masquaret*' meaning a 'galloping ox' (Petit Robert 1996). Technically the tidal bore is a positive surge associated with a sudden rise in water depth and a discontinuity of the velocity and pressure fields (Fig. 1-1 & 1-2).

The bore front is a flow singularity and hydrodynamic shock (LIGHTHILL 1978, LIGGETT 1994). In a system of reference following the bore front, the integral form of the continuity and momentum equations gives a series of relationships between the flow properties in front of and behind the bore (RAYLEIGH 1914, HENDERSON 1966, LIGHTHILL 1978):

$$(V_1 + U) \times A_1 = (V_2 + U) \times A_2 \tag{1-1}$$

$$\rho \times (V_1 + U) \times A_1 \times (\beta_1 \times (V_1 + U) - \beta_2 \times (V_2 + U)) = \iint_{A_2} P \times dA - \iint_{A_1} P \times dA + F_{fric} - W \times \sin\theta \tag{1-2}$$

where V is the flow velocity and U is the bore celerity for an observer standing on the bank (Fig. 1-2), ρ is the water density, g is the gravity acceleration, A is the channel cross-sectional area measured perpendicular to the main flow direction, β is a momentum correction coefficient, P is the pressure, the subscript 1 refers to the initial flow conditions and the subscript 2 refers to the flow conditions immediately after the jump, F_{fric} is the flow resistance force, W is the weight force and θ is the angle between the bed slope and horizontal. Neglecting the flow resistance (F_{fric} = 0), the effect of the velocity distribution ($\beta_1 = \beta_2 = 1$) and for a flat horizontal channel ($\theta \approx 0$), Equations (1-1) and (1-2) give a relationship between the ratio of conjugate cross-section areas A_2/A_1 as a function of the tidal bore Froude number Fr_1 (CHANSON 2012):

$$\frac{A_2}{A_1} = \frac{1}{2} \times \frac{\sqrt{\left(2 - \frac{B'}{B}\right)^2 + 8 \frac{B'/B}{B_1/B} \times Fr_1^2} - \left(2 - \frac{B'}{B}\right)}{\frac{B'}{B}} \tag{1-3}$$

where the Froude number is defined as:

(A) Tidal bore of the Sélune River in Bay of Mont Saint Michel (France) on 19 October 2008 viewed from Pointe du Grouin du Sud - Bore propagation from background right to foreground left

(B) Tidal bore of the Batang Lupar River in Sarawak (Malaysia) in July 2011 (Courtesy of Antony COLAS) - Bore propagation from left to right

(C) Tidal bore of the Garonne River at Podensac (France) on 29 August 2011 (Courtesy of Isabelle

BORDE) - Bore propagation from right to left

(D) Tidal bore of the Sélune River in Bay of Mont Saint Michel (France) on 23 June 2012 - Bore propagation from background to foreground between Ile de Tombelaine and Pointe du Grouin du Sud

Fig. 1-1 - Photographs of tidal bores

$$Fr_1 = \frac{U + V_1}{\sqrt{g \times \frac{A_1}{B_1}}} \quad (1\text{-}4)$$

and B and B' are characteristic the free-surface widths defined as:

$$B = \frac{A_2 - A_1}{d_2 - d_1} \quad (1\text{-}5)$$

$$B' = \frac{\int_{A_1}^{A_2} \int \rho \times g \times (d_2 - y) \times dA}{\frac{1}{2} \times \rho \times g \times (d_2 - d_1)^2} \quad (1\text{-}6)$$

Equation (1-3) is valid for any tidal bore and hydraulic jump in an irregular channel. The effects of the channel cross-sectional shape are accounted for with the ratios B'/B and B_1/B (CHANSON 2012).

In nature, a tidal bore may have a variety of different shapes (CHANSON 2011), and the photographs illustrate in particular that the bore front is not a sharp, vertical discontinuity of the water surface because of the necessary curvature of the streamline and the associated pressure and velocity redistributions (Fig. 1-1). It is estimated worldwide that over 400 estuaries and shallow-water bays are affected by a tidal bore process (CHANSON 2011). A well preserved macro-tidal environment is the Gironde estuary, Garonne River and Dordogne River in south-western France (Fig. 1-1C & 1-3).

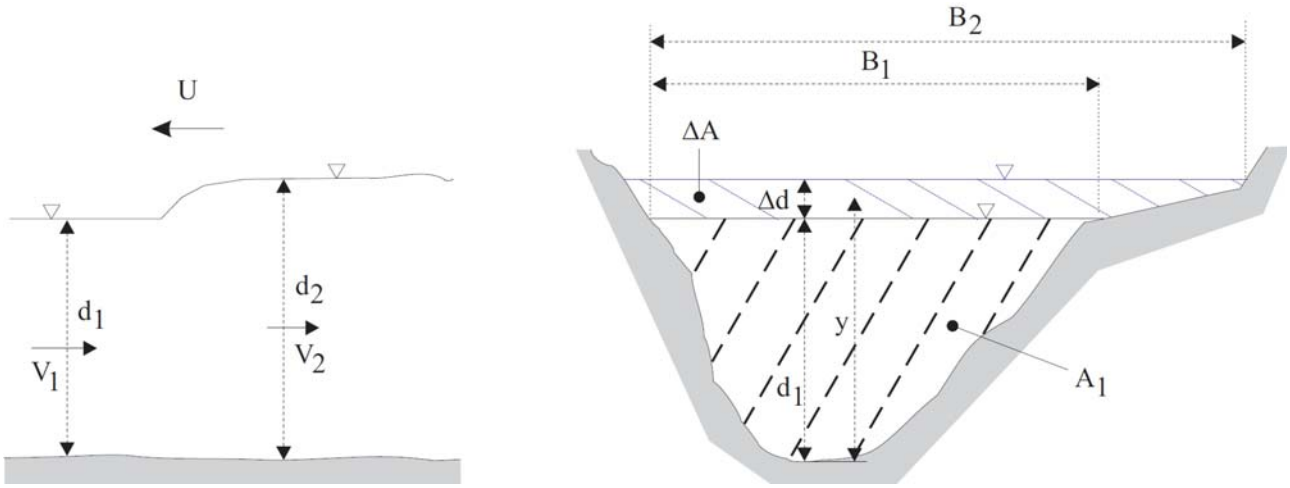

Fig. 1-2 - Definition sketch of a tidal bore propagating in a natural channel

The Gironde estuary flows northwest between Bec d'Ambès at the confluence of the Garonne and Dordogne Rivers, and the Pointe de Grave for about 72 km. It is navigable for oceangoing vessels up to Bordeaux, despite sandbanks and strong tides. Its funnel shape and bathymetry amplifies the tidal range. For example, when the tidal range is 4.5 m at Pointe de Grave, at the mouth of Gironde, the tidal range at Bordeaux is 5.5 m ([1]). The Garonne River is 575 km long plus the Gironde Estuary and its intertidal zone extends up to Castets. The catchment area is 56,000 km^2. The Garonne River tidal bore is observed typically from Pont François Mitterand (Bordeaux) up to Cadillac. A number of visual observations highlighted the rapid evolution of the tidal bore shape and appearance in response to the estuarine bathymetry (CHANSON 2008,2011).

CHANSON et al. (2011) performed a detailed study of the turbulent and sedimentary processes in the tidal bore at Arcins at the end of a dry summer (Fig. 1-3, Table 1-1). The present study was conducted at the same site, but a few weeks after a major flood. The water level was higher in 2012 and the river bed might have been scoured from the soft sediments during the April-May 2012 floods.

[1] Predicted tidal ranges on 7 June 2012.

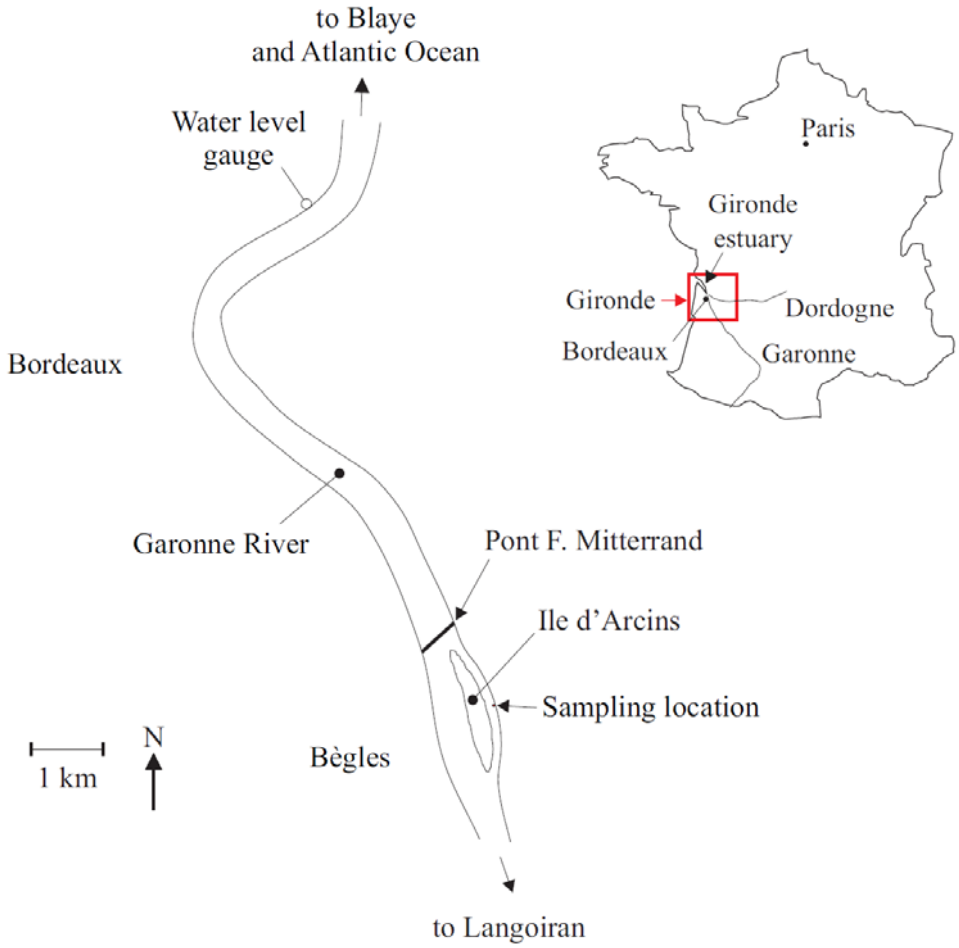

Fig. 1-3 - Map of Garonne River estuarine zone near Arcins (inset: Map of France)

1.2 STRUCTURE OF THE REPORT

A number of field studies experienced some damage to scientific equipments, including in the Rio Mearim (Brazil), in the Daly River (Australia), in the Dee River (UK) and in the Bay of Mont Saint Michel (France) (KJERFVE and FERREIRA 1993, WOLANSKI et al. 2004, SIMPSON et al. 2004, MOUAZE et al. 2010) (Table 1-1). These emphasised the intense turbulent mixing induced by the bore. In the present study, some field measurements were conducted in the Garonne River (France) on 7 June 2012. Some turbulent velocity measurements were performed continuously at high-frequency (50 Hz) in the tidal bore of the Garonne River at Arcins. Despite a number of practical issues and problems, the results provided a detailed characterisation of the unsteady flow features in the tidal bore. The field investigation and instrumentation are described in section 2. The main results are presented in sections 3, 4, and 5. Appendix A lists the field work participants. Appendix B shows a number of photographs of the field study. Appendix C presents the ADV system configurations and discusses the equipment damage. Appendices D, E and F regroup the sediment analyses including the granulometry, rheology and acoustic backscatter results. Appendix G presents the turbulent Reynolds stress data.

Table 1-1 - Field observations of tidal bores

Reference	Initial flow V_1 m/s	d_1 m	Instrument	Channel geometry	Remarks
(1)	(2)	(3)	(4)	(5)	(6)
LEWIS (1972)	0 to +0.2	0.9 to 1.4	Hydro-Products type 451 current meter	Dee River (UK) near Saltney Ferry footbridge. Trapezoidal channel	Field experiments between March and September 1972.
NAVARRE (1995)	0.65 to 0.7	1.12 to 1.15	Meerestechnik-Electronik GmbH model SM11J acoustic current meter (sampling 10Hz)	Dordogne River (France) at Port de Saint Pardon. Width ~ 290 m	Field experiments on 25 & 26 April 1990.
KJERFVE and FERREIRA (1993)			Interocean S4 electro-magnetic current meters (sampling: 1-2 Hz)	Rio Mearim (UK)	Field experiments on 19-22 Aug. 1990 & 28 Jan.-2 Feb. 1991.
WOLANSKI et al. (2001)	--	0.45	Analite nephelometer	Ord River (East Arm) (Australia). Width ~ 380 m	Field experiments in August 1999.
CHEN (2003)	--	--	--	North Branch of the Changjiang River Estuary (China)	Experiments in April 2001.
SIMPSON et al. (2004)	0.1	~0.8	ADCP (1.2 0 MHz) (sampling rate:1 Hz)	Dee River (UK) near Saltney Ferry Bridge. Trapezoidal channel (base width ~ 60 m)	Field experiments in May and September 2002.
WOLANSKI et al. (2004)	0.15	1.5 to 4	Nortek Aquadopp ADCP (sampling rate:2 Hz)	Daly River (Australia). Width ~ 140 m	Field experiments in July and September 2002, and on 2 July 2003.
CHANSON et al. (2011)			ADV Nortek Vector (6 MHz) (sampling: 64 Hz)	Arcins channel, Garonne River (France) Width ~ 76 m	Undular tidal bore.
	0.33	1.40 (*)			10 Sept. 2010.
	0.30	1.43 (*)			11 Sept. 2010.
MOUAZE et al. (2010)			ADV Nortek Vector (6 MHz) (sampling: 64 Hz)	Pointe du Grouin du Sud, Sélune River (France)	Breaking tidal bore.
	0.86	0.15 (*)			24 Sept. 2010.
	0.59	0.11 (*)			25 Sept. 2010.
Present study			microADV Sontek (16 MHz) (sampling: 50 Hz)	Arcins channel, Garonne River (France) Width ~ 78 m	Weak undular tidal bore.
	0.68	2.0 (*)			7 June 2012 morning
	0.59	1.94 (*)			7 June 2012 afternoon

Notes: d_1: initial water depth (at sampling location); V_1: initial flow velocity; (--): information not available; (*): equivalent depth A/B.

2. FIELD INVESTIGATION AND INSTRUMENTATION

2.1 FIELD INVESTIGATION AND SAMPLING SITE

The field study was conducted in the Garonne River (France) in the *Bras d'Arcins* (Arcins channel) between *Île d'Arcins* (Arcins Island) and the right bank close to Lastrene. The location (44°47'58"N, 0°31'07"W) is seen in Figure 1-3. The Arcins channel is about 1.8 km long, 70 m wide and about 1.1 to 2.5 m deep at low tide (Fig. 2-1). Figure 2-1 shows some photographs of the channel and further photographs are presented in Appendix B. Figure 2-2 presents a cross-sectional survey conducted on 7 June 2012, in which it is compared with the bathymetric survey conducted at the same location on 10 September 2010 with z being the vertical elevation ([2]). In Figure 2-2B, the details of the ADV sampling volume location are presented. In Figure 2-2A, all the elevations are shown in m NGF IGN69 ([3]).

Although the tides are semi-diurnal, the tidal cycles have slightly different periods and amplitudes indicating some diurnal inequality (Fig. 2-3). Figure 2-3 presents the water elevation observations at Bordeaux that are compared with the water elevations recorded on-site prior to and shortly after the passage of the tidal bore on 7 June 2012. In Figure 2-3, all the water elevations are presented in m NGF IGN69

(A) Looking downstream at the incoming undular tidal bore in the Arcins channel on 5 June 2012 at 17:33:54 - Note the Airbus barge in the background travelling upstream following the tidal bore

Fig. 2-1 - Photographs of *Bras d'Arcins* (Arcins channel)

[2] The 2012 survey was conducted at the same location as the 2010 survey.

[3] The NGF IGN69 Datum is 1.84 m above the datum of the Bordeaux tidal gauge.

(B) Looking at the pontoon on right bank (Latresne side) on 7 June 2012 at 19:19 (half-hour after tidal bore) - The ADV was mounted at the downstream end (far right) of the pontoon in the foreground

(C) Looking upstream on 7 June 2012 at 17:40 (end of ebb tide)

Fig. 2-1 - Photographs of *Bras d'Arcins* (Arcins channel)

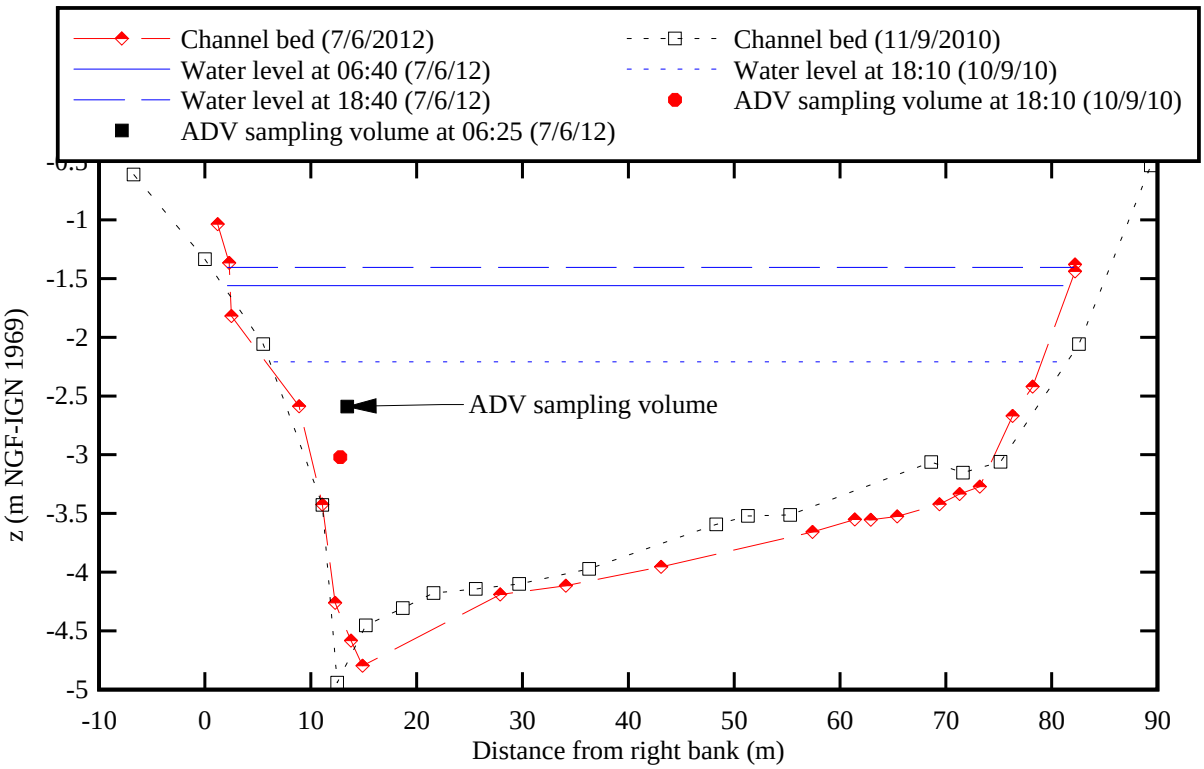

(A) Surveyed (distorted) cross-section looking upstream - Comparison between the 2010 and 2012 surveys at the same cross-section

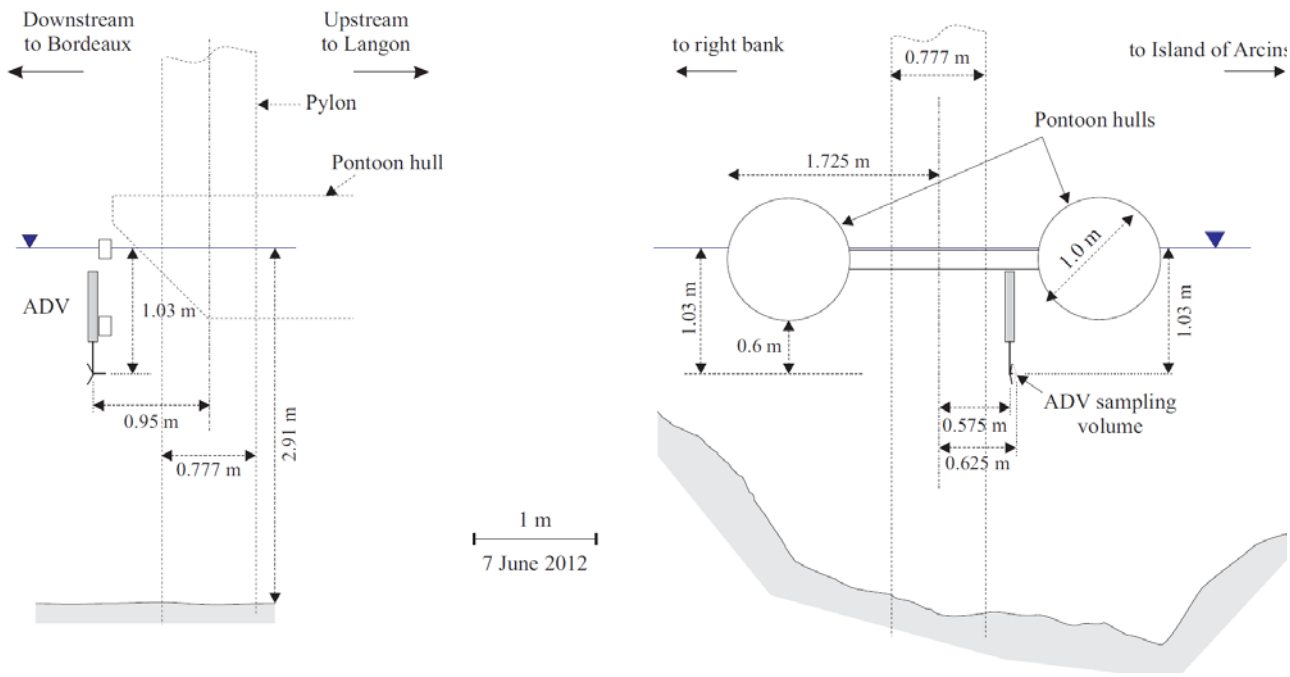

(B) Un-distorted sketch of the ADV mounting, sampling volume location and water surface 20 minutes prior to the tidal bore on 7 June 2012 morning- Left: view from Arcins Island - Right: looking upstream

Fig. 2-2 - Surveyed cross-section of Arcins channel with the low tide water level on 7 June 2012 afternoon and the corresponding ADV sampling volume location

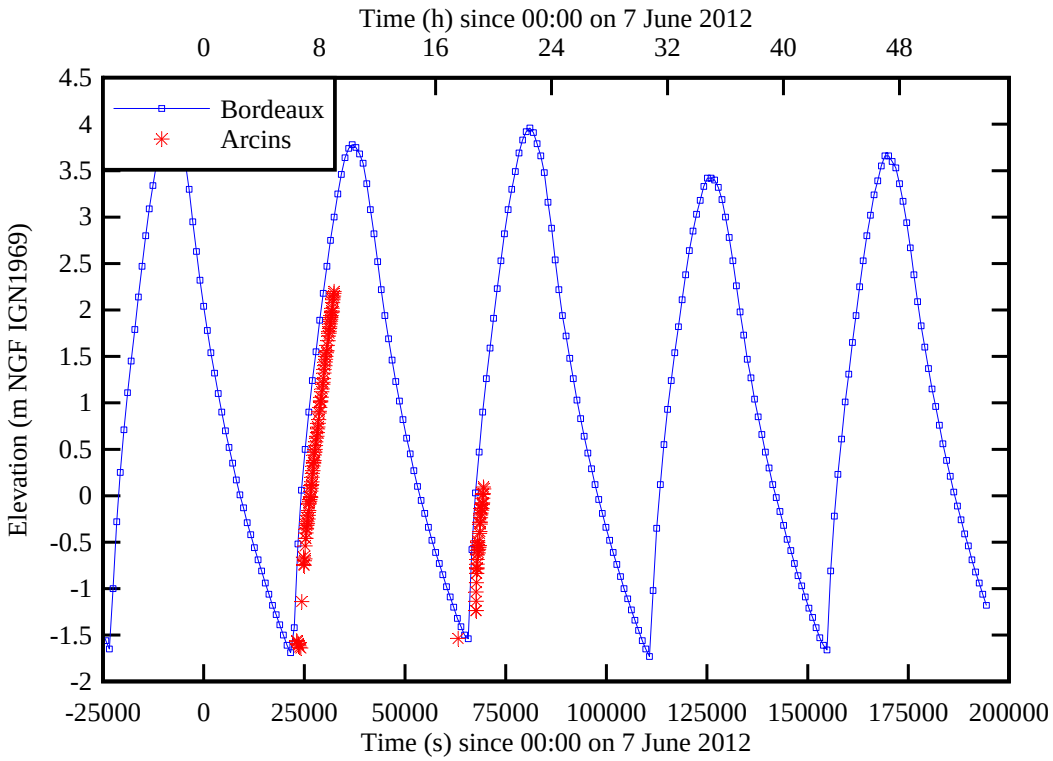

Fig. 2-3 - Measured water elevations at Bordeaux (44°52'N, 0°33'W) (Data: Vigicrue, Ministère de l'Environnement et du Développement Durable) and observations in the Arcins channel on 7 June 2012

Table 2-1 - Tidal bore field measurements in the Arcins channel, Garonne River (France) (Present study, CHANSON et al. 2011)

Date (1)	Tidal range (m) (2)	ADV system (3)	Sampling rate (Hz) (4)	Sampling duration (5)	Start time (6)	Tidal bore time (7)	End time (8)	ADV sampling volume (9)
10/09/2010	6.03	Nortek Vector (6MHz)	64	2h 45 min	17:15	18:17	20:00	About 7 m from right bank waterline (at low tide), 0.81 m below water surface.
11/09/2010	5.89	Nortek Vector (6MHz)	64	2h 20 min	18:00	18:59	20:10	About 7 m from right bank waterline (at low tide), 0.81 m below water surface.
7/06/2012	5.68	Sontek microADV (50 Hz)	50	2h 58 min (10,694 s)	06:01	06:44	09:00	About 11.58 m from right bank waterline (at low tide), 1.03 m below water surface.
	5.5	Visual observations	N/A	N/A	N/A	18:47	N/A	N/A.

Notes: Tidal range: measured at Bordeaux; All times are in French local times.

The field measurements were conducted under spring tide conditions on 7 June 2012 morning and evening. The tidal range data are summarised in Table 2-1 (column 2). During the study, the water elevations and some continuous high-frequency turbulence data were recorded prior to, during and after the passage of the tidal bore for a few hours in the morning. The start and end times are listed in Table 2-1 (columns 6 & 8). No ADV recording was conducted during the afternoon bore because of damage to the ADV unit (see below).

2.2 INSTRUMENTATION

The free surface elevations were measured manually using a survey staff. During the passage of the tidal bore, a video camera recorded the water level and the data were collected at 50 frames per seconds (fps). The survey staff was mounted 2 m beside the ADV unit towards the right bank, to minimise any interference with the ADV sampling volume. The water temperature and salinity were measured with an alcohol thermometer and salinity meter Ebro Electronic SSX56 respectively. The readings were taken about 0.5 m (morning) to 1 m (afternoon) below the free-surface.

During the investigations, the turbulent velocities were measured with a Sontek^{TM} microADV (16 MHz, serial number A1036F) on 7 June 2012 morning. The ADV system was equipped with a 3D side-looking head. The system was fixed at the downstream end of a 23.55 m long heavy, sturdy pontoon. It was mounted vertically, the emitter facing towards Arcins Island, and the positive direction head was pointing downstream. Figure 2-2 shows the location of the ADV sampling volume in the surveyed cross-section. The probe was located between the hulls of the pontoon and the sampling volume was about 1.03 m below the free-surface (Table 2-1, column 9 & Fig. 2-2B). Further details on the ADV settings are reported in Appendix C. All the ADV data underwent a post-processing procedure to eliminate any erroneous or corrupted data from the data sets to be analysed. The post processing was conducted with the software WinADV^{TM} version 2.028, and it included the removal of communication errors, the removal of average signal to noise ratio (SNR) data less than 15 dB and the removal of average correlation values less than 60% (McLELLAND and NICHOLAS 2000). Some discussions on the ADV signal post-processing are developed in Appendix C.

Further observations were recorded with digital cameras Pentax^{TM} K-7, Pentax^{TM} K-01, Sony^{TM} Alpha 33 (30 fps), and a HD digital video camera Canon^{TM} HF10E (50 fps).

2.3 CHARACTERISATION OF THE BED MATERIAL

Some Garonne River bed material was collected at low tide on 7 June 2012 afternoon, as well as at mid-ebb tide on 8 June 2012 afternoon next to the pontoon on the right bank at Arcins. The soil

sample consisted of fine mud and silt materials collected on the stream bed just above the free-surface water mark ([4]). A series of laboratory tests were conducted to characterise the bed material: i.e., the particle size distribution, rheometry and acoustic backscatter properties.

The soil sample granulometry was measured with a Malvern™ laser Mastersizer 2000 equipped with a Hydro 3000SM dispersion unit for wet samples. For each sediment sample (7/6/2012 and 8/6/2012), two mixing techniques were tested: mechanical and ultrasound, for durations ranging from 10 to 30 minutes. For a given configuration, the granulometry was performed four times and the results were averaged. The differences between the 4 runs were checked and found to be negligible.

The rheological properties of mud samples were tested with a rheometer Malvern™ Kinexus Pro (Serial MAL1031375) equipped with either a plane-cone (∅ = 40 mm, cone angle: 4°) or a plane-disk (∅ = 20 mm). The gap truncation (150 μm) was selected to be more than 10 times the mean particle size. The tests were performed under controlled strain rate at constant temperature (25 Celsius). Between the sample collection and the tests, the mud was left to consolidate for 5 days. Prior to each rheological test, a small mud sample was placed carefully between the plate and cone (Fig. 2-4). The specimen was then subjected to a controlled strain rate loading and unloading between 0.01 s^{-1} and 1,000 s^{-1} with a continuous ramp. Figure 2-4 presents some photographs of the tests.

The calibration of the ADV was accomplished by measuring the signal amplitude of known, artificially produced concentrations of material obtained from the bed material sample, diluted in tap water and thoroughly mixed. All the experiments were conducted within 5 days of the experiment. The laboratory experiments were conducted with the same Sontek™ microADV (16 MHz, serial A1036F) system using the same settings as for the field observations on 7 June 2012. For each test, a known mass of sediment was introduced in a water tank which was continuously stirred with a paint mixer (Fig. 2-5). The mixer speed was adjusted during the most turbid water tests to prevent any obvious sediment deposition on the tank bottom. The mass of wet sediment was measured with a Mettler™ Type PM200 (Serial 86.1.06.627.9.2) balance, and the error was less than 0.01 g. The mass concentration was deduced from the measured mass of wet sediment and the measured water tank volume. During the tests, the suspended sediment concentrations (SSCs) ranged from less than 0.01 kg/m^3 to 100 kg/m^3.

The acoustic backscatter amplitude measurements were conducted with the same scan rate and ADV velocity range settings employed in the field. The tank was strongly agitated by the mixer. The ADV signal outputs were scanned at 50 Hz for 180 s for each test. The average amplitude

[4]The mud sample was soft and could be considered somehow as a form of mud cream (*crème de vase*).

measurements represented the average signal strength of the three ADV receivers. They were measured in counts ([5]). For low SSCs, the ADV data were post-processed with the removal of average signal to noise ratio data less than 15 dB, average correlation values less than 60%, and communication errors. For SSC > 60 kg/m^3, unfiltered data were used since both the SNRs and correlations dropped drastically because of signal attenuation.

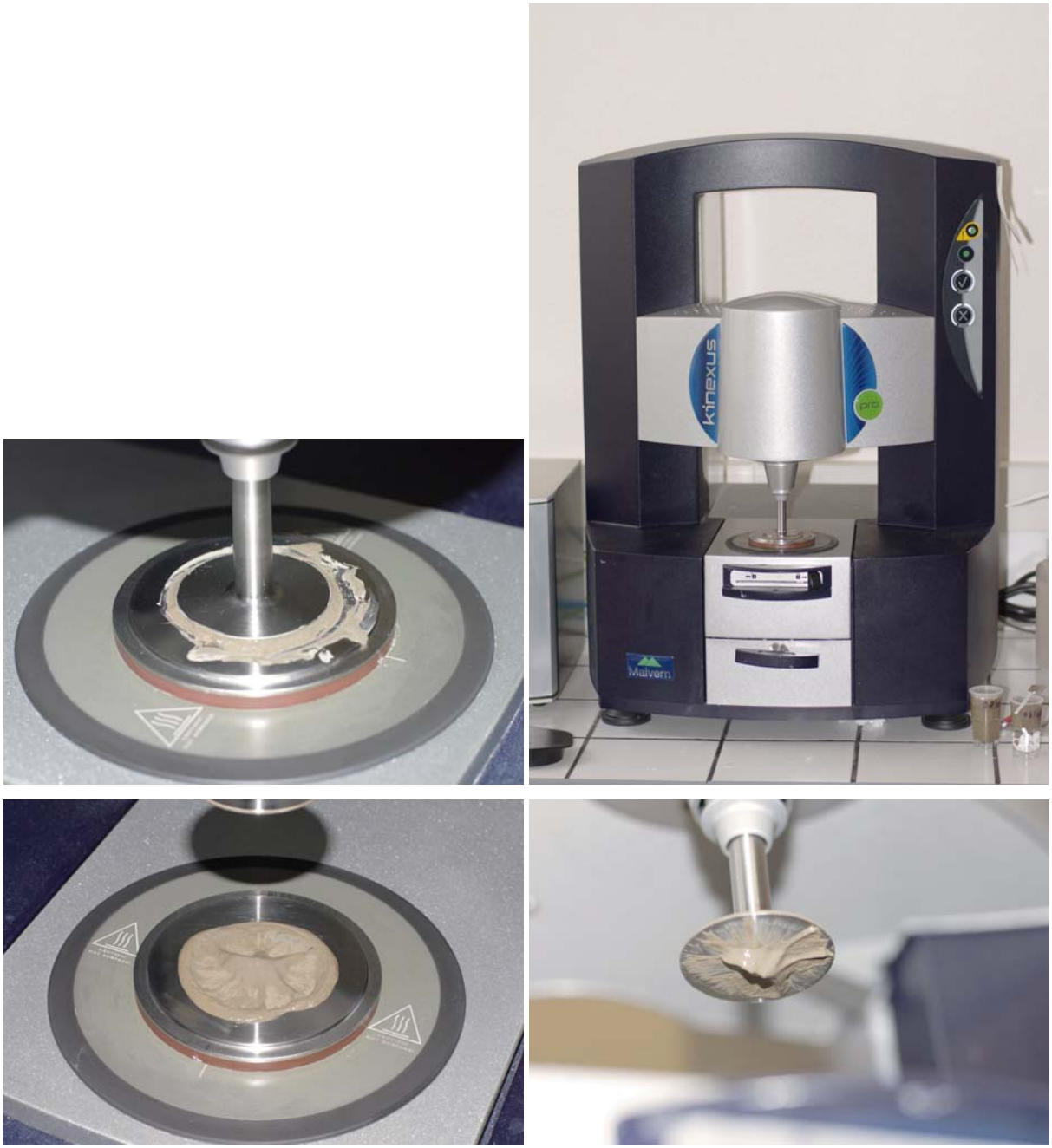

Fig. 2-4 - Photographs of the rheometry tests - From Top left, clockwise: mud sample on the plate during controlled strain rate test, mud pattern on the plane at end of test, mud pattern on the lifted cone at end of test, rheometer unit

[5] One count equals 0.43 dB (Sontek 2006, Person. Comm.).

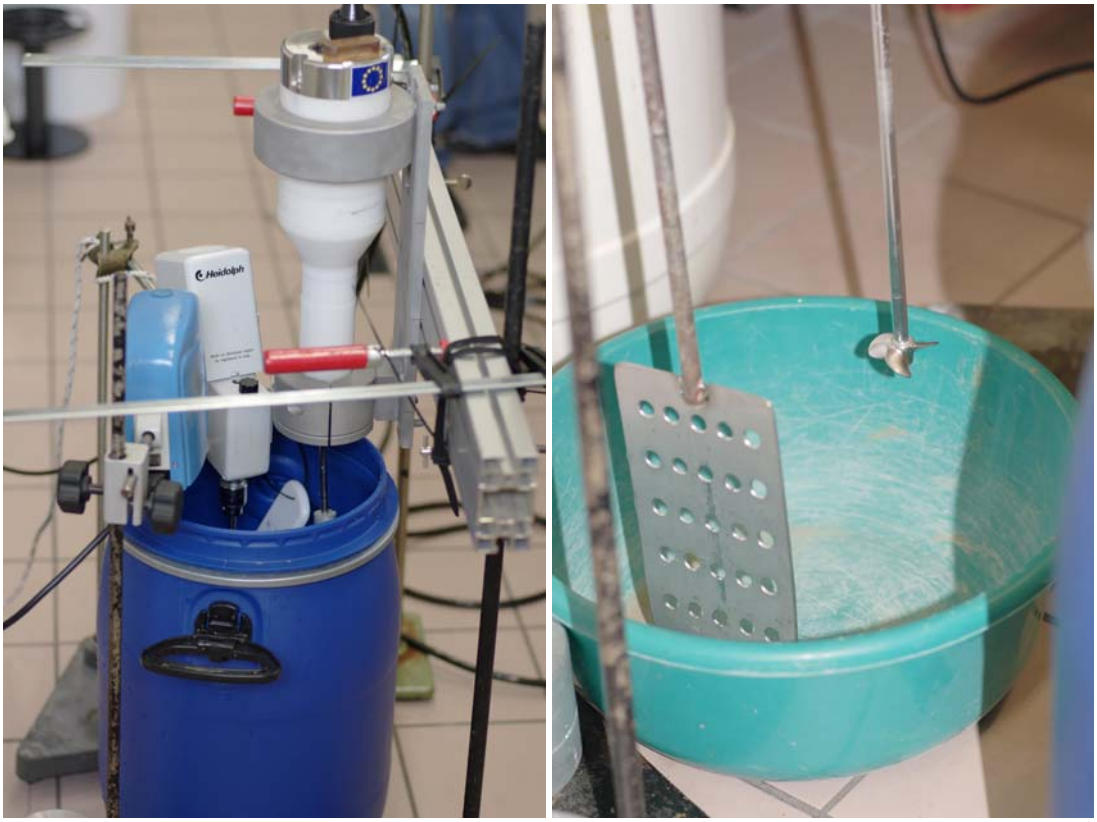

(A, Left) General view - The ADV system is on the right with two water mixers on the left

(B, Right) Details of the mixer blade and propeller

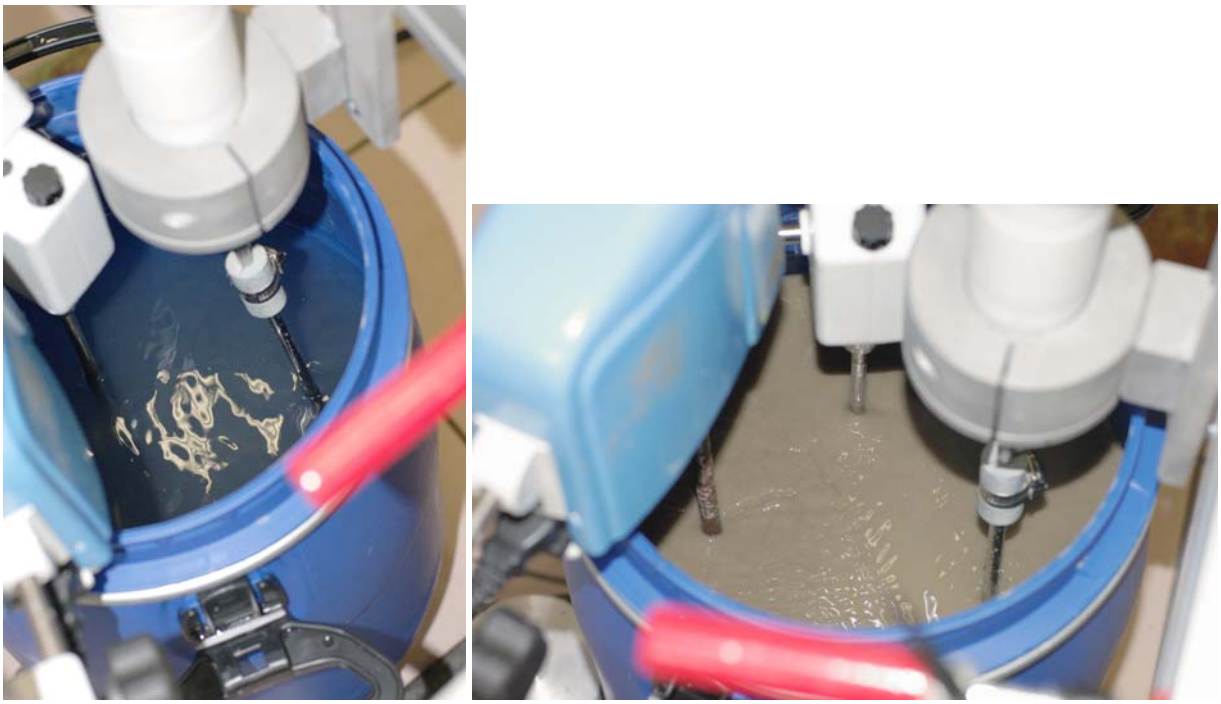

(C, Left) SSC = 0

(D, Right) SSC = 56.3 g/l

Fig. 2-5 - Photographs of the laboratory experiments for ADV calibration (SSC versus signal amplitude)

2.4 REMARKS

2.4.1 ADV synchronisation

The water elevation measurements and ADV data were synchronised within a second. All cameras and digital video cameras were also synchronised together with the same reference time within a second.

2.4.2 Data accuracy

The accuracy on the ADV velocity measurements was 1% of the velocity range (± 2.5 m/s) (Sontek 2008). The accuracy of the water elevation was 0.5 cm prior to the tidal bore and 1-2 cm during the tidal bore passage.

The mass of wet sediment was measured with an accuracy of less than 0.01 g, and the SSC was estimated with an accuracy of less than 0.00025 g/l.

2.4.3 ADV settings and problem

During the field deployment, the authors experienced a major problem: the ADV stem was bent along the main upstream flow direction. The authors found the damaged unit when it was retrieved at the end of the study (Fig. 2-6). Further photographs are presented in Appendix C. Based upon the visual observations and ADV record, it is believed that the ADV unit stem was hit by a submerged debris during the early flood tide, although the authors were constantly looking at the flow free-surface to prevent any impact of floating debris as well as monitoring the ADV data acquisition software and there was no obvious indication of damage to the probe. After the ADV system was brought back in the laboratory, the unit was inspected and checked. While the results were successful, the authors acknowledge that this physical damage might have some effect on the ADV data, in particular the vertical component. Further the suspended sediment tests were performed with the ADV unit four days later and the results indicated no apparent issue with the ADV operation. Nonetheless the velocity data set must be considered with care.

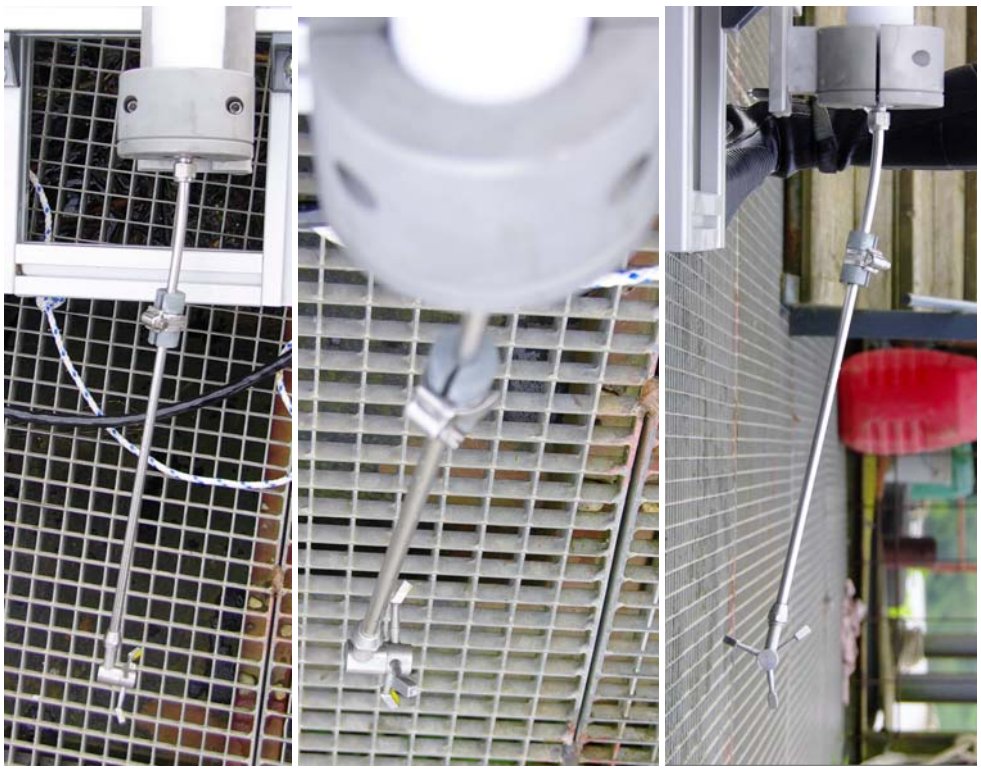

Fig. 2-6 - Photographs of the damaged ADV stem - From left to right: looking upstream, looking downwards, looking towards the Arcins Island

3. SEDIMENT PROPERTIES AND SUSPENDED SEDIMENT CONCENTRATION MEASUREMENTS

3.1 PRESENTATION

The bed sediment material was characterised by a series of laboratory experiments. The relative density of the wet sediment samples was about **s** = 1.36 to 1.48. Assuming a relative sediment density of 2.65, this corresponded to a sample porosity of 0.70 to 0.78. The particle size distribution data presented close results for both samples although they were collected over two different days at different locations (Table 3-1, Fig. 3-1). Herein the type of wet sediment mixing had overall little effect on the results. In Table 3-1, the present results are compared with sediment characteristics of the Brisbane River (Australia) prior to and during a major flood. The full results are reported in Appendix D.

Table 3-1 - Characteristics of sediment samples collected in the Garonne River on 7 and 8 June 2012 - Comparison with Brisbane River sediment samples collected during the 2011 flood (BROWN et al. 2011) and dredged sediment samples (MORRIS and LOCKINGTON 2002)

Reference	Sediment sample	Location	Type	Mixing	d_{50}	d_{10}	d_{90}	$\sqrt{\frac{d_{90}}{d_{10}}}$
					µm	µm	µm	
(1)	(2)	(3)	(4)	(5)	(6)	(7)	(8)	(9)
Garonne River								
Present study	7/06/2012	Garonne River at *Bras d'Arcins* (low tide)	Silt	Mech (10min)	11.86	3.06	50.80	4.07
				Mech (20min)	11.11	2.93	42.19	3.79
				Mech (30min)	12.23	3.10	49.74	4.01
				Ultras (18 min)	13.68	3.19	51.91	4.03
	8/06/2012	Garonne River at *Bras d'Arcins* (mid ebb tide)	Silt	Mech (10min)	13.06	3.75	51.53	3.71
				Mech (20min)	11.05	3.47	38.51	3.33
				Mech (30min)	13.08	3.74	52.15	3.73
				Ultras (14 min)	15.76	3.56	62.97	4.21
Flood deposits								
BROWN et al. (2011)	13/01/2011	Brisbane River at Gardens Point	Silt	--	26.9	3.28	85.1	5.09
	14/01/2011	Brisbane River at Gardens Point	Silt	--	24.6	2.02	88.4	6.62
Dredged sediments								
MORRIS and LOCKINGTON (2002)	2001, Sample 1	Brisbane River at BP Wharf	Clayey sand	--	108.6	--	277.1	--
	2001, Sample 2	Brisbane River at Cairncross Dock	Organic silt	--	< 1.2	--	23.2	--

Notes: Mech: mechanical mixing; Ultras: ultrasound mixing; (--): data not available.

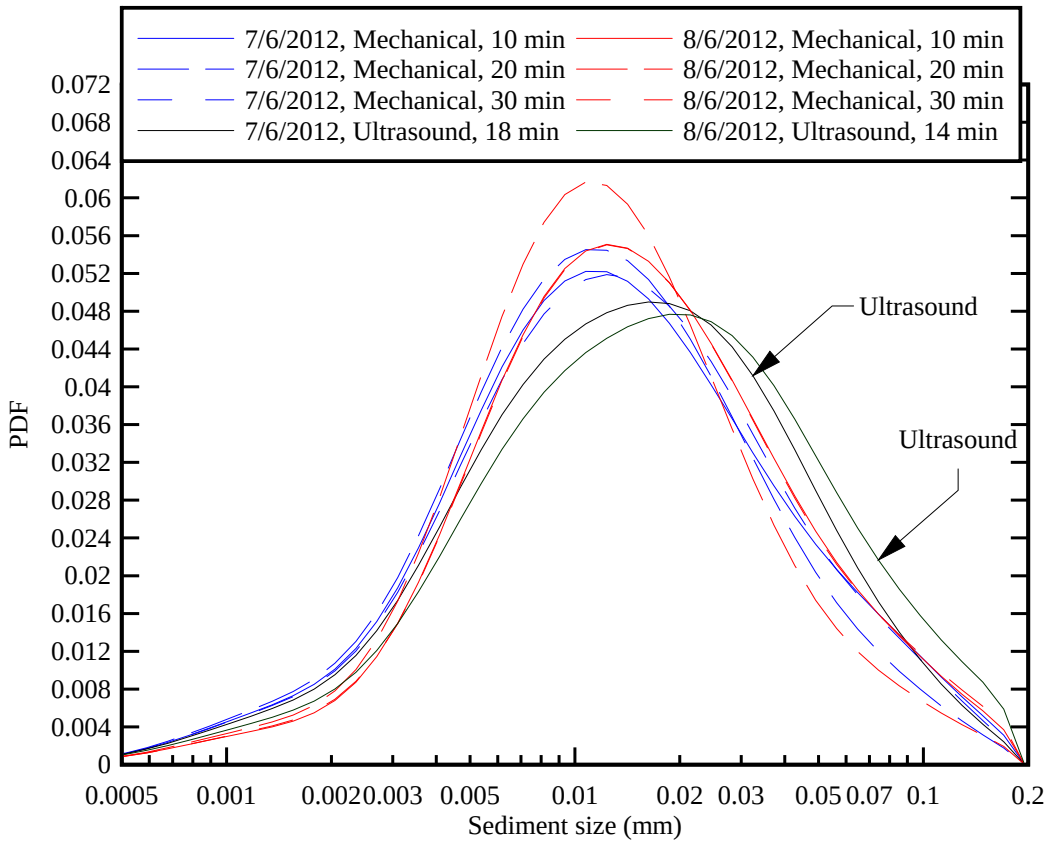

Fig. 3-1 - Particle size distributions of mud samples collected in the Garonne River at Arcins on 7 and 8 June 2012 (Table 3-1)

The median particle size was basically 13 μm corresponding to some silty materials (GRAF 1971, JULIEN 1995, CHANSON 2004). The sorting coefficient $\sqrt{d_{90} / d_{10}}$ ranged from 3.3 to 4.2 (Table 3-1, column 9). The bed material was basically a cohesive mud mixture and the granulometry data were nearly independent of the sample and mixing technique (Table 3-1, Fig. 3-1). The results may be compared with some sediment materials collected in the Brisbane River (Australia) during the January 2011 flood (BROWN et al. 2011) as well as some dredged sediment samples collected also in the Brisbane River during a dry period (MORRIS and LOCKINGTON 2002) (Table 3-1). The Garonne River sediment materials at Arcins channel were typically smaller than the Brisbane River flood sediments, with a smaller sorting coefficient corresponding to a narrower size distribution.

The rheometry tests provided some information on the relationship between shear stress and shear rate during the loading and unloading of small sediment quantities. A range of tests were performed with two configurations, and two sediment samples for each configuration (Appendix E). There were some basic differences between the two sediment samples. The sediment sample collected on 7 June 2012 appeared to be more cohesive and less homogeneous. For example, the authors found some darker sediment inclusions as well as some fibres. Further details on the tests are reported in Appendix D. The relationship between shear stress and shear rate highlighted some basic

differences between the loading and unloading phases typical of some form of material thixotropy ([1]). The magnitude of the shear stress during unloading was smaller than the shear stress magnitude during loading for a given shear rate (Fig. 3-2). Figure 3-2 presents a typical example of rheometry data.

The data were used to estimate an apparent yield stress of the fluid τ_c and effective viscosity μ. Although a complete characterization of rheological behaviour of such thixotropic material would require the determination of all parameters of a thixotropic model, a more rapid but also more approximate characterization of the material was used herein. The yield stress and viscosity were estimated by fitting the rheometer data with a Herschel-Bulkley model, during the unloading phase to be consistent with earlier thixotropic experiments (ROUSSEL et al. 2004, CHANSON et al. 2006). The Herschel-Bulkley fluid model is a simplistic representation of the relationship between shear stress τ and shear rate $\partial V/\partial y$:

$$\tau = \tau_c + \mu \times \left(\frac{\partial V}{\partial y} \right)^m \quad (3\text{-}1)$$

with $0 < m \leq 1$ (HUANG and GARCIA 1998, WILSON and BURGESS 1998). For $m = 1$, Equation (3-1) yields the Bingham fluid behaviour and μ is a material parameter.

Based upon the unloading data, the comparison with Equation (3-1) yielded some basic results in terms of the yield stress τ_c, effective viscosity μ and exponent m which are regrouped in Table 3-2. The findings are compared with other sediment data obtained with a similar characterisation of material.

Quantitatively the findings were consistent with the qualitative observations: that is, a more cohesive sediment mixture was collected on 7 June 2012 associated with larger yield stress and apparent viscosity. On average, the apparent viscosity was between 18 and 36 Pa.s, the yield stress was about 75 to 271 Pa and $m \sim 0.22$ and 0.40 for the sediment sample collected on 7 June 2012 at low tide. For the sediment sample collected on 8 June 2012 at mid-ebb tide, the apparent viscosity was between 2.9 and 13 Pa.s, the yield stress was about 15 to 74 Pa and $m \sim 0.27$ to 0.60 on average. Further the present data were not dissimilar with the sediment characteristics of samples collected at Arcins on 11 September 2010, but it must be stressed that the present study was conducted shortly after a major flood of the Garonne River. An unique feature of the present data set was the range of rheometry data complemented by detailed granulometry tests, although with a limited protocol.

[1] Thixotropy is the characteristic of a fluid to form a gelled structure over time when it is not subjected to shearing and to liquefy when agitated.

The present data scatter suggested that the quantitative results might be closely linked with the testing protocol and configuration. It is conceivable that the in-homogenous nature of the sediment materials collected at low tide on 7 June 2012 might have contributed to the spread of the results. Importantly, the present findings implied that, at high suspended sediment concentrations, the Garonne River waters may have had a non-Newtonian behaviour. Indeed a number of studies showed that hyperconcentrated flood flows are difficult to predict because of their non-Newtonian behaviour (WANG et al. 1994, ANTOINE et al. 1995).

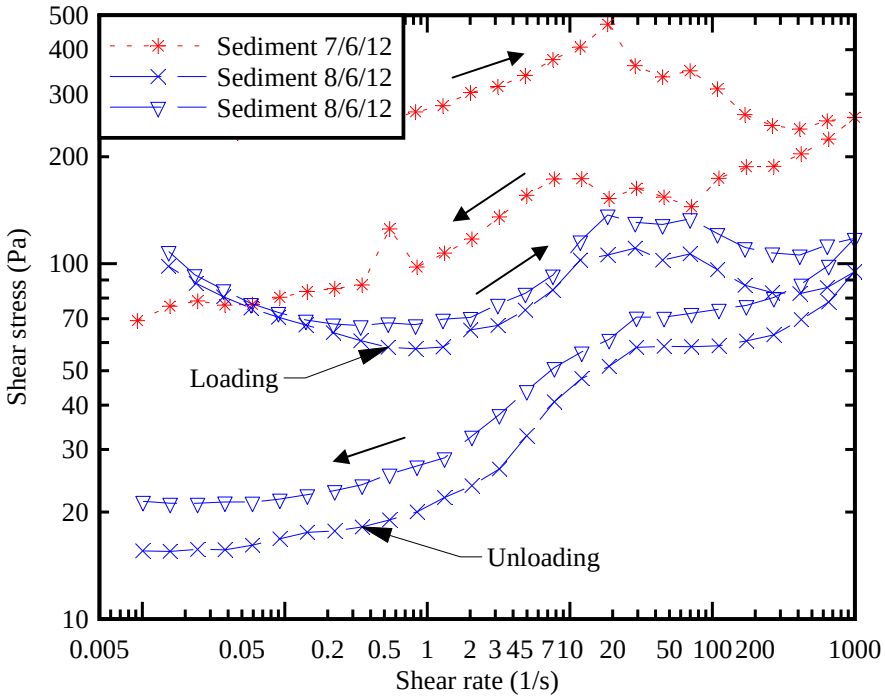

Fig. 3-2 - Mud rheometer test: loading and unloading cycle with a rheometer Malvern Kinexus Pro equipped with a smooth cone (40 mm 4º) - Sediment collection: 7 June 2012 at low tide and 8 June 2012 at mid-ebb tide

Table 3-2 - Measured sediment properties of mud samples collected in the Garonne River on 7 and 8 June 2012 at Arcins - Comparison with Brisbane River flood sediment sample (BROWN et al. 2011) and mud samples collected in the Garonne River at Arcins in September 2010 (CHANSON et al. 2011)

Ref.	River system	Rheometer	Configuration	Loading	Shear rate Min. 1/s	Shear rate Max. 1/s	Temperature Celsius	Sediment collection date	**s**	τ_c Pa	μ Pa.s	m
Present study	Garonne River at Arcins	Malvern Kinexus Pro	Cone 40 mm 4º (smooth)	Continuous ramp	0.01	1,000	25.0	7 June 2012	1.357	75.4	36.1	0.22
								8 June 2012	1.428	15.7	11.4	0.27
								8 June 2012		21.5	13.1	0.28
			Disk 20 mm (smooth)	Continuous ramp	0.01	1,000	25.0	7 June 2012	1.357	271	17.5	0.40
								8 June 2012	1.428	74.2	2.87	0.60
CHANSON et al. (2011)	Garonne River at Arcins	TA-ARG2	Cone 40 mm 2º (smooth)	Steady state flow steps	0.01	1,000	20	11 Sept. 2010	1.41	49.7	44.6	0.28
								(low tide)		61.4	52.9	0.27
BROWN et al. (2011)	Brisbane River in flood at Gardens Point Road	Mettler Viscosimeter	Cylindrical (0.59 mm between cylinders)		0	1,045	25	14 Jan. 2011	1.46	35.5	8.1	0.34

Notes: τ_c: apparent yield stress; μ: effective viscosity; m: Herschel-Bulkley law exponent (Eq. (3-1)).

3.2 ACOUSTIC BACKSCATTER AMPLITUDE AND SUSPENDED SEDIMENT CONCENTRATION

3.1 Experimental calibration

The acoustic Doppler velocimeter (ADV) is designed to measure the velocity components in a small control volume at a relatively high frequency. The ADV signal outputs include the signal strength or acoustic backscatter amplitude which may be related to the suspended sediment concentration (SSC) with proper calibration (KAWANISI and YOKOSI 1997, FUGATE and FRIEDRICHS 2002).

Some early research works were conducted in rivers and coastal zones with non-cohesive sediments, and a number of studies extended the application to cohesive materials (FUGATE and FRIEDRICHS 2002, VOULGARIS and MEYERS 2004, CHANSON et al. 2008). Some thorough experiments indicated that the acoustic backscatter strength increased monotically with increasing SSC for relatively low suspended sediment loads (FUGATE and FRIEDRICHS 2002, CHANSON et al. 2008). For high suspended sediment concentrations, the ADV backscatter amplitude decreased with increasing SSC, the trend highlighting some signal saturation linked to multiple scattering and associated sound absorption (HA et al. 2009, BROWN et al. 2011, CHANSON et al. 2011).

Within the experimental conditions (section 2), the relationships between acoustic backscatter amplitude (Ampl) and suspended sediment concentrations (SSC) were tested systematically for SSCs between 0 and 100 kg/m^3. Two water solutions were used: de-ionised (permutted) water and tap water. Two sediment samples were tested: a sample collected at low tide on 7 June 2012 and another collected at mid-ebb tide on 8 June 2012. The experimental results are summarised in Figure 3-3. The full data sets are reported in Appendix F.

First the results were independent of the water solutions and sediment samples within the experimental setup (App. F). No difference was observed between the de-ionised (permutted) and tap water solutions, nor between the sediment samples collected at low tide on 7 June 2012 and mid-ebb tide on 8 June 2012.

Second there was a good correlation between the results highlighting a characteristic relationship between SSC and amplitude. For SSC $\leq$ 8 kg/m^3, the data indicated a monotonic increase in suspended sediment concentration with increasing backscatter amplitude. For larger SSCs (i.e. SSC > 10 kg/m^3), the experimental results showed a decreasing backscatter amplitude with increasing SSC.

For the laboratory tests with low suspended loads (SSC $\leq$ 8 kg/m^3), the best fit relationships were:

$$SSC = \frac{-8.735}{1 - 35253 \times \exp(-0.1053 \times (Ampl - 92))} \qquad SSC \leq 8 \text{ kg/m}^3 \quad (3\text{-}2)$$

where the suspended sediment concentration SSC is in kg/m^3, and the amplitude Ampl is in counts.

Equation (3-2) was correlated to the data with a normalised correlation coefficient of 0.956.

For large suspended sediment loads (i.e. SSC > 10 kg/m^3), the data were best correlated by

$$SSC = 240.34 - 1.582 \times Ampl + 0.00196 \times Ampl^2 \qquad SSC > 10\ kg/m^3 \quad (3\text{-}3)$$

with a normalised correlation coefficient of 0.993. Equations (3-2) and (3-3) are compared with the data in Figure 3-3. For large suspended sediment concentration within 10 < SSC < 100 kg/m^3, the results showed a good correlation between the acoustic backscatter strength and the SSC, although the ADV signal was saturated.

During the present field investigations, the authors observed that the Arcins channel waters were very turbid before, during and after the tidal bore. In the waters, they could not see their fingers a few centimetres below the free surface and the people who came out of the water were covered by some fine sediment materials. In the Gironde estuary, some SSC observations reported typically values from 0.5 to 2.5 kg/m^3 close to the surface (DOXARAN et al. 2009). Further upstream in the Garonne River, CHANSON et al. (2011) measured SSC levels between 20 and 100 kg/m^3. Herein Equation (3-3) was considered representative of the relationship between the suspended sediment concentration (SSC) and the acoustic backscatter amplitude (Ampl) in the Arcins channel on 7 June 2012.

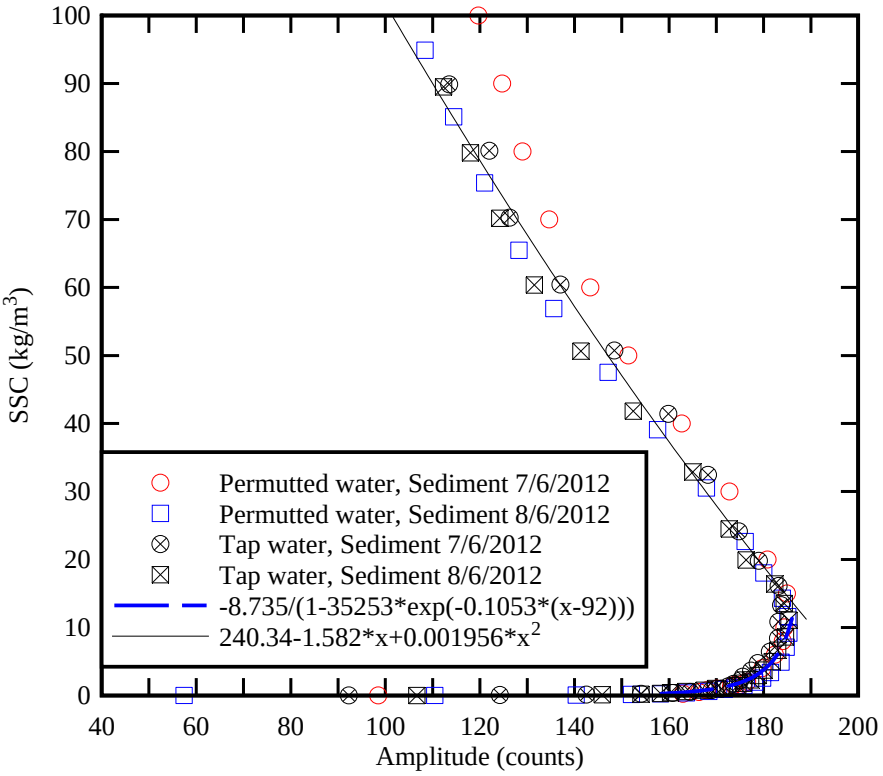

Fig. 3-3 - Relationship between suspended sediment concentration and acoustic signal amplitude with the sediment samples collected at Arcins - Comparison between the data and Equations (3-2) and (3-3)

4. GENERAL OBSERVATIONS

4.1 PRESENTATION

The tidal bore propagation in the Arcins channel (*Bras d'Arcins*) was studied on 7 June 2012 both morning and evening, after being observed on 4 and 5 June 2012 evenings. The tidal bore formed first at the downstream end of the channel (Fig. 4-1A,B,C, 4-2A,B, 4-3A). The tidal bore extended across the entire channel width as an undular bore, even a very flat one as seen on 7 June 2012 morning (Fig. 4-2). When the bore propagated upstream, its shape evolved constantly in response to the local bathymetry. The tidal bore was undular when it passed the sampling location. On 7 June afternoon, the bore front is well marked by the kayakers riding ahead of the first wave crest in Figure 4-3B. Some basic tidal bore characteristics are summarised in Table 4-1 in which they are compared some detailed field observations of tidal bores (Table 1-1). The bore continued to propagate up to the upstream end of the channel for another few minutes. The tidal bore was undular upstream of the sampling point (Fig. 4-1A).

The passage of the tidal bore was characterised by a pseudo-chaotic surface motion lasting for several minutes after the bore front, although the impact on the pontoon was lesser than that observed in September 2010 (CHANSON et al. 2011). At the sampling location, the free-surface elevation rose very rapidly by 0.45 m and 0.52 m in the first 10-15 seconds on 7 June 2012 morning and afternoon respectively. For the next 40 minutes, the water elevation rose further by 1.22 m and 1.33 m on 7 June 2012 morning and afternoon respectively. On the 7 June 2012 morning, the bore front was barely perceptible, but the rapid rise in water elevation was thoroughly documented. More details on the water elevation data are described in the next paragraphs.

(A) Undular tidal bore formation in the Arcins channel at 17:32:42 - Note the Airbus barge in the background travelling upstream following the tidal bore

(B) Tidal bore at 17:33:30

(C) Tidal bore approaching the pontoon at 17:34:05

(D) Tidal bore propagating upstream of the pontoon at 17:34:56

Fig. 4-1 - Undular tidal bore in *Bras d'Arcins* (Arcins channel) on 5 June 2012

(A) Tidal bore approaching the pontoon at 06:51:41 - The red arrow points to the bore front

(B) Tidal bore approaching the pontoon at 06:51:46 - The red arrow points to the bore front

(C) Tidal bore past the pontoon at 06:51:55 - The red arrow points to the bore front in the background

Fig. 4-2 - Field study in *Bras d'Arcins* (Arcins channel) on 7 June 2012 morning

(A) Advancing bore along Arcins Island at 18:54:18 - The red arrow points to the bore front

(B) Sequence of shots as the tidal bore passed the sampling point at 18:54:52 with 0.38 s between each shot - Pierre LUBIN and Bruno SIMON on the kayak tried to surf the bore front

Fig. 4-3 - Field study in *Bras d'Arcins* (Arcins channel) on 7 June 2012 afternoon

Figures 4-1, 4-2 and 4-3 present some photographs of the tidal bore propagation on 5 June 2012 afternoon, 7 June 2012 morning and 7 June 2012 afternoon respectively. Further photographs are presented in Appendix B.

4.2 TIDAL BORE PROPERTIES

4.2.1 Tidal bore celerity and Froude number

A tidal bore is a hydrodynamic shock. The front is characterised by a sudden rise in free-surface elevation and a discontinuity of the pressure and velocity fields. In a tidal bore, the flow properties immediately before and after the bore front must satisfy the equations of conservation of mass and momentum (LIGGETT 1994, CHANSON 2004,2012) (section 1.1). In the system of reference in translation with the bore front, the momentum principle yields a dimensionless relationship between the ratio of conjugate cross-section areas A_2/A_1 and the upstream Froude number Fr_1 (CHANSON 2012):

$$\frac{A_2}{A_1} = \frac{1}{2} \times \frac{\sqrt{\left(2 - \frac{B'}{B}\right)^2 + 8 \times \frac{B'/B}{B_1/B} \times Fr_1^{\,2}} - \left(2 - \frac{B'}{B}\right)}{\frac{B'}{B}} \quad (4\text{-}1)$$

where A_1 and B_1 are respectively the initial cross-section area and free-surface width, A_2 and B_2 are the new cross-section area and free-surface width respectively, and the tidal bore Froude number Fr_1 is defined as:

$$Fr_1 = \frac{V_1 + U}{\sqrt{g \times \frac{A_1}{B_1}}} \quad (4\text{-}2)$$

with V_1 the initial flow velocity, U is the bore celerity for an observer standing on the bank, g the gravity acceleration (section 1.1).

During the present field experiments, the tidal bore was undular at the sampling location, and the tidal Froude number was estimated from the surveyed channel cross-section, water level observations and tidal bore celerity observations (Table 4-1). The tidal bore Froude number (Eq. (4-2)) was Fr_1 = 1.02 and 1.19 for the field observations on 7 June 2012 morning and afternoon respectively.

The present results are shown in Figure 4-4 with the ratio of conjugate cross-sectional areas A_2/A_1 as a function of the tidal bore Froude number Fr_1. The data (solid circles) are compared with Equation (4-1) (Black & white squares) and previous field data (Table 4-1). For completeness, the solution of the momentum equation for a smooth rectangular channel:

$$\frac{A_2}{A_1} = \frac{1}{2} \times \left(\sqrt{1 + 8 \times Fr_1^{\ 2}} - 1 \right) \quad (4\text{-}3)$$

Figure 4-4 illustrates the good agreement between Equation (4-1) and the field data, but for one data point (Sélune River, 25 Sept. 2010). It highlights further the limitations of the Bélanger equation (Eq. (4-3)) in natural irregular channels for which the cross-sectional properties may have a significant impact on the definition of the bore Froude number. The effects of the channel cross-section irregularity increase with increasing Froude number and bore height (d_2-d_1). The Bélanger equation (Eq. (4-3)) based upon the assumption of a rectangular channel is simply inappropriate in an irregular channel, as highlighted by the difference between Equations (4-1) and (4-3) in Figure 4-4.

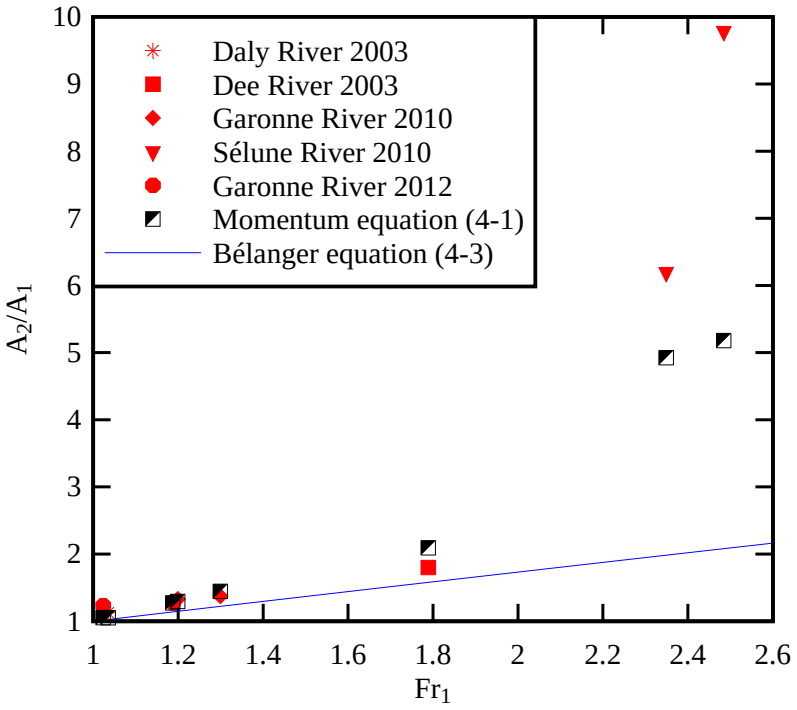

Fig. 4-4 - Dimensionless relationship between the conjugate cross-sectional area ratio A_2/A_1 and tidal bore Froude number Fr_1 - Comparison between the field data, Equation (4-1), previous field observations and the Bélanger equation (Eq, (4-3))

Table 4-1 - Tidal bore properties in the Arcins channel (Garonne River, France) at the sampling location on 7 June 2012 - Comparison with cross-sectional and hydrodynamic properties of tidal bores during field measurements

Reference	River	Date	Bore type	Fr_1	U m/s	V_1 m/s	d_1 m	A_1 m^2	B_1 m	Δd m	ΔA m2	B_2 m	B m	B' m	A_1/B_1	B_2/B_1	B/B_1	B'/B_1	A_2/A_1	Fr_1 Eq. (4-1)
(1)	(2)	(3)	(4)	(5)	(6)	(7)	(8)	(9)	(10)	(11)	(12)	(13)	(14)	(15)	(16)	(17)	(18)	(19)	(20)	(21)
WOLANSKI et al. (2004)	Daly River	2/07/03	Undular	1.04	4.70	0.15	1.50	289.3	129.2	0.28	36.4	130.9	130.1	129.3	2.24	1.013	1.007	1.001	1.13	1.09
SIMPSON et al. (2004)	Dee River	6/09/03	Breaking	1.79	4.1	0.15	0.72	39.3	68.3	0.45	31.4	72.8	70.4	74.1	0.58	1.066	1.030	1.085	1.80	1.58
CHANSON et al. (2011)	Garonne River	10/09/10	Undular	1.30	4.49	0.33	1.77	105.7	75.4	0.50	39.4	81.6	78.5	76.7	1.40	1.083	1.042	1.018	1.37	1.25
		11/09/10	Undular	1.20	4.20	0.30	1.81	108.8	75.8	0.46	36.0	81.6	78.2	77.5	1.43	1.076	1.032	1.021	1.33	1.23
MOUAZE et al. (2010)	Sélune River	24/09/10	Breaking	2.35	2.00	0.86	0.38	5.25	34.7	0.34	27.3	*116.9*	80.9	66.6	0.15	3.37	2.33	1.92	6.19	2.89
		25/09/10	Breaking	2.48	1.96	0.59	0.33	3.56	33.2	0.41	31.3	*117.0*	77.3	65.7	0.11	3.53	2.33	1.98	9.79	4.46
Present study	Garonne River	7/06/12	Undular (very flat)	*1.02*	*3.85*	0.68	2.72	158.9	79.0	0.45	36.71	84.3	81.6	82.4	2.00	1.067	1.033	1.043	1.233	1.15
		7/06/12	Undular	1.19	4.58	0.59	2.65	152.3	78.7	0.52	42.24	84.3	81.2	81.8	1.94	1.071	1.032	1.040	1.278	1.19

Notes: A_1: channel cross-section area immediately prior to the bore passage; B_1: free-surface width immediately prior to the bore passage; d_1: water depth next to ADV immediately prior to the bore passage; Fr_1: tidal bore Froude number (Eq. (4-2)); U: tidal bore celerity positive upstream on the channel centreline; V_1: downstream surface velocity on the channel centreline immediately prior to the bore passage; *Italic data*: incomplete data.

4.2.2 Free-surface properties

The water depth was recorded using a survey staff placed about 1.4 m beside the ADV towards the right bank. The data were recorded visually, although a video camera (50 fps) was also used on 7 June 2012 morning during the bore passage. Figure 4-5 presents the recorded water depth for both field measurements. Figures 4-5A and 4-5B show the entire records and the horizontal axis corresponds to 12,000 s (3 h 20 min). Figure 4-6 highlights the 300 s period around the tidal bore front passage on 7 June 2012 morning.

The water depth data showed qualitatively some similar trend for both data sets. The water depth decreased slowly during the end of the ebb tide prior to the tidal bore arrival. The passage of the bore was associated with a very rapid rise of the water elevation (t = 24,180 s & 67,620 s in Fig. 4-5A & B) and some pseudo-chaotic wave motion shortly after the front. During the following flood flow, the water depth increased rapidly with time: i.e., nearly 1.4 and 1.8 m in 30 minutes on 7 June 2012 morning and afternoon respectively. Such features were previously seen in field experiments of undular tidal bores (WOLANSKI et al. 2004, CHANSON et al. 2011)

There were however some unusual features observed herein. These included (a) a slow rise of water level immediately prior to the bore front on 7 June 2012 morning and (b) some unexpected water level drop about 10 minutes after the front. On 7 June 2012 morning, the free-surface depth data highlighted a gradual rise in water level immediately prior to the bore front (Fig. 4-6). That is, a gentle rise of 0.04 m in about 70 s immediately prior to the bore front discontinuity for $24{,}110 < t < 24{,}180$ s (Fig. 4-6). Although some laboratory experiments reported a gentle rise in water level ahead of breaking bores (KOCH and CHANSON 2009, DOCHERTY and CHANSON 2012, KHEZRI and CHANSON 2012), the present observations might reflect the very flat nature of the tidal bore associated with the bore Froude number ($Fr_1 \approx 1.02$) close to unity. On both morning and afternoon of 7 June 2012, the authors were surprised by a rapid and short drop in water elevation about 10 minutes after the passage of the bore front. This feature is highlighted in Figures 4-5A and 4-5B with a black arrow, and it will be further discussed in section 5. No physical explanation can be proposed definitely, but it might be conceivable that the sudden drop 10 minutes after the main bore front was due to the tidal bore of the main Garonne River channel entering into the southern end of the Arcins channel and propagating northwards against the flood flow (Fig. 4-7). The situation is sketched in Figure 4-7. Such a backward bore was previously seen at the southern end of the Arcins channel during previous tidal bore events and it occurs because the tidal bore front travels faster in the deeper waters of the Garonne River main channel. A similar phenomenon was observed in the River Trent (UK) (JONES 2012, *Pers. Comm.*).

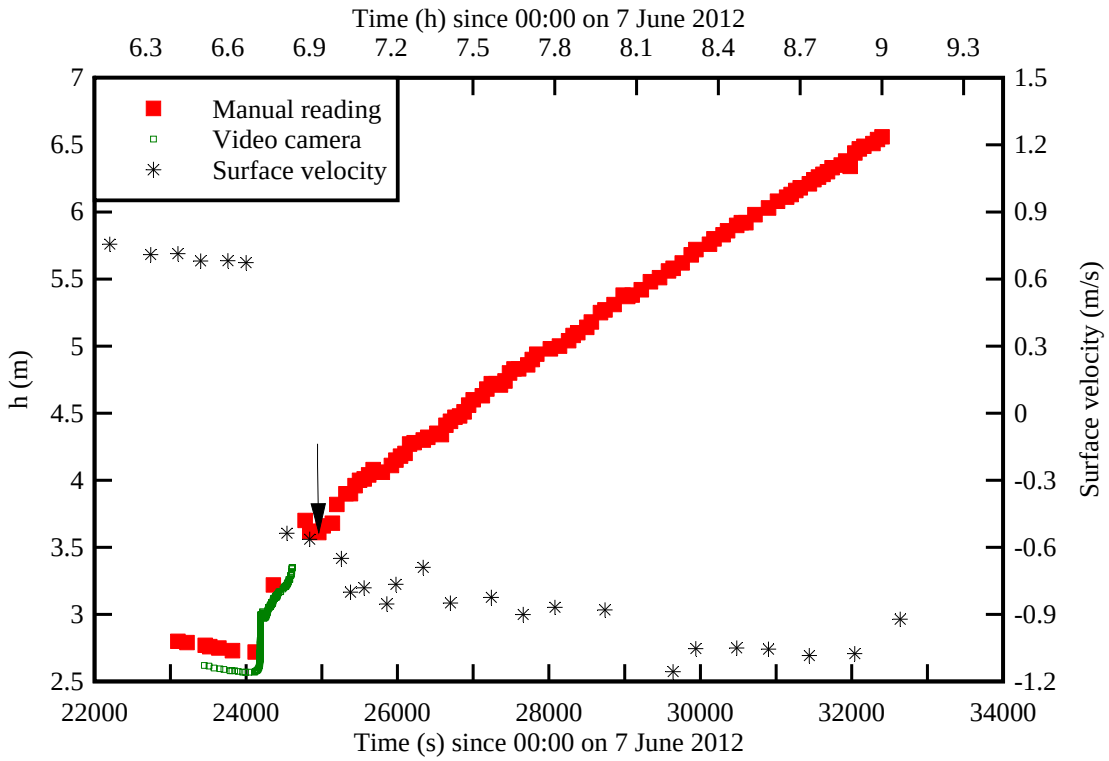

(A) On 7 June 2012 morning

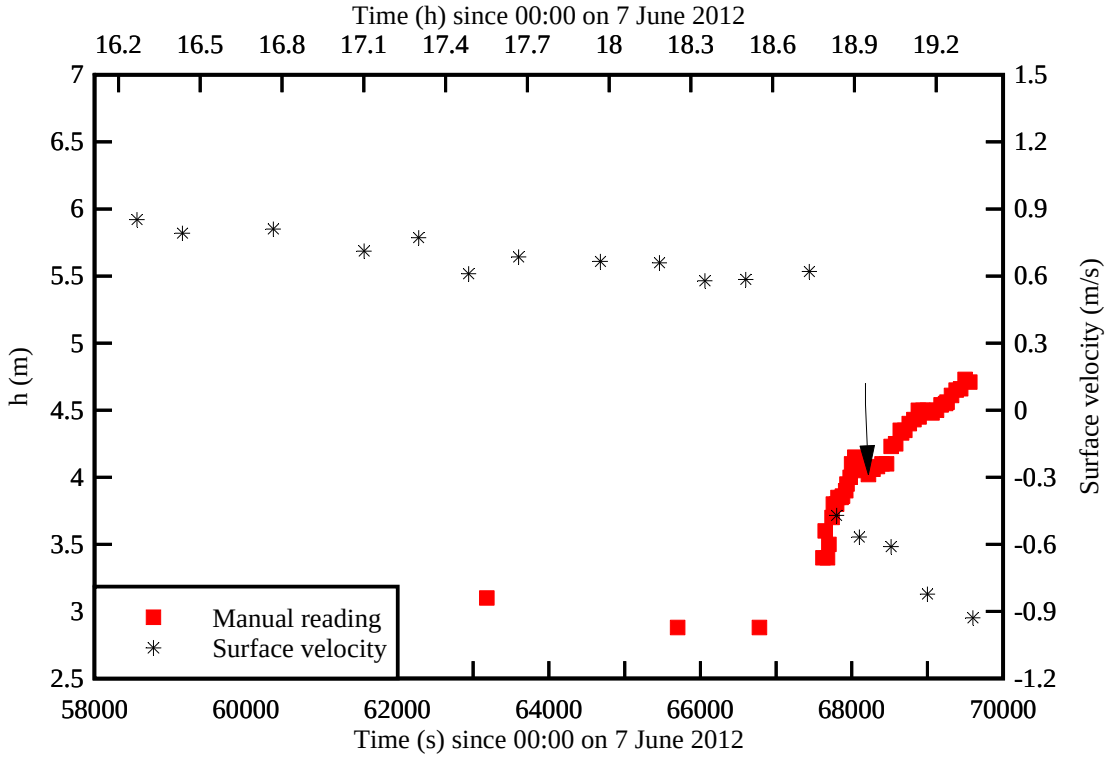

(B) On 7 June 2012 afternoon

Fig. 4-5 - Time variations of the water depth next to ADV unit and free-surface velocity in the channel centre during the field experiments - Survey staff depth and surface velocity data - The black arrow points to a transient water elevation lowering

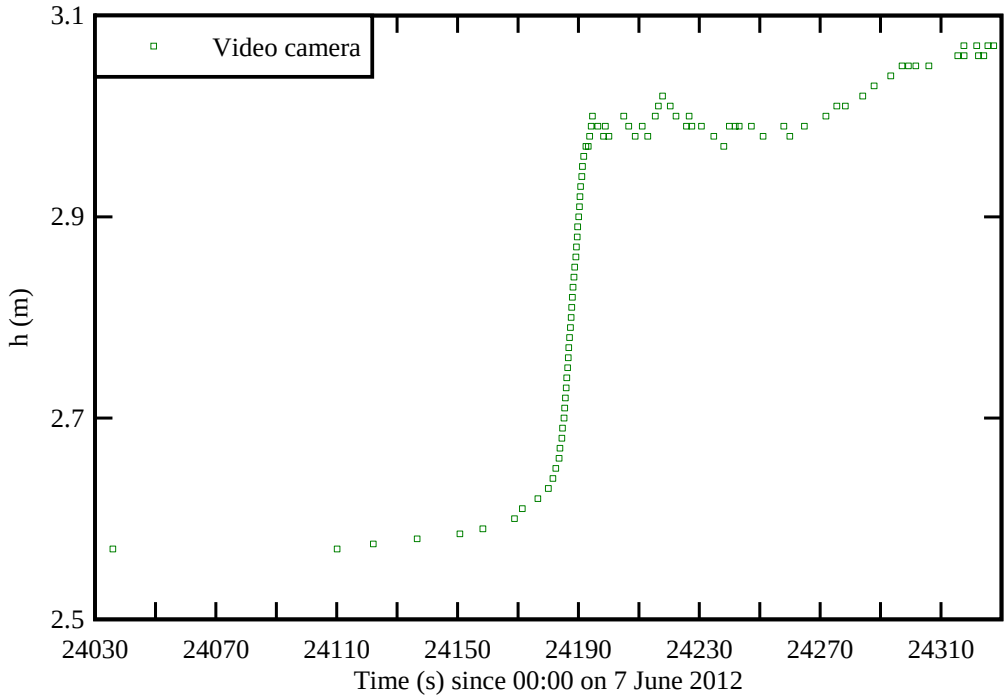

Fig. 4-6 - Time variations of the water depth next to ADV unit on 7 June 2012 morning - Survey staff depth data

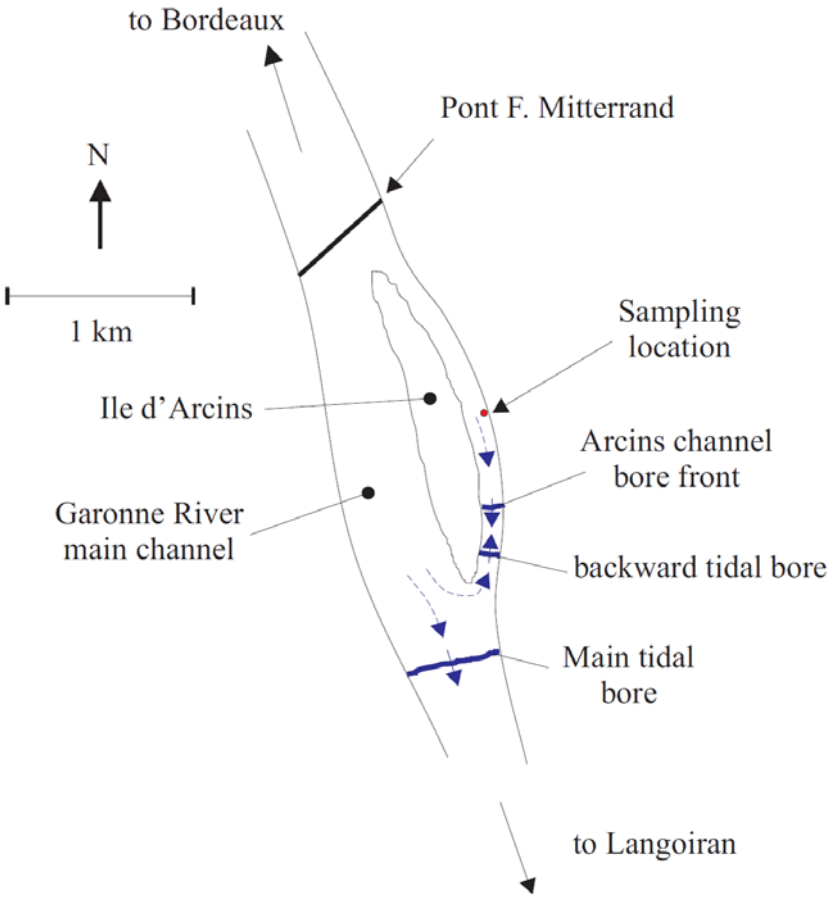

Fig. 4-7 - Sketch of the tidal bore of the Garonne River main channel entering into the southern end of the Arcins channel and propagating northwards against the flood flow in the Arcins channel

Figure 4-5 includes further the surface velocity data. These were recorded in the middle of the Arcins channel using floating debris and carefully measured with stopwatches between two locations 20 to 30 m apart. The surface velocity observations highlighted the sudden flow reversal associated with the passage of the tidal bore. However, next to the ADV, the video observations indicated that the surface flow direction reversed about 6 s after the bore front on 7 June 2012 morning. This time lag will be discussed in the next section together with the ADV data. Some related time lags were previously documented in other tidal bores (see review in CHANSON 2011) and are discussed in section 5.1.

4.3 WATER TEMPERATURE AND SALINITY

The time-variations of water temperature and salinity data are presented in Figure 4-8, in which they are compared with the water depth data. The water temperature varied from 20 to 21 Celsius in the morning of 7 June 2012 and between 18 and 21 Celsius in the afternoon. The salinity of water ranged from 0.055 to 0.08 kg/m^3, or 55 to 80 ppm ([1]). These values corresponded mostly to freshwater and the finding was consistent with the observations of those who "tasted" the waters while installing and dismantling the setup in water. The result implied that the effects of the recent (April-May 2012) flood of the Garonne River were still felt at the sampling site on 7 June 2012. Importantly the present observations did not show any evidence of saline front nor temperature front on both morning and evening tidal bores on 7 June 2012.

While some salinity and temperature fronts were sometimes reported behind tidal bores (review in CHANSON 2011, pp. 118-120), the present findings were collected at a sampling site located at about 100 km from the river mouth (Pointe de Grave). It is likely that the upstream location together with the relatively large freshwater runoff prevented the occurence of any salinity and temperature front.

[1] The sodium chloride solubility is 36 kg/m^3 (36,000 ppm) at 25 Celsius (BURGESS 1978) which is about the salinity of sea water.

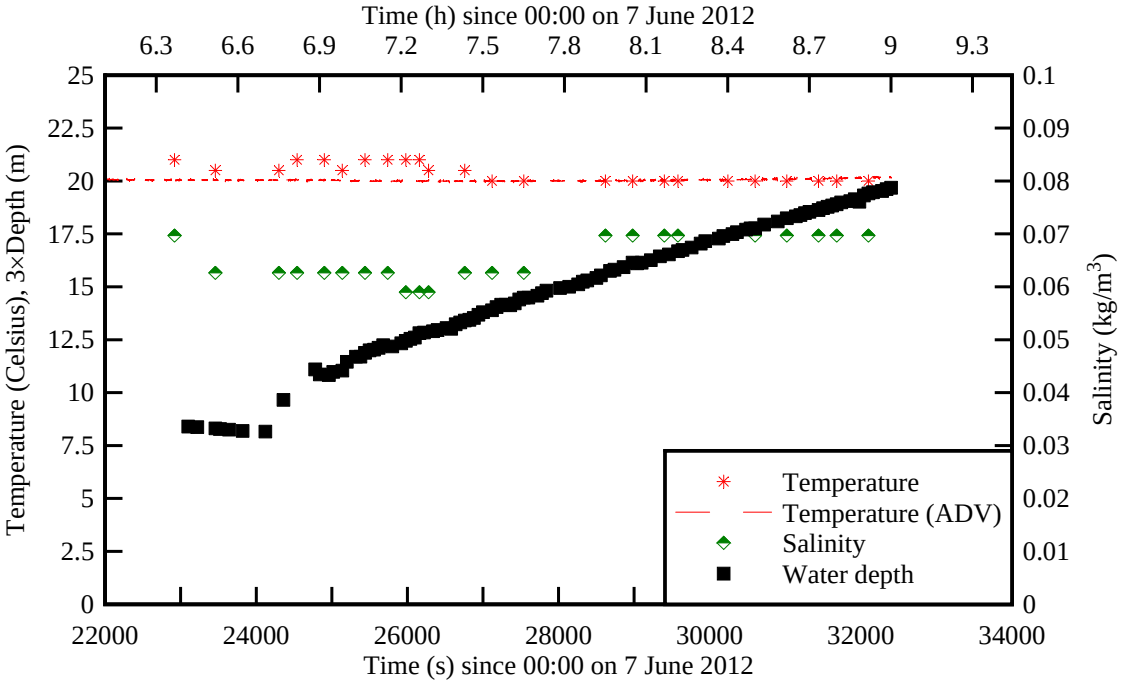

(A) On 7 June 2012 morning

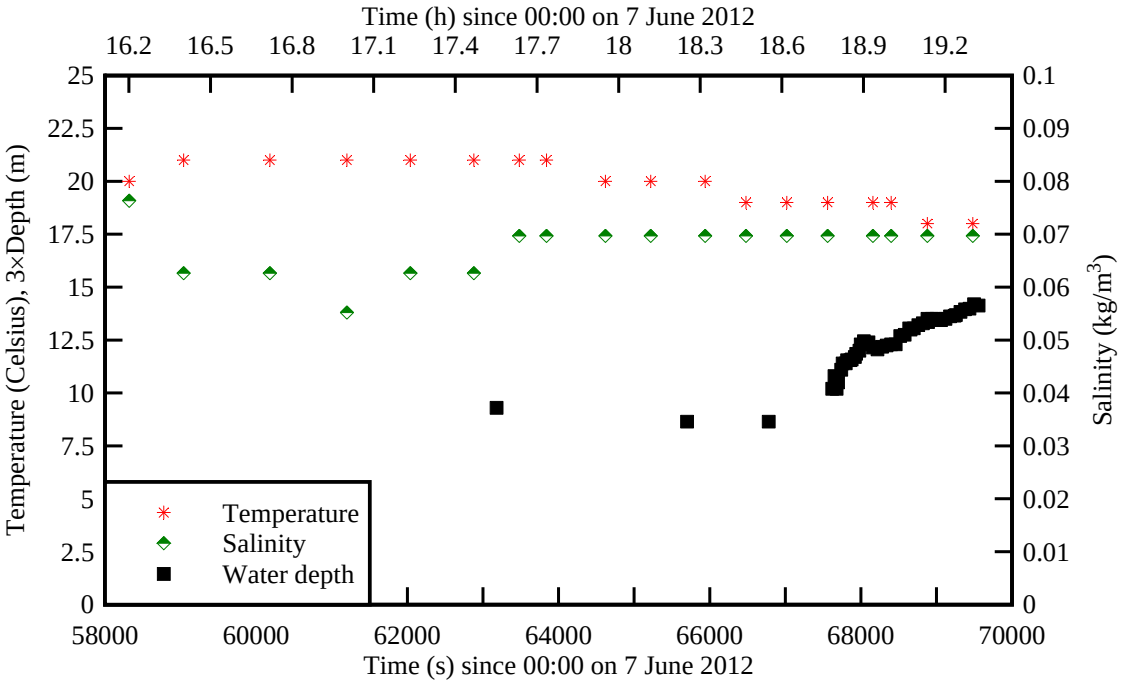

(B) On 7 June 2012 afternoon

Fig. 4-8 - Time variations of the water temperature (Celsius) and salinity (kg/m^3) on 7 June 2012 - Comparison with water depth data

5. TURBULENT VELOCITY CHARACTERISTICS

5.1 TURBULENT VELOCITY DATA

On 7 June 2012 morning, the instantaneous velocity data showed the drastic impact of the tidal bore propagation ([1]). Figure 5-1 presents the time-variations of the ADV velocity components, with the longitudinal velocity component V_x positive downstream towards Bordeaux, the transverse velocity component V_y positive towards the Arcins Island, and the vertical velocity component V_z positive upwards. The time-variations of the water depth at the survey staff are shown together with the surface velocity data (Fig. 5-1A). The surface velocity was recorded with stop watches using floating debris on the channel centreline.

The turbulent velocity data showed the marked effect of the passage of the bore front at t = 24,180 s despite the small bore height (Fig. 5-1 & 5-2). The longitudinal velocity component data showed some rapid flow deceleration associated with the passage of the bore front although with some delay. The surface velocity data exhibited a general pattern similar to the ADV data (Fig. 5-1A). However the surface velocity magnitude was consistently larger than the longitudinal velocity magnitude recorded by the ADV. The ADV sampling volume was only 7 m from the river bank water line at low tide, and the slower ADV data might reflect the effect of river bank proximity.

The tidal bore passage was observed about t ≈ 24,180 s with the sudden rise in free-surface elevation of the bore front. A time delay between the bore front passage and longitudinal flow reversal was observed and this is highlighted in Figure 5-2. That is, the data showed the reversal in longitudinal flow direction about 50 s after the bore front: i.e., t ≈ 24,330 s (Fig. 5-1A & 5-2). For comparison, the free-surface velocity next to the survey staff reversed direction about 6 s after the bore front (section 4.2.2). This unusual flow reversal differed from a number earlier observations including WOLANSKI et al. (2004), SIMPSON et al. (2004), CHANSON et al. (2011) and MOUAZE et al. (2010) in the field, and HORNUNG et al. (1995), KOCH and CHANSON (2009), CHANSON (2010) and DOCHERTY and CHANSON (2012) in laboratory. All these studies showed the flow reversal at the same time as the bore passage. However a few field studies reported some usual delay between the bore front arrival and the flow reversal (Table 5-1). These are summarised in Table 5-1 together with the present observations. As an example, M. PARTIOT conducted some classical experiments in the Seine River tidal bore (BAZIN 1865) showing some delay between bore passage and velocity reversal. (Table 5-1). In the Severn River, ROWBOTHAM (1983) observed some delayed flow reversal depending upon the relative water

[1] Herein, only the data collected on 7 June 2012 morning are discussed. The ADV unit was not deployed on 7 June 2012 afternoon following some instrument damage (section 2).

elevation and bore strength: "*the water near the bed still flowing downwards for up to ten minutes after the surface has been suddenly reversed by the passage of a fairly large bore*", "*with small bores the normal downward flow comes gently to a standstill after the bore had gone by and it may be a minute before the upward stream gathers momentum*" (ROWBOTHAM 1983, p. 32). On the other hand, KJERFVE and FERREIRA (1993) reported an early flow reversal in the Rio Mearim (Brazil): "*The current began changing directions 1 min ahead of arrival of the bore*" (Table 5-1). While the authors do not have a definite explanation for the flow reversal delay, it is conceivable that the significant freshwater flow prior to the bore arrival tended to delay the flow reversal at the ADV control volume. It is also possible that some flow stratification might have impacted the velocity field with the denser saltwater close to the channel bed, although no vertical distribution of salinity was measured (section 4).

Table 5-1 - Unusual observations of delays between tidal bore passage and flow reversal (Field observations)

Reference	River	Date	Location	Flow reversal delay	Remarks
(1)	(2)	(3)	(4)	(5)	(6)
PARTIOT in BAZIN (1865)	Seine (France)	13/09/1855	Chapel Barre-y-Va		Undular bore
			Next to surface	+130 s	
			3.3 m below surface	+90 s	
		25/09/1855	Vallon de Caudebecquet,		Undular bore
			Next to surface	+145 s	
			1.5 m below surface	+60 s	
			next to bottom	+60 s	
KJERFVE and FERREIRA (1993)	Rio Mearim (Brazil)	30/01/1991	Location D, 0.7 m above bottom	-60 s	Undular bore
Present study	Garonne	7/06/2012	Arcins,		Undular
			Surface data	+6 s	(Fr_1 = 1.02)
	(France)	morning	1.03 m below surface	+50 s	

Note: Flow reversal delay positive when the longitudinal velocity direction changed after the bore passage.

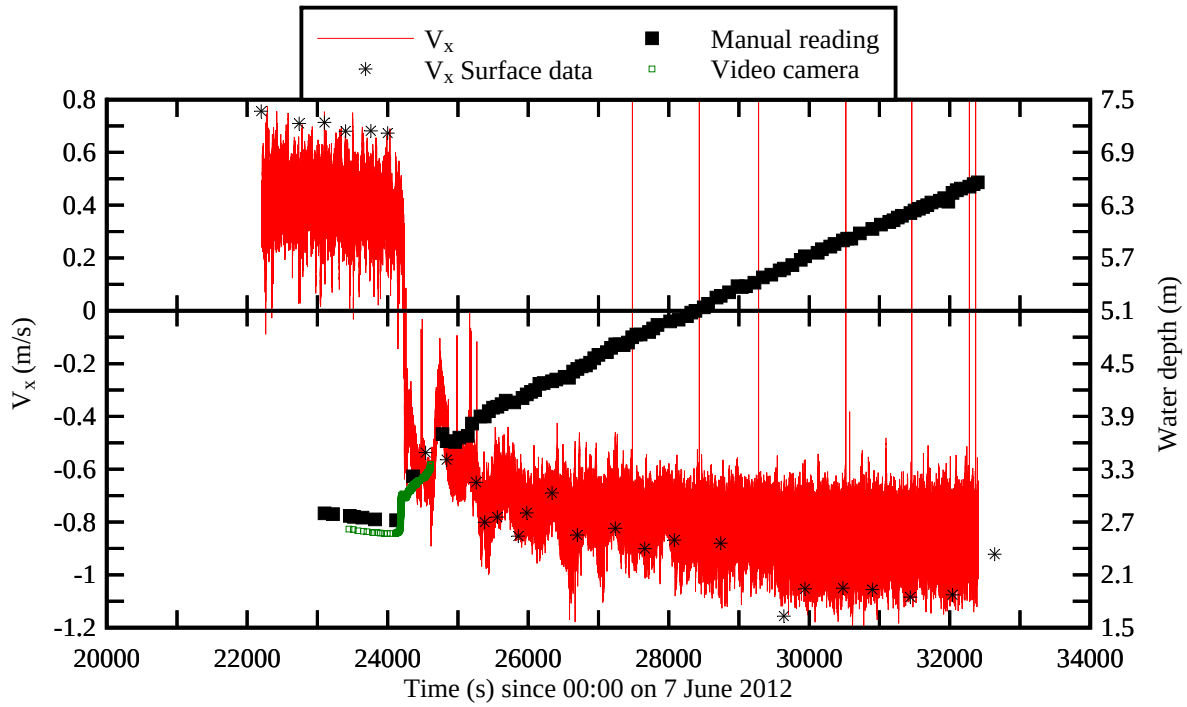

(A) Water depth, longitudinal velocity component V_x, and surface velocity on the channel centreline

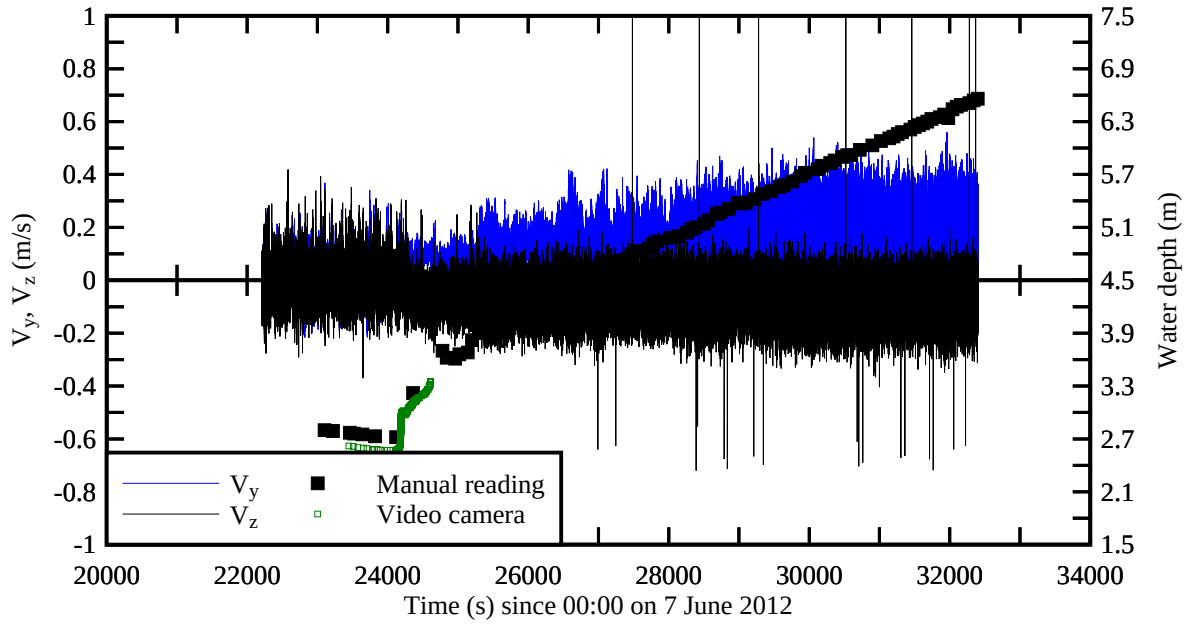

(B) Transverse velocity component V_y and vertical velocity component V_z

Fig. 5-1 - Time variations of the turbulent velocity components and water depth in the tidal bore of the Garonne River on 7 June 2012 - Post-processed ADV data, sampling rate: 50 Hz

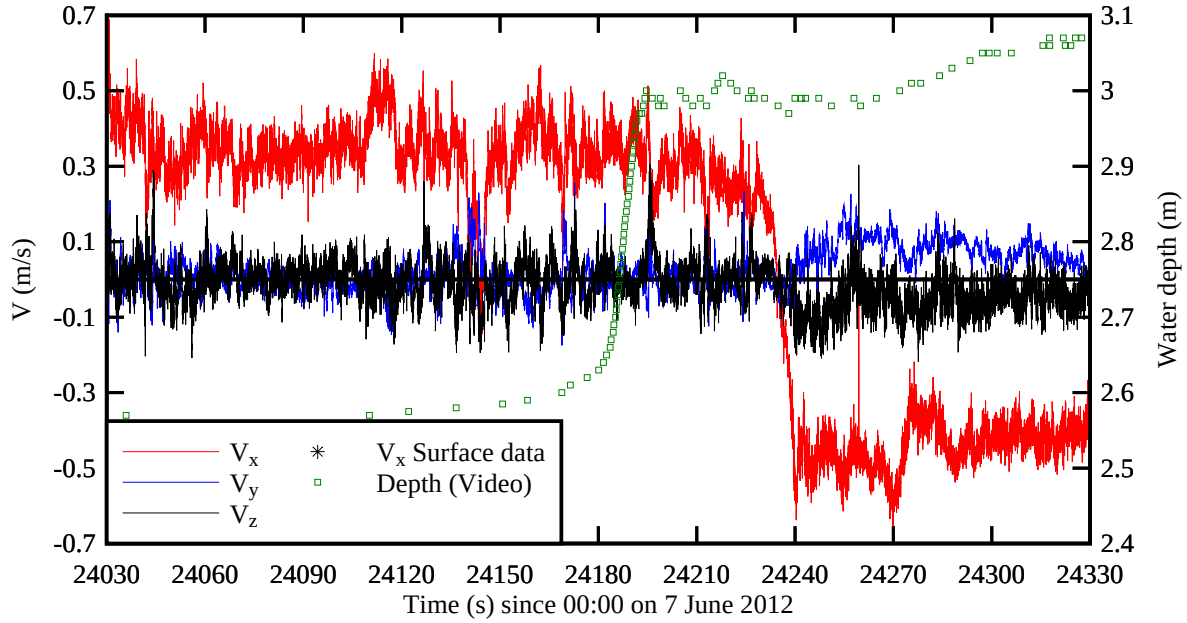

Fig. 5-2 - Details of the time variations of the turbulent velocity components and water depth in the tidal bore of the Garonne River on 7 June 2012 about the tidal bore passage - Post-processed ADV data, sampling rate: 50 Hz

The tidal bore passage was characterised by some large fluctuations of all three turbulent velocity components. The longitudinal flow component changed from +0.4 m/s oriented downriver to -0.65 m/s oriented upriver immediately after the passage of the bore, with turbulent fluctuations between 0 to -1 m/s. The large velocity fluctuations lasted for the entire sampling duration (Fig. 5-1A). The longitudinal velocity results were consistent with the free-surface velocity observations before and after the tidal bore passage, although the surface current was stronger on the channel centreline.

After the passage of the bore, the transverse velocities fluctuated between -0.25 and +0.55 m/s, and the time-averaged transverse velocity component was +0.16 m/s (Fig. 5-1B). The finding implied some net transverse circulation towards the left bank at 1.03 m beneath the free-surface. This flow pattern was possibly linked with the irregular channel cross-section and the existence of some secondary flow motion.

The vertical velocity data highlighted a marked effect of the tidal bore. After the bore passage, the vertical velocity fluctuated between -0.1 and +1.3 m/s, with a time-averaged value of about -0.08 m/s (Fig. 5-1B).

Note that the ADV sampling volume depth was about 1.03 m for the entire study duration. That is, the velocity data characterised the turbulence in the upper water column. The ADV unit was fixed to a pontoon, whose vertical motion of the pontoon cannot be ignored.

Discussion

The arrival of the bore was characterised with a rapid rise of the water elevation associated with a delayed flow deceleration. The flow reversal process lasted about 5-7 s, compared to about 10 s for the bore front passage. The flow deceleration was followed with large and rapid fluctuations of all three velocity components. These large and rapid fluctuations lasted several minutes after the bore passage (Fig. 5-1 & 5-2). The longitudinal velocity data presented some long-period fluctuations with periods of about 40 s (Fig. 5-1A) starting after the bore passage and flow reversal. These might be caused by some form of seiche which was possibly linked with some transverse sloshing in the Arcins channel.

The ADV sampling volume was located 1.03 m beneath the free-surface. That is, the data are not true Eulerian data.

5.2 TURBULENT SHEAR STRESSES

A turbulent Reynolds stress is proportional to the product of two velocity fluctuations characterising a transport effect resulting from the turbulent motion induced by velocity fluctuations with its subsequent increase of momentum exchange (BRADSHAW 1971, PIQUET 1999). The turbulent velocity fluctuation is the deviation of the instantaneous velocity from an average velocity component $\overline{V}$. In an unsteady flow, $\overline{V}$ may be the low-pass filtered velocity component, also called the variable interval time average VITA (PIQUET 1999, CHANSON and DOCHERTY 2012). A VITA method was applied to the present field data set using a cut-off frequency derived upon a sensitivity analysis conducted between an upper limit of filtered signal (herein 25 Hz, the Nyquist frequency) and a lower limit corresponding to a period of about 4-6 s of the bore undulations on 7 June 2012 morning ([2]). The results yielded an optimum threshold: F_{cutoff} = 0.5 Hz. The filtering was applied to all velocity components, and the turbulent Reynolds stresses were calculated from the high-pass filtered signals. For completeness, KOCH and CHANSON (2008) and CHANSON and DOCHERTY (2012) selected similarly a cutoff period $1/F_{cutoff}$ that was close to half the undulation period, as in the present study.

Some basic results in terms of normal and tangential Reynolds stress components are presented in Figure 5-3 and Table 5-2, and the full data set is presented in Appendix G. Figure 5-3 shows the time-variations of the Reynolds stresses before and after the tidal bore. Table 5-2 gives the time-average and standard deviation of each Reynolds stress component immediately prior to the tidal bore (i.e. 23,130 < t < 24,130 s) and following the flow reversal (i.e. 24,250< t < 25,250 s).

[2] The period of the undulations of the tidal bore on 7 June 212 afternoon was about 2 s.

Table 5-2 - Time-averages and standard deviations of Reynolds stress components before and after the tidal bore of the Garonne River on 7 June 2012 morning

Description	Reynolds stress					
	$\rho \times v_x^2$ Pa	$\rho \times v_y^2$ Pa	$\rho \times v_z^2$ Pa	$\rho \times v_x \times v_z$ Pa	$\rho \times v_x \times v_y$ Pa	$\rho \times v_y \times v_z$ Pa
Time-averaged data						
Before bore	14.66	0.206	0.261	0.074	-0.186	-0.013
After bore	5.66	0.435	0.489	1.959	1.779	0.324
Standard deviation						
Before bore	28.23	0.712	0.541	3.417	4.30	0.495
After bore	9.535	0.447	0.494	2.153	1.92	0.334

Notes: Before bore: 23,130 < t < 24,130 s; After bore: 24,250< t < 25,250 s.

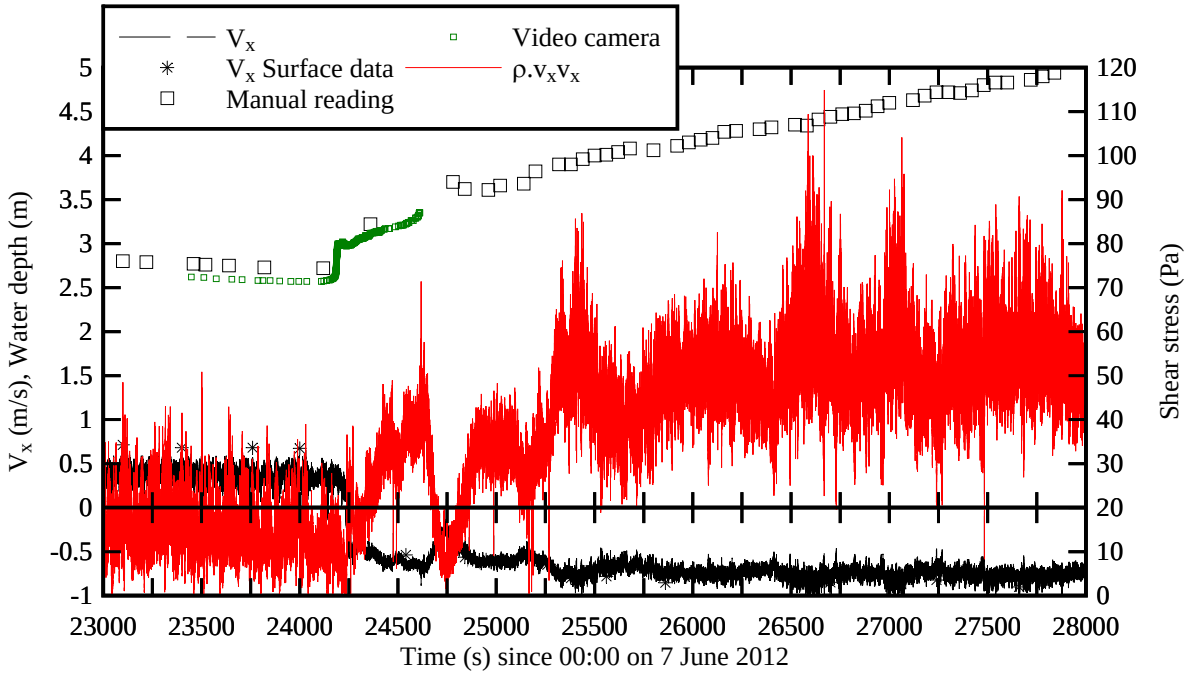

(A) $\rho \times v_x^2$, water depth and longitudinal velocity component V_x

Fig. 5-3 - Time-variations of Reynolds stresses, water depth and longitudinal velocity component during the tidal bore passage on 7 June 2012 morning - Post-processed ADV data, sampling rate: 50 Hz

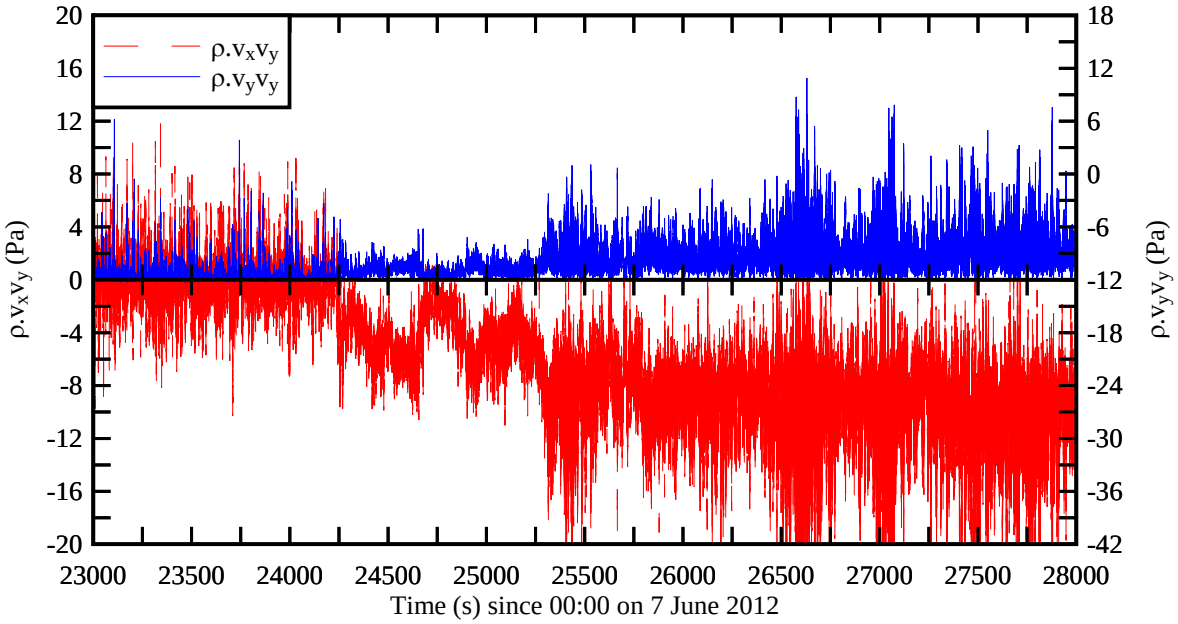

(B) $\rho \times v_y^2$ and $\rho \times v_x \times v_y$

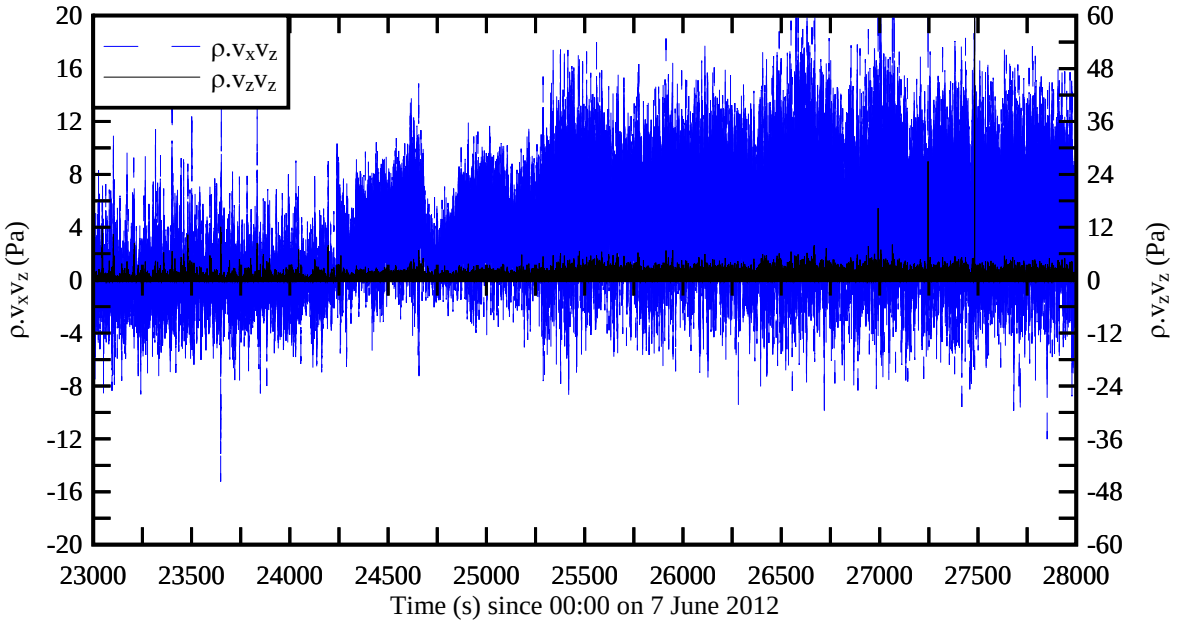

(C) $\rho \times v_x^2$ and $\rho \times v_x \times v_z$

Fig. 5-3 - Time-variations of Reynolds stresses, water depth and longitudinal velocity component during the tidal bore passage on 7 June 2012 morning - Post-processed ADV data, sampling rate: 50 Hz

The present data showed large and rapid turbulent Reynolds stress fluctuations during the tidal bore and flood flow (Figure 5-3). During the tidal bore and flood flow, the amplitudes of instantaneous Reynolds stresses were significant, with normal stress magnitudes up to 120 Pa and tangential stress magnitudes up to 30 Pa. Some large fluctuations in normal and tangential stresses were also

observed (Fig. 5-3). While these instantaneous levels were less than those observed by CHANSON et al. (2011) in the Garonne River in 2010, the findings were comparable to the results of MOUAZE et al. (2010) in the Sélune River tidal bore. Such values were significantly larger than previous laboratory data (KOCH and CHANSON 2009, CHANSON 2010, CHANSON and DOCHERTY 2012). The Reynolds stress levels were basically larger than those during the ebb tide, with normal stresses between 2 and 3.5 times larger on average than before the bore front (Table 5-2). Similarly the tangential stresses were significantly larger on average after the bore, while the fluctuations in tangential stresses were on average 10% larger than those at the end of ebb tide.

Figure 5-4 details the Reynolds shear stress data for a 1,000 s period encompassing the bore front passage ($t \approx 24{,}180$ s), the flow reversal ($t \approx 24{,}330$ s) and the short drop in water elevation ($t \approx 24{,}780$ s) about 10 minutes after the bore front (section 4.2.2). The results highlighted that the flow reversal was characterised by a very significant increase in all the shear stress components (Fig. 5-4). That is, the magnitude of shear stresses during the flow reversal was about 2 to 10 times larger than that during the end of ebb tide. The sudden increase in shear stress was caused by the flow reversal rather than the bore front passage.

On the other hand, the lowering in water elevation about 10 minutes after the bore front tended to be associated with a significant and unusual drop in shear stress magnitude: that is, about $t \approx 24{,}780$ s in Figure 5-4. The finding was observed for all Reynolds stress tensor components.

Discussion

The calculations of the Reynolds stresses yielded some unusually high level of normal stress $\rho \times v_x^2$ (Fig. 5-3). All calculations were double-checked and it is the authors' opinion that the issue might be linked with some internal problem of the ADV unit (See also Appendix C). Despite this issue, the present field measurements demonstrated the intense turbulent mixing during the tidal bore. Herein large and rapid fluctuations of the Reynolds stress component were observed. For a non-cohesive sediment material, the Shields diagram gives a critical shear stress for sediment bed load motion about: $(\tau_o)_c = 0.1$ Pa for 0.1 mm size quartz particles (GRAF 1971, JULIEN 1995). In the present study, the instantaneous shear stress magnitudes ranged up to more than 120 Pa. The Reynolds stress levels were up to three orders of magnitude larger than the critical threshold for sediment motion, although the comparison has some limitations. For example, the Garonne River bed material was cohesive and had a thixotropic behaviour (section 3).

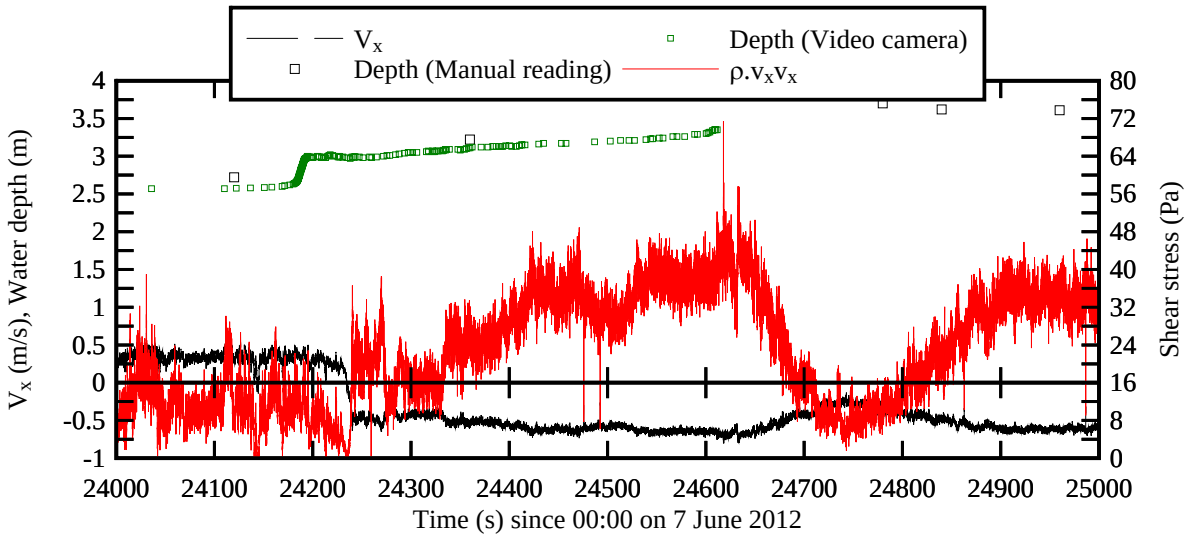

(A) $\rho \times v_x^2$, water depth and longitudinal velocity component V_x

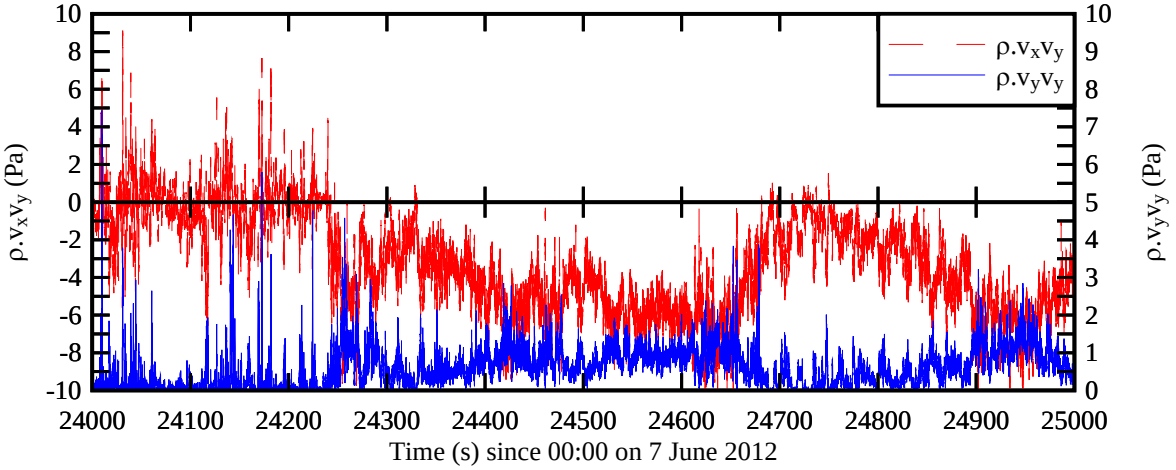

(B) $\rho \times v_y^2$ and $\rho \times v_x \times v_y$

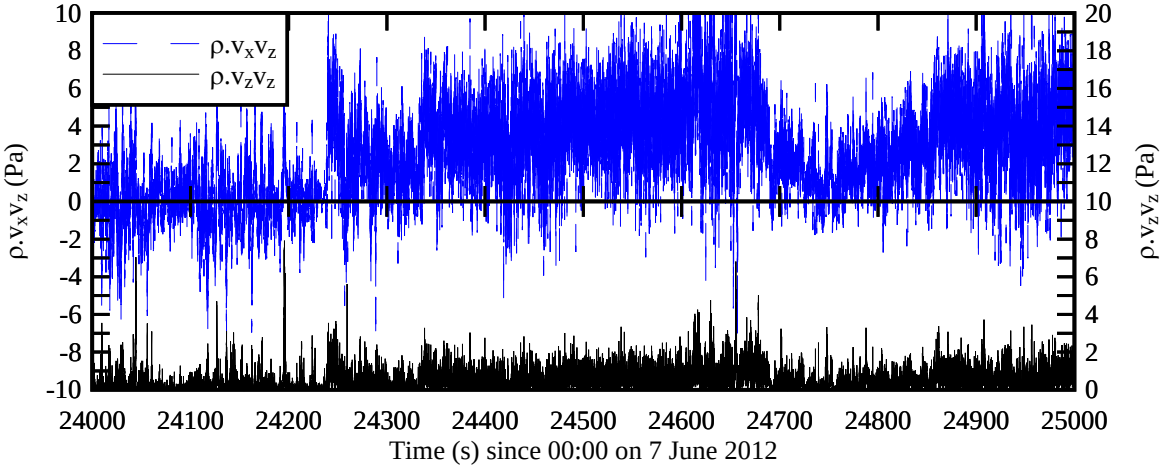

(C) $\rho \times v_x^2$ and $\rho \times v_x \times v_z$

Fig. 5-4 - Details of the Reynolds stress time-variations of Reynolds stresses during the passage of the bore front and flow reversal on 7 June 2012 morning - Post-processed ADV data, sampling rate:

50 Hz

During the tidal bore passage and ensuing flood flow, some large scale vortices were observed and these played an important role in terms of sediment material pickup and upward advection (CHANSON 2004,2011). The sediment motion induced by large eddies occurs by convection since the turbulent mixing length is much larger than the sediment distribution length scale. The validity of the Shields diagram and of the associated critical shear stress estimate is quite debatable.

A comparison between field and laboratory results for comparable Froude number may be pertinent. For an undistorted Froude similitude, the shear stress scaling ratio equals the geometric scaling ratio (LIGGETT 1994, CHANSON 2004, DOCHERTY and CHANSON 2012). The geometric scaling ratio between the present field study and the undular bore experiments of KOCH and CHANSON (2008) and CHANSON (2010) was 14:1 to 25:1. In the Garonne River bore, the shear stress magnitudes were typically 20 to 100 times larger than the physical model data, highlighting the limitations of the Froude similitude.

5.3 SUSPENDED SEDIMENT PROCESSES

The time-variations of the acoustic backscatter amplitude, and the corresponding suspended sediment concentration (SSC) deduced from Equation (3-3), are presented in Figure 5-5 for the field study on 7 June 2012 morning. The water depth data are reported also in Figure 5-5.

The complete data set showed some nearly constant SSC (~ 34 kg/m^3 on average) during the end of the ebb tide prior to the tidal bore arrival (Fig. 5-5). The passage of the tidal bore and ensuing flow reversal were associated with large fluctuations of the backscatter amplitude and SSC about 100 s after the bore passage (Fig. 5-6). The details are shown in Figure 5-6 for a 300 s period about the bore front passage. A similar unusual event was observed about 100 s after the tidal bore front during a previous study on 10 and 11 September 2010 in the Garonne River (CHANSON et al. 2011). For both studies (CHANSON et al. 2011, Present study), the event data indicated a significant decrease in SSC after the bore front passage (e.g. t = 24,300 s in Fig. 5-6), followed by a major event with large and rapid fluctuations in SSC: e.g., between t = 24,250 and 24,350 s in Figure 5-6.

During the flood flow, the SSC seemed to decrease down to 26 kg/m^3 on average about 22 minutes (1350 s) after the bore passage. Afterwards the average SSC increased up to a level about 32 kg/m^3, comparable to those observed at the end of ebb tide.

Visually, the authors observed some turbulent patches of muddy waters at the free-surface during the flood flow after the tidal bore. The free-surface waters appeared murkier than those at the end of ebb tide before the tidal bore.

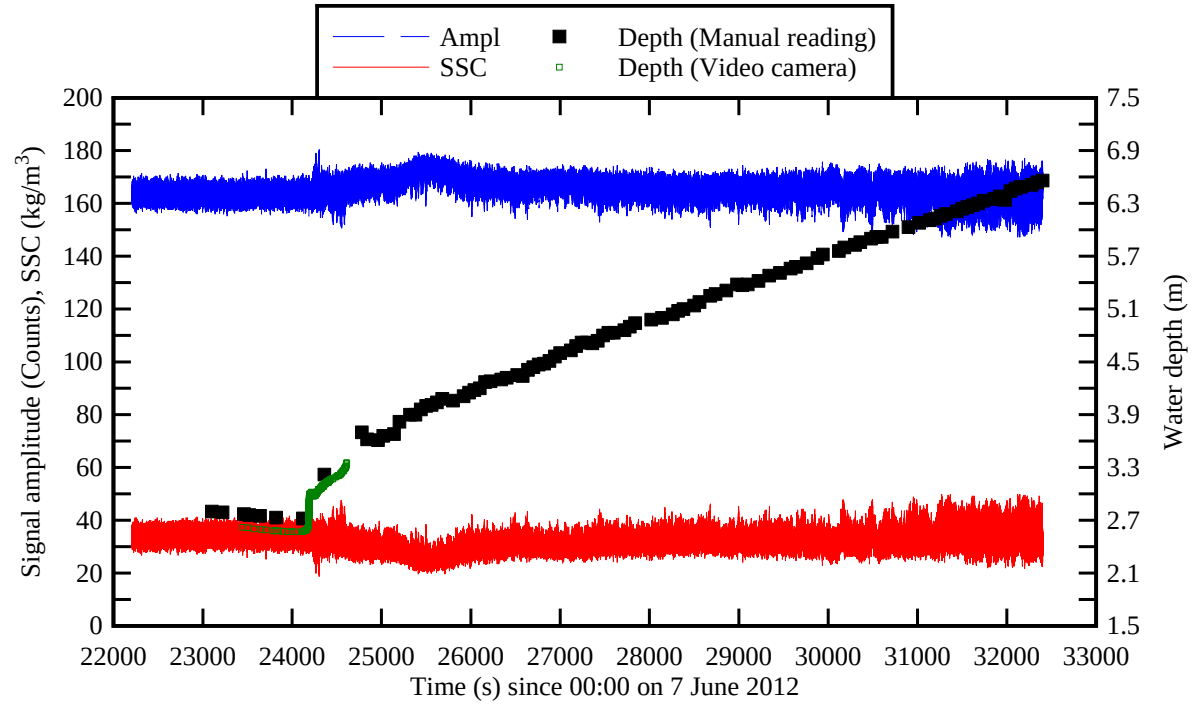

Fig. 5-5 - Time variations of the acoustic backscatter amplitude and suspended sediment concentration (SSC) on 7 June 2012 - Post-processed ADV data, sampling rate: 50 Hz

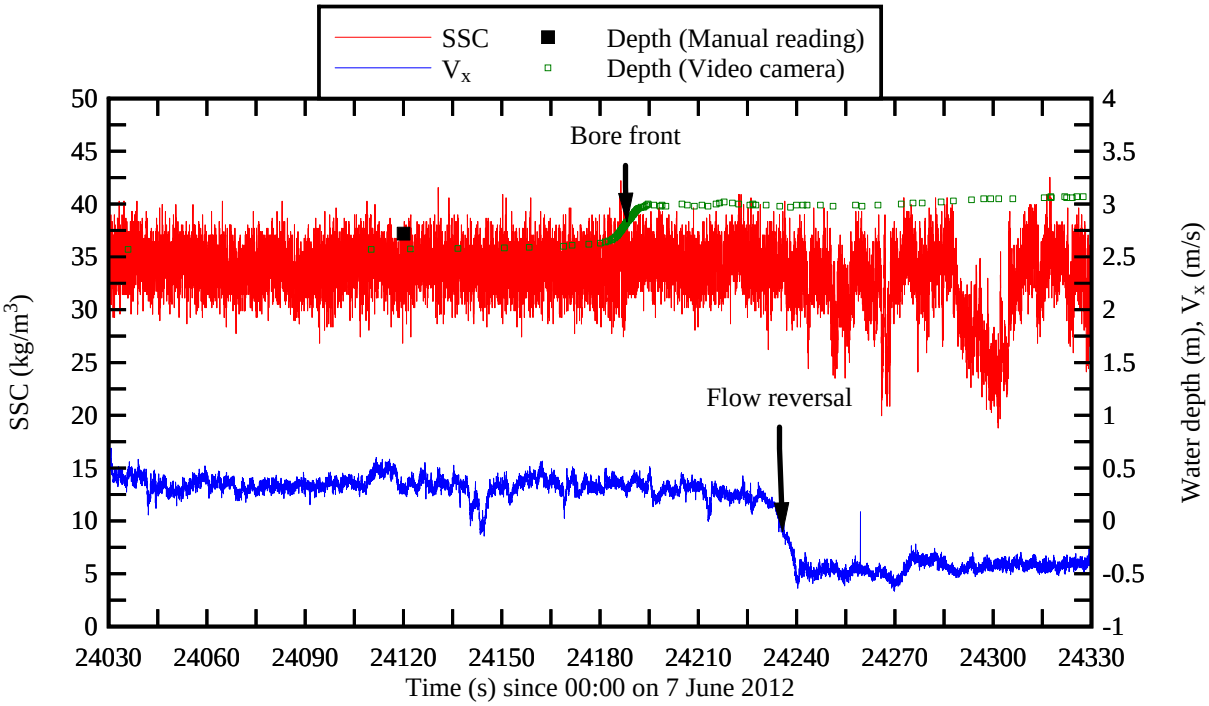

Fig. 5-6 - Details of the time-variations of suspended sediment concentration (SSC), longitudinal velocity V_x and water depth during the tidal bore passage on 7 June 2012 - Post-processed ADV data, sampling rate: 50 Hz

Lastly and importantly, the present data set were recorded 1.03 m beneath the free-surface. The data were not true Eulerian data and they could not be representative to the entire water column or channel cross-section.

5.4 SUSPENDED SEDIMENT FLUX

The velocity and SSC data were used to calculate the instantaneous suspended sediment flux per unit area q_s defined as:

$$q_s = SSC \times V_x \quad (5\text{-}1)$$

where q_s and V_x are positive in the downstream direction. In this equation, the SSC is in kg/m^3, the longitudinal velocity component V_x is in m/s and the sediment flux per unit area q_s is in kg/m^2/s. Herein q_s represents a sediment flux per unit area. The suspended sediment concentration (SSC) was calculated using Equation (3-3) applied to the post-processed backscatter amplitude signal. The results are presented in Figure 5-7 in terms of the instantaneous sediment flux q_S.

The sediment flux data showed typically a downstream positive suspended sediment flux during the end of the ebb tide prior to the tidal bore (Fig. 5-7). On average, the suspended sediment flux per unit area was 14 kg/m^2/s prior to the bore. The arrival of the tidal bore was characterised by a rapid flow reversal and the suspended sediment flux was negative during the flood tide after the flow reversal. The instantaneous sediment flux data q_s showed some large and rapid time-fluctuations that derived from a combination of velocity and suspended sediment concentration fluctuations. The high-frequency fluctuations in suspended sediment flux were likely linked with some sediment flux bursts caused by some turbulent bursting phenomena next to the boundaries. Some low-frequency fluctuations in sediment flux were also observed after the bore passage with a period of about 10 minutes (Fig. 5-7).

With the present data set, the sediment flux data were integrated with respect of time to yield the net sediment mass transfer per unit area during a period T:

$$\int_T SSC \times V_x \times dt \quad (5\text{-}2)$$

The results are presented in Figure 5-8 showing the net mass transfer per unit area since the start of the ADV sampling. Prior the tidal bore (22,125 < t < 24,340 s), the net sediment mass transfer per unit area was positive (Fig. 5-8) and Equation (5-2) yielded +28,040 kg/m^2 during the 37 minutes of data prior the tidal bore. Since the flow reversal following the bore passage, the net sediment mass transfer per unit area was negative and equalled -201,650 kg/m^2 for 24,340 < t < 32,400 s (i.e. 136 minutes). That is, the net sediment flux was about two times larger in magnitude after the bore than the sediment flux prior to the tidal bore.

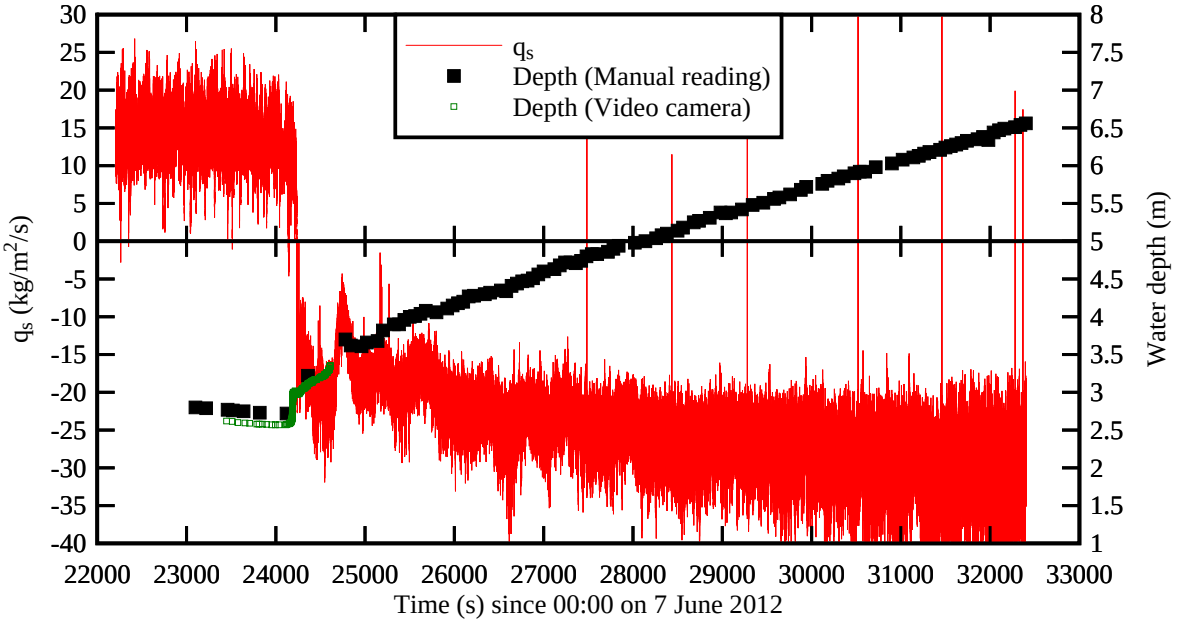

Fig. 5-7 - Time variations of the suspended sediment flux per unit area (q_s = SSC×V_x) and water depth on 7 June 2012 - Post-processed ADV data, sampling rate: 50 Hz

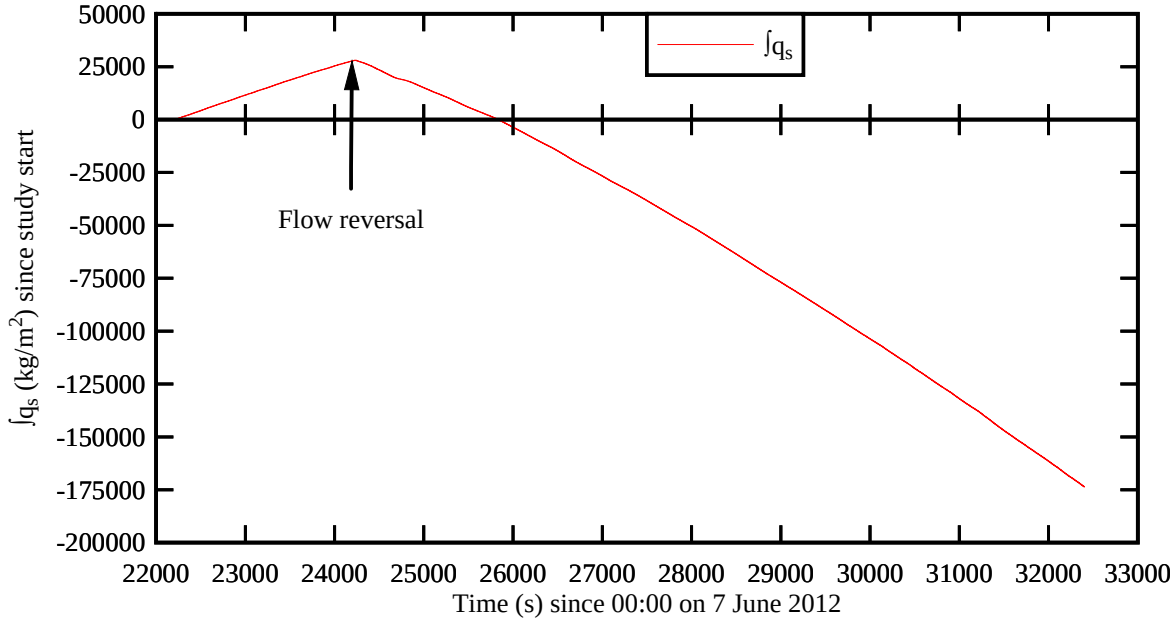

Fig. 5-8 - Net sediment mass transfer per unit area (q_s = SSC×V_x) since the start of the study on 7 June 2012

The present findings may be compared with the results of CHANSON et al. (2011) in the Arcins channel on 11 September 2010. That study was conducted at the end of a dry summer, and the net suspended sediment flux per unit area was 8 times less prior to the bore than that observed in 2012.

The difference was likely linked with the relatively stronger freshwater flow in June 2012. After the bore passage, the magnitude of suspended sediment flux per unit area was twice as large in 2010 as that in 2012. That is, the tidal bore re-mobilised a larger suspended sediment flux in September 2010. The difference may be the combined result of the slightly less vigorous flood flow in June 2012 together a lesser amount of available sediment materials following some bed scour during the April-May 2012 floods of the Garonne River.

A number of studies highlighted that the tidal bore passage was linked with some intense sediment mixing and upstream advection of suspended matters (CHEN et al. 1990, TESSIER and TERWINDT 1994, GREB and ARCHER 2007, CHANSON et al. 2011). The present data set supported the same trend (Fig. 5-7 and 5-8).

A basic feature of the present data set was the rapid fluctuations in suspended sediment flux during the tidal bore passage and flood flow. This feature was not documented, but by CHANSON et al. (2011). A key difference between the ADV data sets (CHANSON et al. 2011, Present study) from earlier field works was the continuous record at relatively high frequency (50 Hz herein) during a relatively long period. It is however acknowledged that the investigation was a point measurement about 1.03 m beneath the free-surface and any extrapolation should not be conducted because that the sampling volume was unlikely representative of the entire Arcins channel cross-section.

5.5 DISCUSSION

Some basic results in terms of the longitudinal velocity, suspended sediment concentration and suspended sediment flux before and after the tidal bore are presented in Table 5-3. Table 5-3 gives the first four statistical moments of each parameter immediately prior to the tidal bore (i.e. 23,130 < t < 24,130 s) and following the flow reversal (i.e. 24,250< t < 25,250 s). Table 5-3 includes further the integral time scale of the longitudinal velocity, SSC and sediment flux, denoted T_{Vx}, T_{SSC} and T_{qs} respectively, and defined as:

$$T_{Vx} = \int_0^{\tau(R_{XX}=0)} R_{xx}(V_x(t), V_x(t+\tau)) \times d\tau \quad (5\text{-}3)$$

$$T_{SSC} = \int_0^{\tau(R_{XX}=0)} R_{xx}(SSC(t), SSC(t+\tau)) \times d\tau \quad (5\text{-}4)$$

$$T_{qs} = \int_0^{\tau(R_{XX}=0)} R_{xx}(q_s(t), q_s(t+\tau)) \times d\tau \quad (5\text{-}5)$$

where τ is the time lag and R_{xx} is the normalised auto-correlation function. The integral time scale T_{Vx}, or Taylor macro scale, is a rough measure of the longest connection in the turbulent behaviour of the longitudinal velocity.

Table 5-3 - Statistical summary of longitudinal velocity V_x, suspended sediment concentration SSC and sediment flux q_s data before and after the tidal bore of the Garonne River on 7 June 2012 morning

Flow parameter	Statistical property	Before bore 23,130 < t < 24,130 s	After bore 24,250< t < 25,250 s	Units
V_x	Mean	0.394	-0.548	m/s
	Median	0.393	-0.578	m/s
	Std	0.080	0.106	m/s
	Skewness	0.0103	0.972	--
	Kurtosis	0.314	0.335	--
	T_{Vx}	2.4	52	s
SSC	Mean	34.3	31.3	kg/m^3
	Median	34.2	31.1	kg/m^3
	Std	1.90	2.93	kg/m^3
	Skewness	-0.0237	0.430	--
	Kurtosis	0.00590	0.497	--
	T_{SSC}	0.22	8.0	s
q_s	Mean	13.51	-17.15	$kg/m^2/s$
	Median	13.41	-17.58	$kg/m^2/s$
	Std	2.80	3.73	$kg/m^2/s$
	Skewness	0.0826	0.434	--
	Kurtosis	0.313	0.116	--
	T_{qs}	2.6	52	s

Notes: Before bore: 23,130 < t < 24,130 s; After bore: 24,250< t < 25,250 s; Skewness: Fisher skewness; Kurtosis: Fisher kurtosis; T: auto-correlation time scale.

The results showed some key differences in the statistical flow properties between before and after the bore (Table 5-3). The flow field after the bore passage was more turbulent and the integral time scales were on average 20 times larger after the bore passage. The larger time scales may reflect the production of large eddies by the bore front and their upstream advection behind the bore. Further a comparison between turbulent and SSC integral time scales showed some key differences. The ratio of sediment to turbulent integral time scales was basically $T_{SSC}/T_{Vx} \approx 0.1$ both before and after the bore. The finding demonstrated conclusively some quantitative differences in timescales between the turbulent velocities and suspended sediment concentrations in a tidal bore flow, as discussed previously by CHANSON et al. (2007), TOORMAN (2008) and CHANSON and TREVETHAN (2011) in open channel and estuarine flows.

Altogether the physical data highlighted some significant sediment load with large SSCs and suspended sediment fluxes per unit area during the tidal bore event. Figure 5-9 shows the

relationship between the average suspended sediment flux per unit area data as a function of the mean suspended sediment concentration after the tidal bore for the present study. The present data were compared with physical data recorded in rivers during floods and in estuaries (Table 5-3 & Fig. 5-9). Table 5-4 lists a number of seminal field observations of suspended sediment loads in major river systems, including the Amazon, Mississippi and Nile Rivers, as well as hyperconcentrated flows, together with estuarine flow data including the observations in the Garonne River tidal bore on 11 September 2010 by CHANSON et al. (2011). Figure 5-9 demonstrates that high suspended sediment fluxes per unit area and SSC data were observed in the Garonne River tidal bore. While larger values were measured in some hyperconcentrated flows, the present results showed higher suspended sediment concentrations and fluxes than in most rivers in flood. The high suspended sediment concentration data combined with the rheology data (section 3) implied that the flood flow was likely non-Newtonian.

Owing to the fine sediment material and relatively fast and turbulent motion, the sediment motion was dominated by sediment suspension. Importantly the present data were point measurements. They should not be extrapolated to the Arcins channel or even the main channel of the Garonne River.

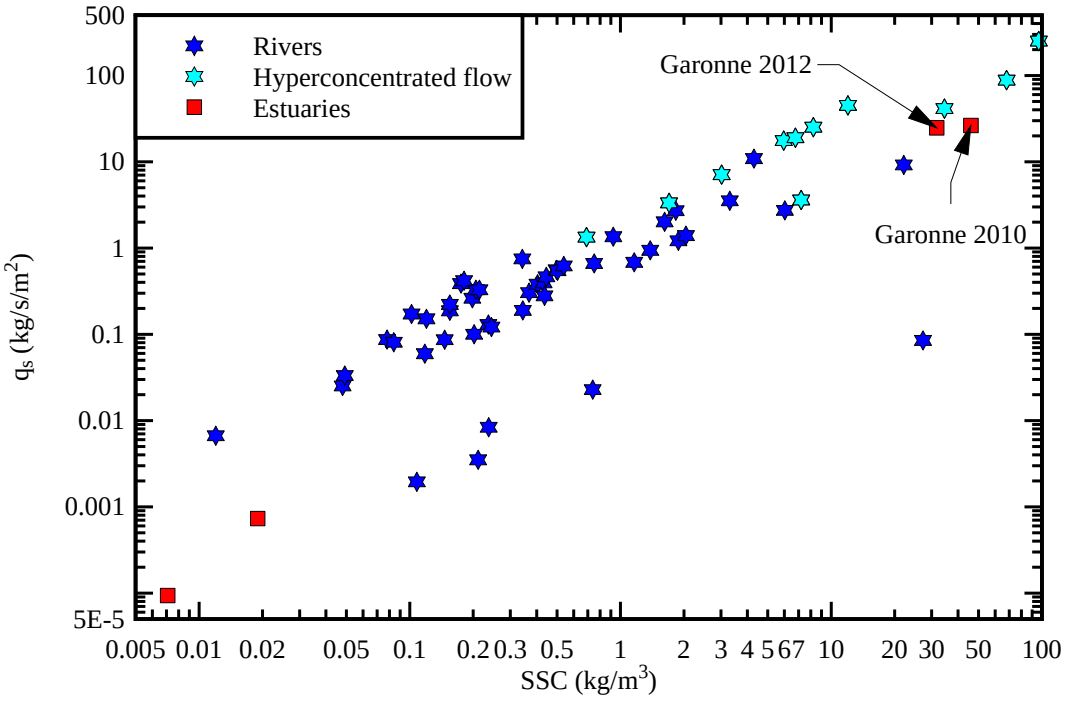

Fig. 5-9 - Suspended sediment flux q_s (kg.s^{-1}.m^{-2}) as function of the suspended sediment concentration SSC - Comparison between present data (Garonne 2012), the 2010 observations (Garonne 2010) together with observations in estuaries and rivers during flood including hyperconcentrated flows (Table 5-4)

Table 5-4 - Measurements of suspended sediment concentrations and suspended sediment flux per unit area in tidal bores, rivers during floods and in estuaries

Ref.	River	Location	Date	Q m^3/s	V m/s	SSC kg/m^3	q_s $kg..s^{-1}m^{-2}$	Remarks
(1)	(2)	(3)	(4)	(5)	(6)	(7)	(8)	(9)
Rivers								
BOUCHEZ et al. (2011)	Solimoes (Brazil)	Manacapuru	1/03/2006	109,200	--	0.237	0.008352	([1])
	Madeira (Brazil)	Foz Madeira	1/03/2006	47,200	--	0.738	0.022834	([1])
	Amazonas (Brazil)	Iracema	1/03/2006	134,500	--	0.108	0.001948	([1])
	Amazonas (Brazil)	Obidos	1/03/2006	168,900	--	0.211	0.003508	([1])
HORN et al. (1998)	Fitzroy (Australia)	Laurel Banks	12/03/1994	2,700	1.07	3.3	3.53	([1])
	Brisbane (Australia)	College Crossings	5/05/1996	1,984	--	0.925	1.35	([1])
BROWN et al. (2011)	Brisbane (Australia)	Gardens Point, Brisbane	12/1/2011	--	0.46	6.03	2.73	([3])
	Brisbane (Australia)	Gardens Point, Brisbane	13/1/2011	--	0.45	22.1	9.18	([3])
	Brisbane (Australia)	Gardens Point, Brisbane	13/1/2011	--	0.0018	27.3	0.085	([3])
VAN DEN BERG	Huanghe (China)	Li-Jin	2/09/1987	1,212	1.30	68.02	88.45	Hyperconcentrated flow ([2])
and VAN GELDER	Huanghe (China)	Li-Jin	9/09/1987	1,050	1.2	34.50	41.40	Hyperconcentrated flow ([2])
(1993)	Huanghe (China)	Li-Jin	22/09/1987	185	0.5	7.21	3.60	Hyperconcentrated flow ([2])
LI et al. (1998)	Huanghe (China)	Li-Jin	13/08/1993	2,500	2.6	96.7	250.4	Hyperconcentrated flow ([1])
VANONI (1975)	Missouri (USA)	Omaha (Nebraska)	Oct.1951	--	2.53	4.3	10.88	([1])
	Rio Puerco (USA)	Bernado (New Mexico)	19/08/1961	--	1.58	131.2	206.75	Hyperconcentrated flow ([1])
AKALI (2002)	Mississippi (USA)	Union Point (Mississippi)	27/02/1998	28,624	1.78	0.50	0.559	([1])
	Mississippi (USA)	Union Point (Mississippi)	23/03/1998	30,110	1.55	0.50	0.546	([1])
	Mississippi (USA)	Union Point (Mississippi)	10/04/1998	31,368	1.66	0.40	0.380	([1])
	Mississippi (USA)	Union Point (Mississippi)	17/04/1998	30,282	1.67	0.54	0.620	([1])
	Mississippi (USA)	Union Point (Mississippi)	8/05/1998	34,544	1.93	0.45	0.464	([1])
	Mississippi (USA)	Union Point (Mississippi)	9/06/1998	21,344	1.30	0.43	0.394	([1])
	Mississippi (USA)	Union Point (Mississippi)	3/08/1998	16,195	1.29	0.37	0.304	([1])
JORDAN (1965)	Mississippi (USA)	St Louis, Missouri	17/4/1951	14,753	2.25	0.342	0.750	([1])
	Mississippi (USA)	St Louis, Missouri	21/5/1951	10,251	1.61	0.206	0.329	([1])
	Mississippi (USA)	St Louis, Missouri	16/7/1951	19,935	2.21	0.175	0.387	([1])
	Mississippi (USA)	St Louis, Missouri	22/7/1951	21,606	2.30	0.181	0.418	([1])
	Mississippi (USA)	St Louis, Missouri	30/7/1951	13,252	1.64	0.102	0.172	([1])
	Mississippi (USA)	St Louis, Missouri	17/9/1951	10,987	1.53	0.214	0.328	([1])
	Mississippi (USA)	St Louis, Missouri	24/9/1951	8,070	1.32	0.078	0.087	([1])
	Mississippi (USA)	St Louis, Missouri	8/10/1951	5,890	1.12	0.120	0.151	([1])
	Mississippi (USA)	St Louis, Missouri	15/10/1951	5,154	1.02	0.084	0.081	([1])

	Mississippi (USA)	St Louis, Missouri	13/11/1951	6,201	1.21	0.155	0.187	([1])
	Mississippi (USA)	St Louis, Missouri	3/12/1951	5,380	1.14	0.155	0.222	([1])
PITLICK (1992)	North Fork Toutle (USA)	Hoffstadt Creek Bridge	17/02/1989	--	2.96	5.95	17.61	Hyperconcentrated flow ([1])
	North Fork Toutle (USA)	Hoffstadt Creek Bridge	10/03/1989	--	3.75	12	45.00	Hyperconcentrated flow ([1])
	North Fork Toutle (USA)	Hoffstadt Creek Bridge	21/03/1989	--	2.81	6.76	19.00	Hyperconcentrated flow ([1])
	North Fork Toutle (USA)	Hoffstadt Creek Bridge	28/03/1989	--	3.06	8.23	25.18	Hyperconcentrated flow ([1])
	North Fork Toutle (USA)	Hoffstadt Creek Bridge	11/04/1989	--	2.35	3.02	7.10	Hyperconcentrated flow ([1])
	North Fork Toutle (USA)	Hoffstadt Creek Bridge	21/04/1989	--	1.96	1.7	3.33	Hyperconcentrated flow ([1])
	North Fork Toutle (USA)	Hoffstadt Creek Bridge	27/04/1989	--	1.94	0.69	1.34	Hyperconcentrated flow ([1])
BUCKLEY (1921)	Nile	Beleida (Egypt)	1/08/1921	906	0.51	0.118	0.0596	([2])
	Nile	Beleida (Egypt)	13/08/1921	2,571	0.88	0.75	0.663	([2])
	Nile	Beleida (Egypt)	22/08/1921	4,980	1.24	1.62	2.01	([2])
	Nile	Khannaq (Egypt)	15/09/1920	7,220	1.48	1.83	2.71	([2])
	Nile	Khannaq (Egypt)	16/09/1920	6,400	1.32	0.198	0.261	([2])
	Diversion channel	Ismailia (Egypt)	1/07/1922	50.5	0.56	0.012	0.00667	([2])
	Diversion channel	Ismailia (Egypt)	22/07/1922	47.5	0.52	0.048	0.0251	([2])
	Diversion channel	Ismailia (Egypt)	1/08/1922	68.3	0.68	0.0491	0.0333	([2])
	Diversion channel	Ismailia (Egypt)	8/08/1922	66	0.64	0.436	0.279	([2])
	Diversion channel	Ismailia (Egypt)	15/08/1922	66	0.68	1.38	0.942	([2])
	Diversion channel	Ismailia (Egypt)	19/08/1922	66	0.68	2.05	1.40	([2])
	Diversion channel	Ismailia (Egypt)	9/09/1922	62.5	0.64	1.88	1.21	([2])
	Diversion channel	Ismailia (Egypt)	7/10/1922	53.3	0.59	1.16	0.683	([2])
	Diversion channel	Ismailia (Egypt)	25/11/1922	51.5	0.55	0.344	0.189	([2])
	Diversion channel	Ismailia (Egypt)	2/12/1922	42.9	0.50	0.244	0.121	([2])
	Diversion channel	Ismailia (Egypt)	9/12/1922	49.9	0.55	0.236	0.130	([2])
	Diversion channel	Ismailia (Egypt)	16/12/1922	42.9	0.50	0.202	0.100	([2])
	Diversion channel	Ismailia (Egypt)	20/12/1922	55.5	0.59	0.147	0.086	([2])
Estuaries								
TREVETHAN et al. (2007)	Eprapah (Australia)	Site 3	5-7/6/2006	--	--	0.0071	9.37E-5	([3]) ([4])
CHANSON et al. (2006)	Eprapah (Australia)	Site 2B	16-18/5/2005	--	--	0.0190	0.000732	([3]) ([4])
CHANSON et al. (2011)	Garonne (France)	Arcins	11/09/2010	--	--	46.02	26.33	Tidal bore ([3]) ([4])
Present study	Garonne (France)	Arcins	7/06/2012	--	--	31.7	24.73	Tidal bore ([3]) ([4])

Notes: ([1]) depth-averaged data; ([2]) data measured close to the bed; ([3]) point measurement data; ([4]) time-averaged flux amplitude; (--): data not available.

6. CONCLUSION

Some field observations were conducted in the tidal bore of the Garonne River on 7 June 2012 in the Arcins channel. The channel was about 1.8 km long, 70 m wide and about 1.6 to 3.4 m deep at low tide. The tidal bore propagation in the Arcins channel was observed on 7 June 2012 morning and afternoon, although the velocity measurements were conducted in the morning bore only because of some instrumentation damage. The velocity components were sampled continuously at relatively high-frequency (50 Hz) with an acoustic Doppler velocimeter (ADV), its sampling volume being about 1.03 m beneath the free-surface. The present study was conducted at the same site as a series of field measurements performed in 2012 (CHANSON et al. 2011), but a few weeks after a major flood. The water level was higher in 2012 and the river bed might have been scoured from the soft sediments during the April-May 2012 flood.

The sediment bed material was cohesive with a median particle size of about 13 μm, and the mud exhibited a non-Newtonian behaviour. The rheometry results suggested that the quantitative characterisation of the material was closely linked with the testing protocol and configuration. Some experiments under controlled conditions were performed to use the acoustic backscatter amplitude of the ADV as a surrogate estimate of the suspended sediment concentration (SSC). The laboratory data showed that the relationship between SSC and backscatter amplitude had two distinct trends: a monotonic increase in signal amplitude with small SSCs, and a decrease in backscatter amplitude with increasing SSC for larger suspended loads. The latter was linked with some signal saturation at large sediment concentrations.

On 7 June 2012, the tidal bore was a flat undular bore with a Froude number close to unity: Fr_1 = 1.02 and 1.19 in the morning and afternoon respectively. A feature of the study was some effect of recent floods (April-May 2012) of the Garonne River. At the end of ebb tide, the current was strong, the water level was relatively high and the water was predominantly some freshwater. Despite the high initial water level and strong fluvial current, the bore front exhibited a sharp discontinuity in terms of free-surface elevation: the bore front was 0.45 m and 0.52 m high on the morning and afternoon respectively. The field observations highlighted a number of unusual features on the morning of 7 June 2012. These included (a) a slight rise in water elevation starting about 70 s prior to the front, (b) a flow reversal about 50 s after the bore front, (c) some large fluctuations in suspended sediment concentration (SSC) about 100 s after the bore front and (d) a transient water elevation lowering about 10 minutes after the bore front passage. The measurements of water temperature and salinity showed nearly identical results before and after the tidal bore: there was no evidence of saline or thermal front.

The turbulent velocity data showed a marked impact of the tidal bore. The longitudinal velocity

component highlighted some rapid flow deceleration with the passage of the tidal bore, although the flow reversal took place about 50 s after the bore front passage. While unusual, such a delayed flow reversal was previously documented in other estuaries. Herein it is hypothesised that the flow reversal delay was caused by the significant freshwater flow prior to the bore passage, although the effect of any water column stratification could not be checked. The flow reversal was characterised by some large fluctuations of all velocity components. The turbulent Reynolds stress data indicated some large and rapid turbulent stress fluctuations during the tidal bore and flood flow. The turbulent stress magnitudes were larger than during the ebb tide, and some large fluctuations in normal and tangential stresses were observed. The time-variations of shear stresses highlighted a drastic increase by nearly one order of magnitude in shear stress levels during the flow reversal, as well as an unusual drop in shear stress magnitudes during the transient water elevation lowering. These features were observed with all Reynolds stress tensor components.

The data set yielded the time-variations in instantaneous suspended sediment concentrations and suspended sediment flux per unit area at the sampling site during the tidal bore event. The suspended sediment concentration (SSC) data indicated sediment concentrations between 20 and 40 kg/m^3 typically. Some large fluctuations in suspended sediment concentrations were observed about 100 s after the bore front, while some lower SSC levels were seen about 22 minutes after the tidal bore, before the SSC levels increased up to levels comparable to those before the bore. The data set yielded some substantial suspended sediment flux amplitudes consistent with the murky appearance of waters. The results indicated a downstream positive suspended sediment flux during the end of the ebb tide prior to the tidal bore. The arrival of the tidal bore and flow reversal was characterised by a rapid reversal in suspended sediment flux during the flood tide. After the passage of the bore, the net sediment mass transfer per unit area was negative (i.e. upriver) and its magnitude was twice as large as the net flux at the end of the ebb tide. Overall the sediment concentration and data highlighted some very significant suspended sediment load. The findings coupled with the rheology findings might imply that the flood flow had likely some non-Newtonian behaviour.

The present field data set presented a number of striking features rarely documented to date, including a delayed flow reversal and a transient water elevation lowering. These might be linked with the bore Froude number close to unity and the effects of a recent flood. On the other hand, the data highlighted a number of flow features previously documented in the field, including the large and rapid fluctuations in velocities and suspended sediment flux during the tidal bore. Importantly the present velocity record was a point measurement located 1.03 m beneath the free-surface, and any extrapolation to the entire channel cross-section would be inappropriate.

7. ACKNOWLEDGEMENTS

The authors thank Prof. Michele MOSSA (Politecnico di Bari, Italy) and Dr Eric JONES (Proudman Oceanographic Laboratory, UK) for their detailed review of the report and valuable comments. They acknowledge the helpful comments of Dr Mouldi BEN MEFTAH (Politecnico di Bari, Italy).

The ADV was provided kindly by Prof Laurent DAVID (University of Poitiers, France). The authors acknowledge the assistance of Patrice BENGHIATI and the permission to access and use the pontoon in the *Bras d'Arcins*. They thank all the people who participated to the field works (Appendix A), without whom the study could not have been conducted. The helpful discussion with Dr Sébastien JARNY (University of Poitiers, France) is acknowledged. The authors acknowledge the financial assistance of the Agence Nationale de la Recherche (Projet Mascaret), and they thank the project leader Dr Pierre LUBIN (University of Bordeaux, France) for his generous support.

APPENDIX A - LIST OF FIELD WORK PARTICIPANTS (FIELD STUDY G12, 7 JUNE 2012)

THURSDAY 7 JUNE 2012

David REUNGOAT

Hubert CHANSON

Bastien CAPLAIN

Pierre LUBIN

Bruno SIMON

Alexandre IDARO

Benjamin REAU

Louis HERNANDO

Cédric LE BOT

Ludovic OSMAR

Valérie THOUARD

Stéphane VINCENT

(A, Left) David REUNGOAT at the downstream end of the pontoon

(B, Right) Pierre LUBIN in wet suit and Hubert CHANSON

(C) From left to right, Bastien CAPLAIN, Valérie THOUARD et Stéphane VINCENT

(D) From left to right: David REUNGOAT, Pierre LUBIN, Alexandre IDARO, Bastien CAPLAIN

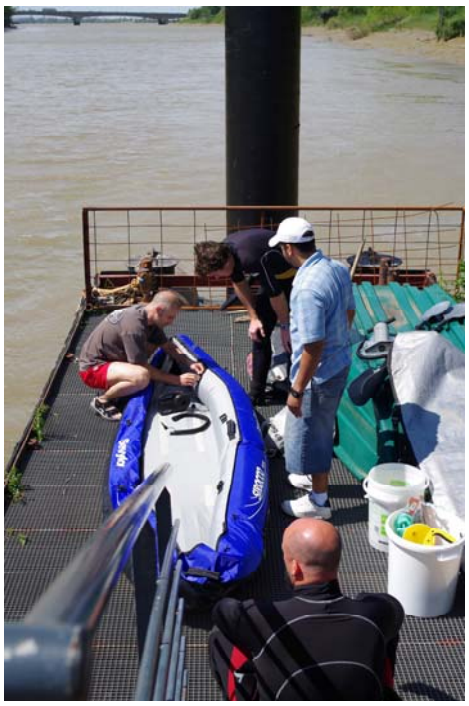

(E) Top, from left to right: Stéphane VINCENT, Bruno SIMON, Ludovic OSMAR; Foreground: Pierre LUBIN

(F) Pierre LUBIN and Bruno SIMON during the survey of the channel

(G) Benjamin REAU and Alexandre IDARO

(H) From left to right: Bastien CAPLAIN, Cédric LE BOT, Bruno SIMON, Louis HERNANDO, David REUNGOAT, Pierre LUBIN

Fig. A-1 - Photographs of the participants

APPENDIX B - PHOTOGRAPHS OF THE FIELD STUDY G12 (7 JUNE 2012)

(A) Looking downstream on 7 June 2012 at 17:40

(B) Looking at the pontoon on 7 June 2012 at 07:03

(C) Looking at the pontoon on 7 June 2012 at 19:19

(D) Looking upstream on 7 June 2012 at 17:40

Fig. B-1 - Sampling site on the Garonne River between *Île d'Arcins* (Arcins Island) and Latresne

(A) Undular tidal bore formation in the Arcins channel at 17:32:42 - Note the Airbus barge in the background travelling upstream following the tidal bore

(B) Tidal bore at 17:33:30

(C) Tidal bore at 17:33:54

(D) Tidal bore approaching the pontoon at 17:34:05

Fig. B-2 - Tidal bore in Arcins channel on 5 June 2012 afternoon during some preparation works

(A) Upstream propagation of the bore at 06:51:29 - The red arrow points to the bore front

(B) Tidal bore approaching the pontoon at 06:51:41 - The red arrow points to the bore front

(C) Tidal bore approaching the pontoon at 06:51:46 - The red arrow points to the bore front

(D) Tidal bore past the pontoon at 06:51:55 - The red arrow points to the bore front in the background

Fig. B-3 - Tidal bore on 7 June 2012 morning

Fig. B-4 - Arcins channel after the tidal bore on 7 June 2012 morning, looking downstream - From left to right, top to bottom: (a) at 07:03:18 (b) at 07:03:51 (c) at 07:20:01 (d) at 07:43:28 (e) 08:24:26 (f) at 09:04:30

(A) Advancing bore viewed from the pontoon at 18:54:05 - The arrow points to the bore front

(B) Advancing bore along Arcins Island at 18:54:18 - The arrow points to the bore front

(C) Tidal bore approaching the sampling point at 18:54:40

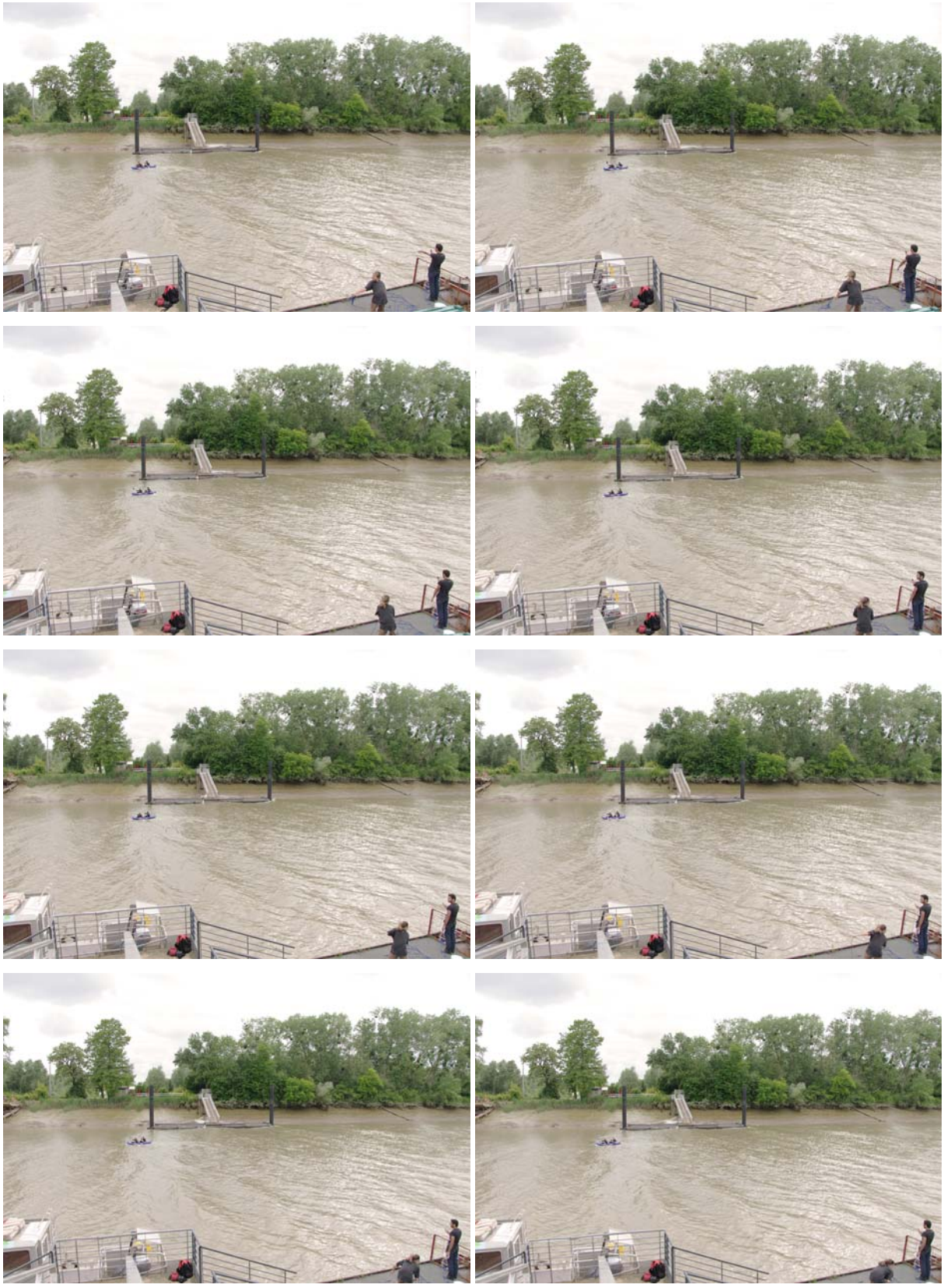

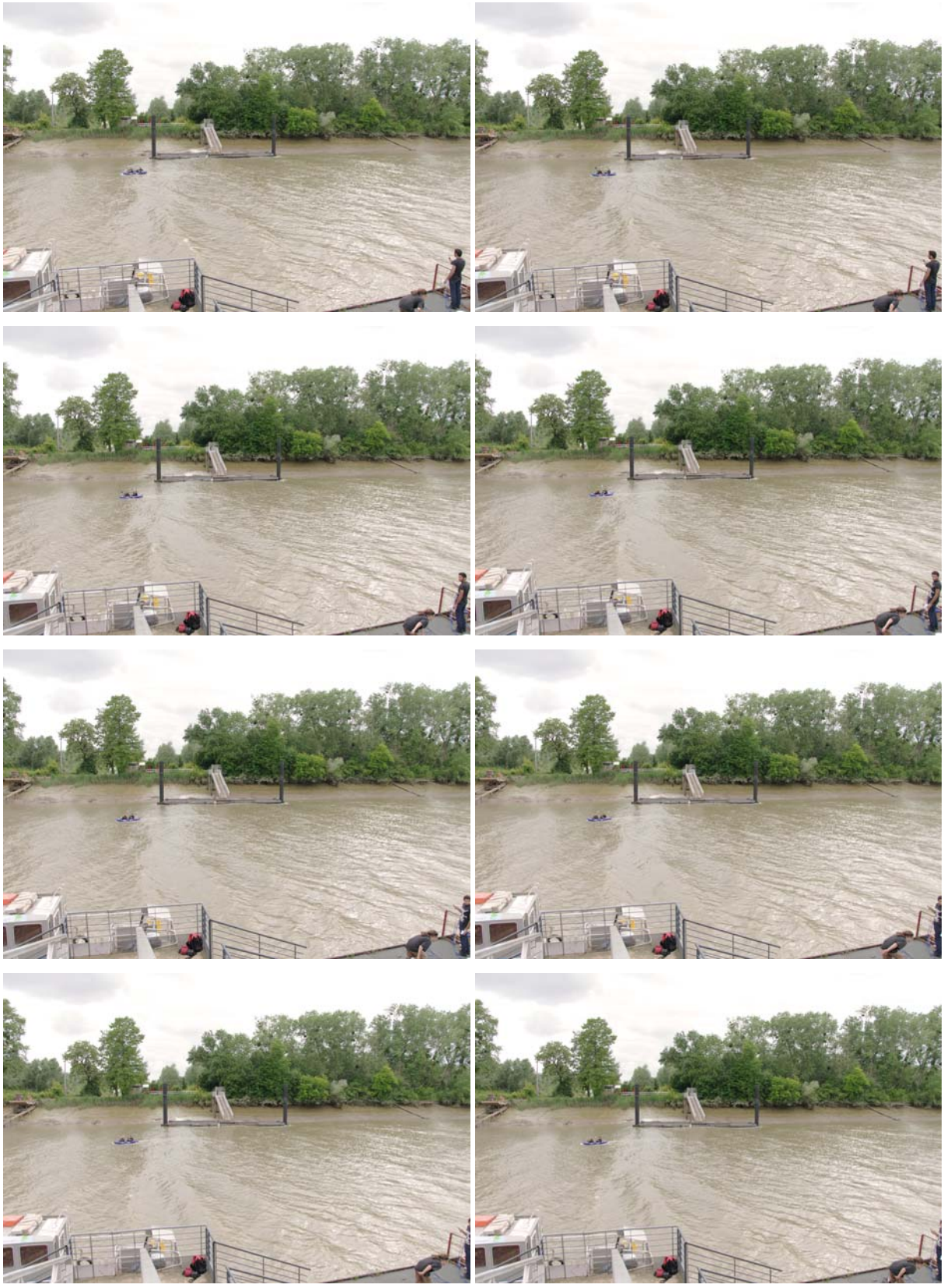

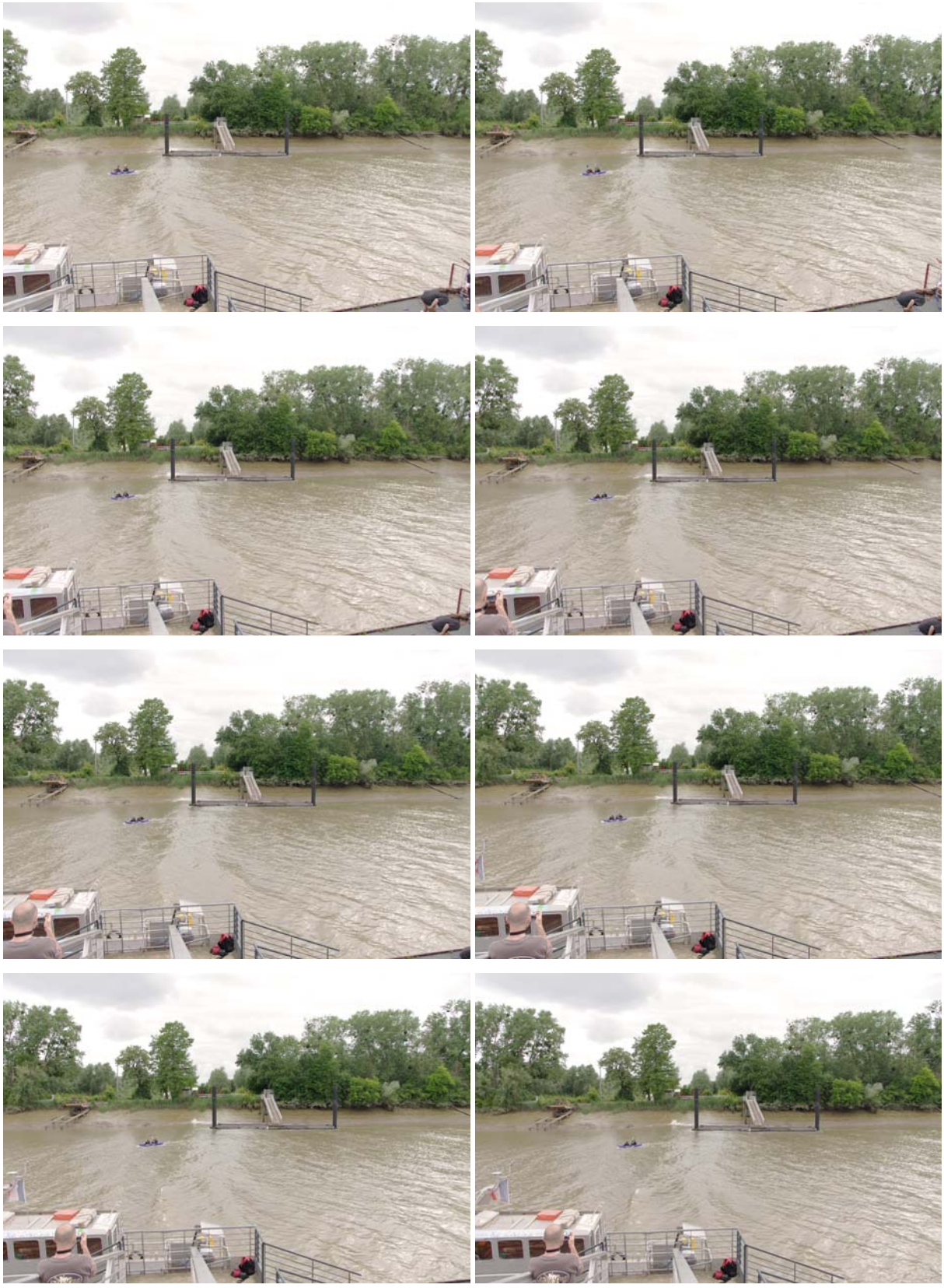

(D) Sequence of shots as the tidal bore passed the sampling point at 18:54:47 with 0.38 s between each shot - Pierre LUBIN and Bruno SIMON on the kayak tried to surf the bore front

(E) Arcins channel at 19:19:05

Fig. B-5 - Tidal bore on 7 June 2012 afternoon

APPENDIX C - ACOUSTIC DOPPLER VELOCIMETER CONFIGURATIONS (FIELD STUDY G12, 7 JUNE 2012)

C.1 PRESENTATION

During the field investigation, a Sontek™ microADV (16 MHz, serial number A1036F) was deployed. The ADV was equipped with a 3D side-looking head. The ADV longitudinal direction was pointed upstream.

The ADV was fixed at the downstream end of a 23.55 m long heavy, sturdy pontoon and it was logged in real-time with the software HorizonADV running on a nearby notebook computer. The probe was located between the hulls and the sampling volume was 1.03 m below the free-surface. The paragraph C.2 lists the ADV settings on 7 June 2012.

C.2 CONFIGURATION THURSDAY 7 JUNE 2012

Start:	7 June 2012 at 06:01:49
Nb samples:	534689
Probe	A1036
System:	16000 kHz MicroADV XZ 5 cm SIDE
CPU/DSP Software version:	8.5/4.1
Sensor:	None
Recorder:	No
Velocity range:	+/- 250 cm/s
Sampling mode:	normal
Lag adjustment:	NO
Coordinate system:	XYZ
Sound speed:	1481.6 m/s (Temperature = 20 C, Salinity = 0 ppt)
Sampling rate:	50 Hz
Recording mode:	Continuous

C.3 PRACTICAL ISSUES

The ADV unit was positioned vertically with the side-looking head facing towards Arcins Island. The raw data are shown in Figure C-1. The first velocity component (V_1) corresponded to about the vertical component, the V_2 component to about the longitudinal component and the V_3 component to the transverse component. Some basic post-processing showed a significant number of spikes during the first 2,477 seconds of the record. This was illustrated by the removal of more than 98% of data using the phase-space thresholding despiking technique (GORING and NIKORA

2002, WAHL 2003). Therefore the signal processing was restricted herein to the removal of communication errors, the removal of average signal to noise ratio data less than 15 dB and the removal of average correlation values less than 60% (McLELLAND and NICHOLAS 2000). In comparison, the processing of the ADV signal during the study G10 (CHANSON et al. 2011) included the removal of communication errors, the removal of average signal to noise ratio data less than 15 dB, the removal of average correlation values less than 60%, and the phase-space thresholding technique. Although the exact cause of the large number of spikes remains unknown, it is suspected that there might be some internal problem with the ADV unit.

The first 500 s of the ADV signal record were removed because David REUNGOAT and Pierre LUBIN were in the water at the time to secure the ADV unit. With the post-processed data, the system of co-ordinates was rotated by 1.78º around the V_1 axis, by 12.73º around the V_y axis and by 180º around the V_z axis to yield a Cartesian system of co-ordinate with V_x being the longitudinal velocity component positive downstream, V_y being the transverse velocity component positive towards Arcins Island and V_z the vertical velocity component positive upwards. The resulting post-processed signal is presented in Figure C-2.

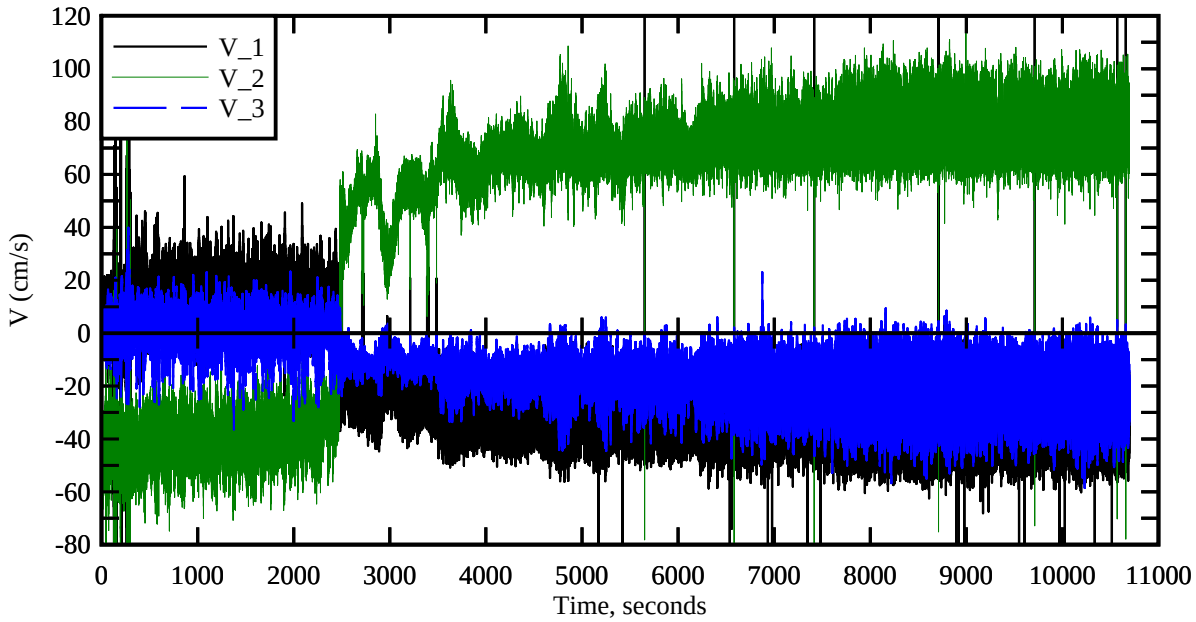

Fig. C-1 - Raw velocity data without post-processing

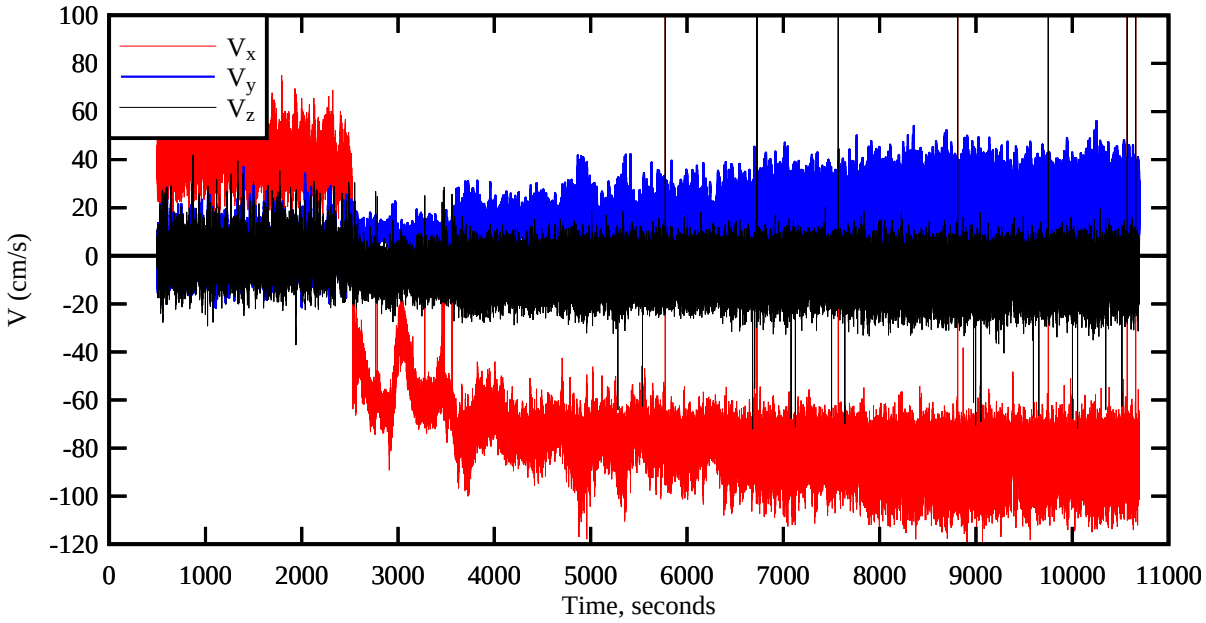

Fig. C-2 - Post-processed velocity data with V_x being the longitudinal velocity component positive downstream, V_y being the transverse velocity component positive towards Arcins Island and V_z the vertical velocity component positive upwards

The authors experienced a major problem: they found the ADV stem bent along the main upstream flow direction when the unit was retrieved at the end of the study (Fig. C-3). Based upon the visual observations and ADV record, it is suspected that the ADV unit was hit by a submerged debris during the early ebb tide, about 6,185 s after the start of the record. This was inferred by a relatively large number of erroneous data from 6,185 s onwards: that is, for t > 27,894 s since 00:00 on 7 June 2012 (or after 07:44:54).

During the field investigation on Thursday 7 June 2012, the authors were constantly looking at the free-surface to prevent any impact of floating debris as well as monitoring the ADV data acquisition software. There was at least one person checking the free-surface ahead of the ADV at any time. There was no obvious prior indication of probe damage. After the ADV system was brought back in the laboratory, the unit was inspected and checked. While the results were successful, the authors acknowledge that this physical damage might have some effect on the ADV data, in particular the vertical component. Further the suspended sediment tests were performed with the ADV unit four days later and the results indicated no apparent issue with the ADV operation. Nonetheless the velocity data set must be considered with care.

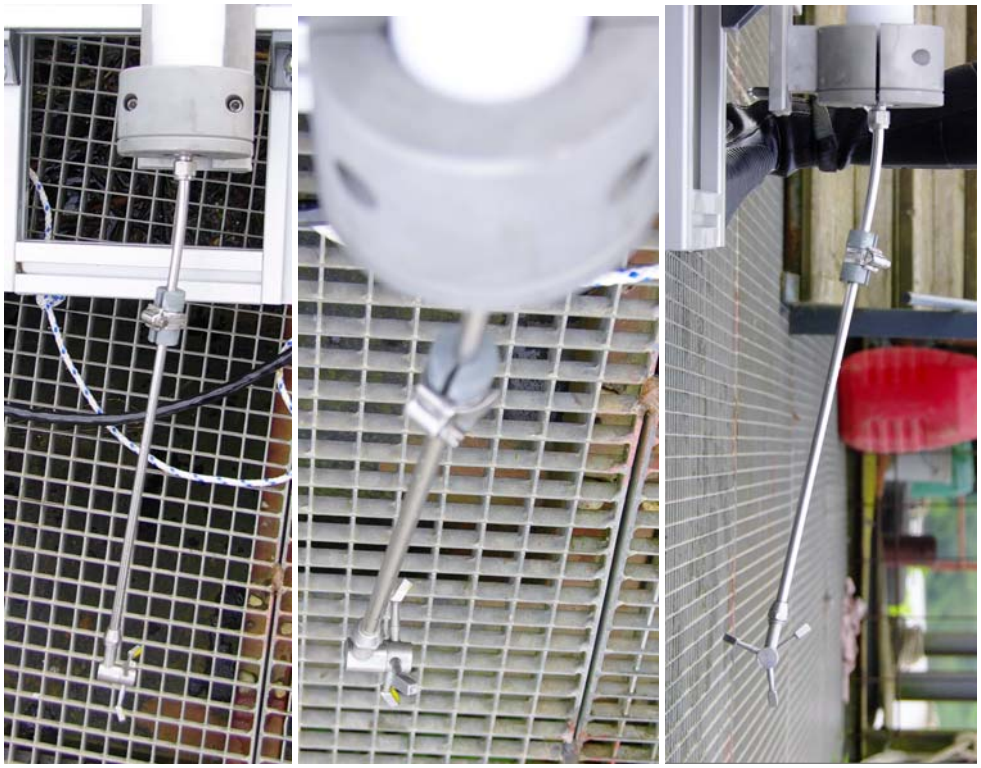

Fig. C-3 - Photographs of the bent ADV stem on 7 June 2012 at 10:30 - On the lower photographs, from left to right: looking upstream, looking downwards, looking towards the Arcins Island

APPENDIX D - GRANULOMETRY OF GARONNE RIVER SEDIMENT SAMPLES

D.1 PRESENTATION

Some Garonne River bed materials were collected at low tide on 7 June 2012 afternoon and on 8 June 2012 afternoon at mid ebb tide, next to the right bank at Arcins. The soil samples consisted of fine mud and silt materials collected on the stream bed just above the water surface mark (Fig. E-1, App. E). The granulometry and rheological properties of mud samples were tested. The results are summarised in Appendices D and E.

The soil sample granulometry was measured with a Malvern^{TM} laser Mastersizer 2000 with Hydro 3000SM dispersion unit for wet samples. For each sediment sample (7/6/2012 and 8/6/2012), two mixing techniques were tested: mechanical and ultrasound, for durations ranging from 10 to 30 minutes. For a given configuration, the granulometry was performed four times and the results were averaged. The differences between the 4 runs were checked and found to be negligible.

D.2 GRANULOMETRY DATA

The data are reported in Table D-1 and the results are presented in Figure D-1.

Table D-1 - Volume fraction of sediment particle sizes in percentage - The first column indicates the lower sediment size boundary

Size (microns)	Volume fraction							
Sediment:	7/06/2012	7/06/2012	7/06/2012	7/06/2012	8/06/2012	8/06/2012	8/06/2012	8/06/2012
Mixer:	Mechanical	Mechanical	Mechanical	Ultrasound	Mechanical	Mechanical	Mechanical	Ultrasound
Duration:	10 min.	20 min.	30 min.	18 min.	10 min.	20 min.	30 min.	14 min.
Nb runs:	4	4	4	4	4	4	4	4
0.363	0.00001	0.00058	0.00001	0.00001	0.00000	0.00000	0.00000	0.00001
0.417	0.00080	0.00084	0.00081	0.00081	0.00062	0.00064	0.00062	0.00078
0.479	0.00118	0.00124	0.00118	0.00118	0.00092	0.00095	0.00091	0.00110
0.55	0.00172	0.00180	0.00171	0.00168	0.00125	0.00132	0.00125	0.00153
0.631	0.00235	0.00248	0.00234	0.00226	0.00168	0.00180	0.00168	0.00202
0.724	0.00310	0.00326	0.00307	0.00294	0.00214	0.00232	0.00214	0.00258
0.832	0.00388	0.00409	0.00384	0.00365	0.00261	0.00286	0.00262	0.00316
0.955	0.00469	0.00495	0.00464	0.00439	0.00307	0.00340	0.00311	0.00377
1.096	0.00549	0.00581	0.00543	0.00514	0.00352	0.00394	0.00359	0.00438
1.259	0.00635	0.00672	0.00626	0.00594	0.00401	0.00453	0.00411	0.00503
1.445	0.00731	0.00775	0.00720	0.00686	0.00461	0.00526	0.00474	0.00577
1.66	0.00852	0.00904	0.00837	0.00801	0.00549	0.00629	0.00563	0.00673
1.905	0.01012	0.01074	0.00993	0.00953	0.00680	0.00782	0.00693	0.00802
2.19	0.01230	0.01304	0.01203	0.01156	0.00873	0.01007	0.00883	0.00978

2.51	0.01516	0.01605	0.01479	0.01418	0.01143	0.01321	0.01147	0.01208
2.88	0.01873	0.01980	0.01824	0.01738	0.01496	0.01732	0.01493	0.01494
3.31	0.02297	0.02425	0.02233	0.02111	0.01931	0.02239	0.01921	0.01831
3.80	0.02767	0.02918	0.02687	0.02515	0.02431	0.02825	0.02415	0.02203
4.37	0.03265	0.03438	0.03166	0.02932	0.02977	0.03466	0.02958	0.02594
5.01	0.03753	0.03946	0.03636	0.03334	0.03531	0.04117	0.03511	0.02977
5.75	0.04211	0.04420	0.04078	0.03705	0.04070	0.04747	0.04051	0.03340
6.61	0.04602	0.04822	0.04459	0.04024	0.04551	0.05297	0.04533	0.03662
7.59	0.04913	0.05139	0.04770	0.04293	0.04955	0.05741	0.04941	0.03942
8.71	0.05119	0.05349	0.04995	0.04503	0.05252	0.06035	0.05241	0.04172
10.00	0.05222	0.05451	0.05135	0.04666	0.05439	0.06168	0.05431	0.04363
11.48	0.05218	0.05444	0.05187	0.04784	0.05507	0.06131	0.05502	0.04514
13.18	0.05115	0.05335	0.05155	0.04862	0.05467	0.05934	0.05463	0.04635
15.14	0.04930	0.05135	0.05044	0.04897	0.05328	0.05603	0.05326	0.04721
17.38	0.04672	0.04851	0.04853	0.04882	0.05103	0.05162	0.05100	0.04767
19.95	0.04364	0.04506	0.04592	0.04804	0.04810	0.04654	0.04806	0.04761
22.91	0.04021	0.04108	0.04267	0.04653	0.04459	0.04105	0.04453	0.04690
26.30	0.03662	0.03682	0.03896	0.04423	0.04072	0.03555	0.04061	0.04542
30.20	0.03301	0.03242	0.03498	0.04116	0.03660	0.03024	0.03645	0.04314
34.67	0.02954	0.02811	0.03097	0.03746	0.03245	0.02537	0.03225	0.04014
39.81	0.02629	0.02404	0.02715	0.03332	0.02843	0.02107	0.02821	0.03657
45.71	0.02333	0.02037	0.02368	0.02902	0.02472	0.01741	0.02449	0.03270
52.48	0.02067	0.01715	0.02065	0.02481	0.02141	0.01442	0.02122	0.02880
60.26	0.01823	0.01436	0.01800	0.02085	0.01850	0.01199	0.01838	0.02507
69.18	0.01595	0.01198	0.01564	0.01726	0.01595	0.01002	0.01594	0.02166
79.43	0.01372	0.00988	0.01339	0.01401	0.01362	0.00834	0.01374	0.01857
91.20	0.01151	0.00800	0.01117	0.01114	0.01146	0.00686	0.01171	0.01579
104.7	0.00928	0.00624	0.00890	0.00854	0.00937	0.00547	0.00974	0.01322
120.2	0.00719	0.00464	0.00675	0.00629	0.00746	0.00423	0.00792	0.01092
138.0	0.00517	0.00315	0.00466	0.00428	0.00569	0.00310	0.00618	0.00872
158.5	0.00312	0.00176	0.00266	0.00243	0.00370	0.00194	0.00409	0.00589
182.0	0	0	0	0	0	0	0	0

Notes:

- Volume fraction of sediment particle sizes in percentage; that is, 0.012 equals 1.2%.

- The first column indicates the lower sediment size boundary; for example, the row 0.417 list the fraction of particles between 0.417 and 0.479 microns.

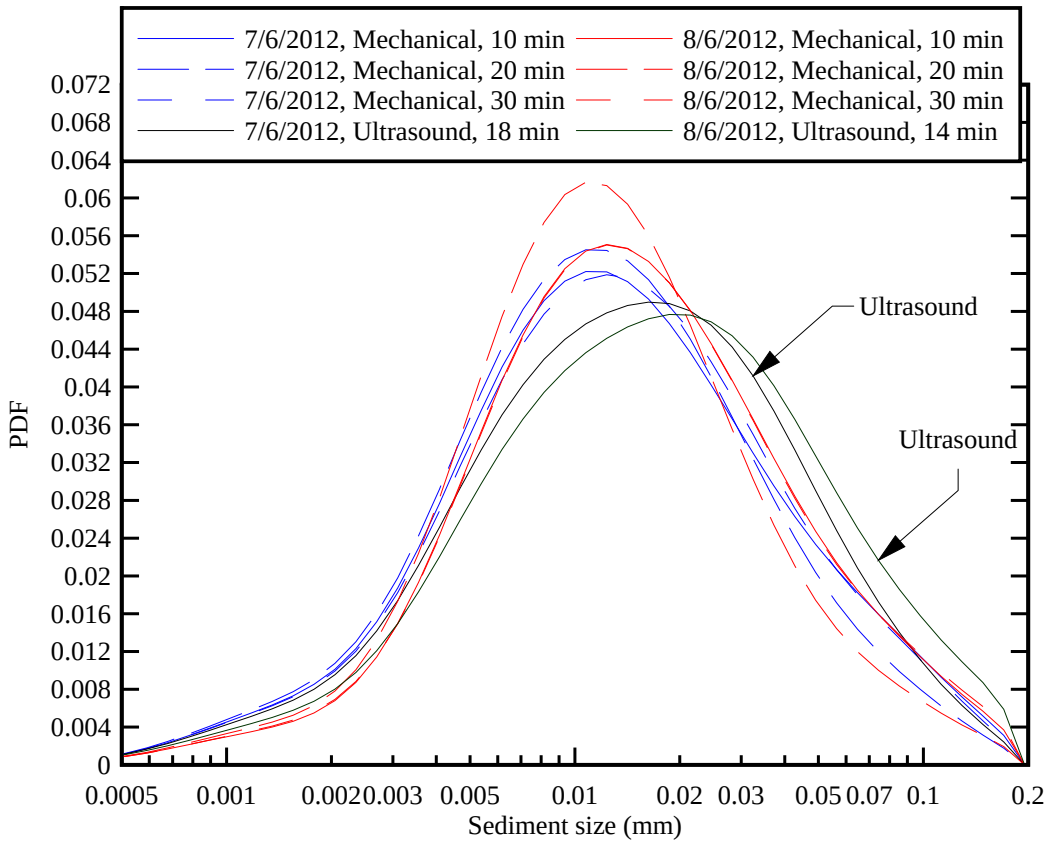

(A) Probability distribution functions of the data

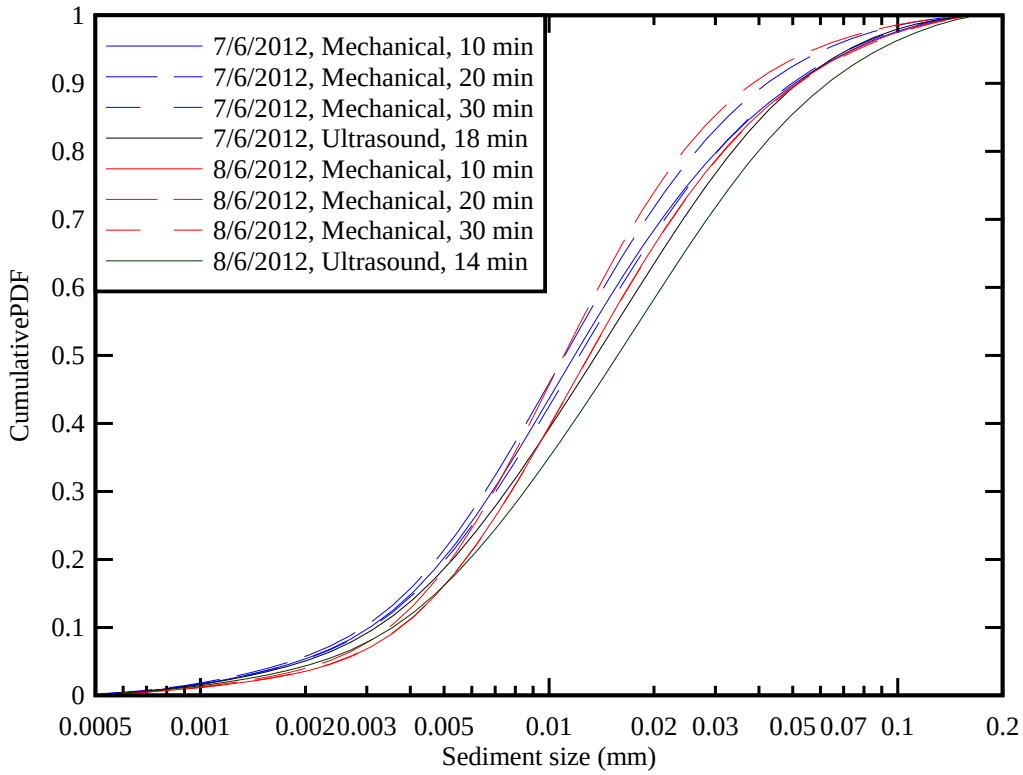

(B) Cumulative probability distribution functions

Fig. D-1 Granulometry data for Garonne River sediment samples collected in the *Bras d'Arcins* on 7 and 8 June 2012

D.3 DISCUSSION

The bed sediment material was characterised by a series of laboratory experiments. The relative density of the wet sediment samples was about **s** = 1.36 to 1.48. Assuming a relative sediment density of 2.65, this corresponded to a sample porosity of 0.70 to 0.78.

The particle size distribution data (Table D-1, Fig. D-1) presented close results for both samples although they were collected over two different days at different locations. The type of wet sediment mixing had overall little effect on the results.

The median particle size was basically 13 μm corresponding to some silty materials (GRAF 1971, JULIEN 1995, CHANSON 2004). The sorting coefficient $\sqrt{d_{90} / d_{10}}$ ranged from 3.3 to 4.2 (Table D-2, column 9). The bed material was basically a cohesive mud mixture and the granulometry data were nearly independent of the sample and mixing technique (Table D-2, Fig. D-1). The results may be compared with some sediment materials collected in the Brisbane River during the January 2011 flood (BROWN et al. 2011) as well as some dredged sediment samples collected also in the Brisbane River during a dry period (MORRIS and LOCKINGTON 2002) (Table D-2). The Garonne River sediments at Arcins channel were typically smaller than the Brisbane River flood sediments, with a smaller sorting coefficient corresponding to a narrower size distribution.

Table D-2 - Characteristics of sediment samples collected in the Garonne River on 7 and 8 June 2012 - Comparison with Brisbane River sediment samples collected during the 2011 flood (BROWN et al. 2011) and dredged sediment samples (MORRIS and LOCKINGTON 2002)

Reference	Sediment sample	Location	Type	Mixing	d_{50}	d_{10}	d_{90}	$\sqrt{\frac{d_{90}}{d_{10}}}$
					µm	µm	µm	
(1)	(2)	(3)	(4)	(5)	(6)	(7)	(8)	(9)
Garonne River								
Present study	7/06/2012	Garonne River at *Bras d'Arcins* (low tide)	Silt	Mech (10min)	11.86	3.06	50.80	4.07
				Mech (20min)	11.11	2.93	42.19	3.79
				Mech (30min)	12.23	3.10	49.74	4.01
				Ultras (18 min)	13.68	3.19	51.91	4.03
	8/06/2012	Garonne River at *Bras d'Arcins* (mid ebb tide)	Silt	Mech (10min)	13.06	3.75	51.53	3.71
				Mech (20min)	11.05	3.47	38.51	3.33
				Mech (30min)	13.08	3.74	52.15	3.73
				Ultras (14 min)	15.76	3.56	62.97	4.21
Flood deposits								
BROWN et al. (2011)	13/01/2011	Brisbane River at Gardens Point	Silt	--	26.9	3.28	85.1	5.09
	14/01/2011	Brisbane River at Gardens Point	Silt	--	24.6	2.02	88.4	6.62
Dredged sediments								
MORRIS and LOCKINGTON (2002)	2001, Sample 1	Brisbane River at BP Wharf	Clayey sand	--	108.6	--	277.1	--
	2001, Sample 2	Brisbane River at Cairncross Dock	Organic silt	--	< 1.2	--	23.2	--

Notes: Mech: mechanical mixing; Ultras: ultrasound mixing; (--): data not available.

APPENDIX E - RHEOMETRY OF GARONNE RIVER SEDIMENT SAMPLES

E.1 PRESENTATION

Some Garonne River bed materials were collected at low tide on 7 June 2012 afternoon and on 8 June 2012 afternoon at mid ebb tide, next to the right bank at Arcins. The soil samples consisted of fine mud and silt materials collected on the stream bed just above the water surface mark (Fig. E-1). The rheological properties of mud samples were tested with several configurations (Table E-1). These included a rheometer Malvern^{TM} Kinexus Pro (Serial MAL1031375) equipped with either a plane-cone (∅ = 40 mm, cone angle: 4°) or a plane-disk (∅ = 20 mm). The gap truncation (150 μm) was selected to be more than 10 times the mean particle size. The tests were performed under controlled strain rate at constant temperature (25 Celsius). Between the sample collection and the tests, the mud was left to consolidate for 5 days. Prior to each rheological test, a small mud sample was placed carefully between the plate and cone (Fig. E-2). The specimen was then subjected to a controlled strain rate loading and unloading between 0.01 s^{-1} and 1,000 s^{-1} with a continuous ramp. All rheometry tests were performed with a smooth fixed disk. More a new soil sample was used for each test. No soil sample was used for more than once. All the tests were conducted shortly after the field study to prevent the deterioration of the sediment material samples.

Table E-1 - Rheometry tests with Garonne River estuarine sediment samples collected on 7 and 8 June 2012

Series	Rheometer	Configuration	Loading	Shear rate		Temperature	Sediment collection date
				Min. 1/s	Max. 1/s	Celsius	
1	Malvern Kinexus Pro (Serial MAL1031375)	Cone 40 mm 4º (smooth) Smooth fixed disk	Continuous ramp	0.01	1,000	25.0	7 June 2012 8 June 2012
2	Malvern Kinexus Pro (Serial MAL1031375)	Disk 20 mm (smooth) Smooth fixed disk	Continuous ramp	0.01	1,000	25.0	7 June 2012 8 June 2012

Fig. E-1 - Sediment sample collection on 7 June 2012 - Sample collection next to the water line by Pierre LUBIN and Bruno SIMON at 18:36 - Sample test series 1

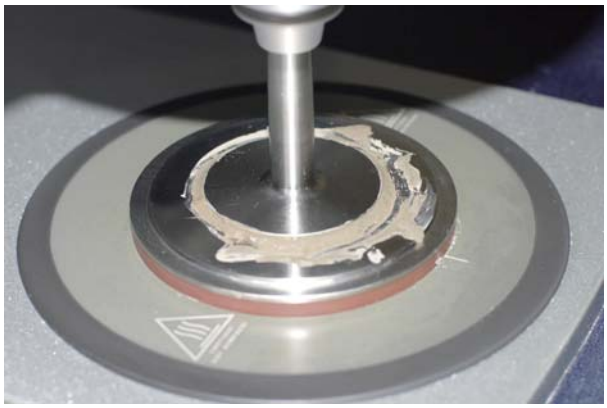

Fig. E-2 - Photographs of the rheometry tests with the Malvern™ Kinexus Pro rheometer - From Top left, clockwise: mud sample on the plate during controlled strain rate test, mud pattern on the plane at end of test, mud pattern on the lifted cone at end of test, rheometer unit

E.2 RESULTS

The basic results are presented in Figures E-3.

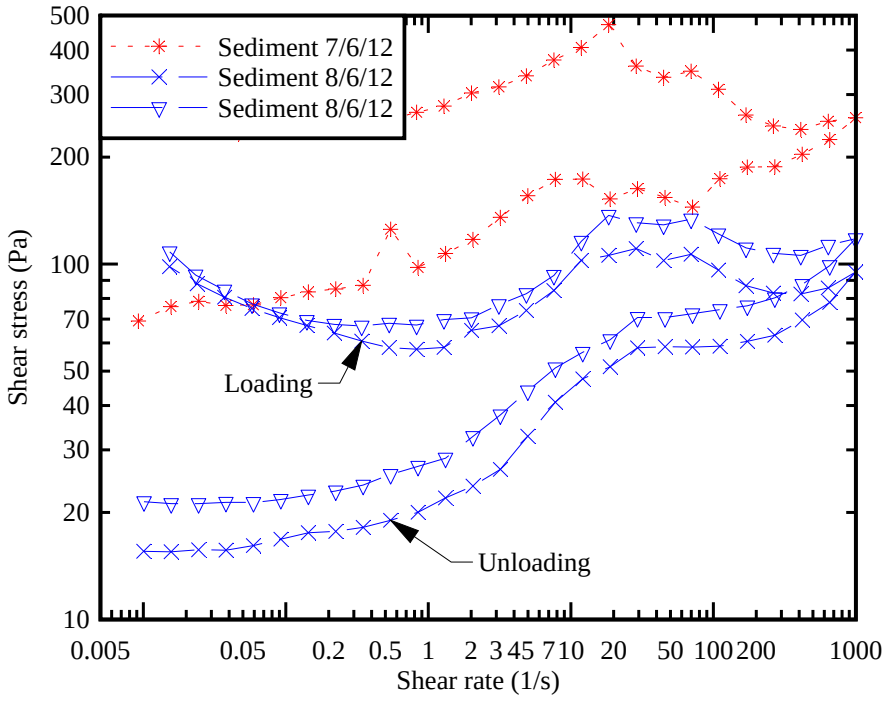

(A) Rheometer Malvern Kinexus Pro (Serial MAL1031375) with smooth cone (40 mm 4º) - Sediment collection: 7 June 2012 at low tide and 8 June 2012 at mid-ebb tide

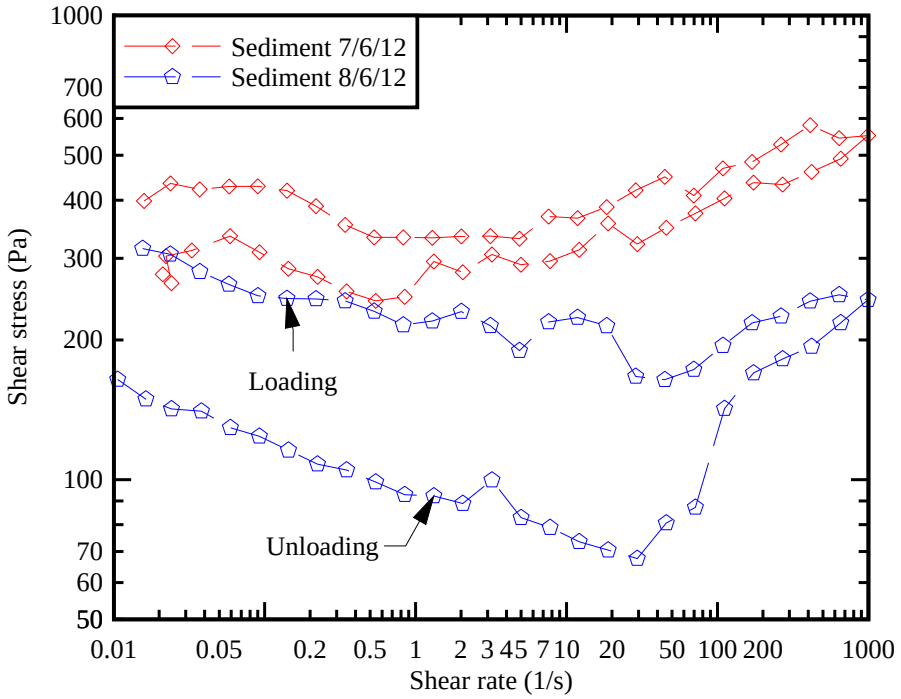

(B) Rheometer Malvern Kinexus Pro (Serial MAL1031375) with smooth disk (20 mm) - Sediment collection: 7 June 2012 at low tide and 8 June 2012 at mid-ebb tide

Fig. E-3 - Results of mud sample rheometry tests

E.3 DISCUSSION

The results highlighted some differences between the various data, depending upon the sediment sample and rheometer configuration (disk versus cone) (Fig. E-3). There were some distinct differences between the two types of sediments. The sediment sample collected on 7 June 2012 appeared to be more cohesive and less homogeneous. For example, the authors found some darker sediment inclusions as well as some fibres in the 7 June 2012 sample. It must be added that a number of tests were discarded because of obvious slippage during the loading/unloading sequence. These were not included herein nor discussed any further.

The relationship between shear stress and shear rate highlighted some basic differences between the loading and unloading which were typical of a thixotropic material. The magnitude of the shear stress during unloading was smaller than the shear stress magnitude during loading for a given shear rate. The rheometry data were used to estimate an apparent yield stress of the fluid τ_c and effective viscosity μ. Importantly a more complete characterization of the rheological behaviour of such thixotropic material would require the determination of the parameters of a thixotropic model. Herein a more rapid but also more approximate characterization of the material was used. The yield stress and apparent viscosity were estimated during the unloading phase, to be consistent with earlier thixotropic experiments (ROUSSEL et al. 2004, CHANSON et al. 2006). The yield stress

and viscosity estimates were calculated by fitting the rheometer data with a Herschel-Bulkley model. In a Herschel-Bulkley fluid, the relationship between shear stress τ and shear rate $\partial V/\partial y$ is assumed to follow:

$$\tau = \tau_c + \mu \times \left(\frac{\partial V}{\partial y} \right)^m \quad \text{(E-1)}$$

where $0 < m \leq 1$ (HUANG and GARCIA 1998, WILSON and BURGESS 1998). For $m = 1$, Equation (E-1) yields the Bingham fluid behaviour and μ is a material parameter. For $m = 1$ and $\tau_c = 0$, μ is the dynamic viscosity of a Newtonian fluid in a laminar flow motion. Based upon the unloading data, the comparison with Equation (E-1) yielded some basic results in terms of the yield stress τ_c, effective viscosity μ and exponent m which are regrouped in Table E-2. The data are compared with earlier results obtained with a similar approach.

On average, the apparent viscosity was between 18 and 36 Pa.s, the yield stress was about 75 to 271 Pa and m ~ 0.22 and 0.40 for the sediment sample collected on 7 June 2012 at low tide (Fig. E-1). For the sediment sample collected on 8 June 2012 at mid-ebb tide, the apparent viscosity was between 2.9 and 13 Pa.s, the yield stress was about 15 to 74 Pa and m ~ 0.27 to 0.60 on average. The results are summarised in Table E-3.

Quantitatively the findings were consistent with the qualitative observations of a more cohesive sediment mixture collected on 7 June 2012 (Table E-3). Further they were not dissimilar with the sediment characteristics of samples collected at Arcins on 11 September 2010 (Table E-2), but it must be stressed that the present study was conducted shortly after a major flood of the Garonne River.

Table E-3 - Summary of rheometry test results with Garonne River estuarine sediment samples collected on 7 and 8 June 2012

Sediment sample	τ_c Pa	μ Pa.s	m
7 June 2012	173	26.8	0.31
8 June 2012	37.1	9.1	0.38

Note: average results between cone and disk configurations

Table E-2 - Measured properties of mud samples collected in the Garonne River on 7 and 8 June 2012 at Arcins - Comparison with Brisbane River flood sediment sample (BROWN et al. 2011) and mud samples collected in the Garonne River at Arcins in September 2010 (CHANSON et al. 2011)

Ref.	River system	Rheometer	Configuration	Loading	Shear rate		Temperature	Sediment collection	**s**	τ_c	μ	m
					Min. 1/s	Max. 1/s	Celsius	date		Pa	Pa.s	
Present study	Garonne River at Arcins	Malvern Kinexus Pro	Cone 40 mm 4º (smooth)	Continuous ramp	0.01	1,000	25.0	7 June 2012	1.357	75.4	36.1	0.22
								8 June 2012	1.428	15.7	11.4	0.27
								8 June 2012		21.5	13.1	0.28
			Disk 20 mm (smooth)	Continuous ramp	0.01	1,000	25.0	7 June 2012	1.357	271	17.5	0.40
								8 June 2012	1.428	74.2	2.87	0.60
CHANSON et al. (2011)	Garonne River at Arcins	TA-ARG2	Cone 40 mm 2º (smooth)	Steady state flow steps	0.01	1,000	20	11 Sept. 2010 (low tide)	1.41	49.7	44.6	0.28
										61.4	52.9	0.27
BROWN et al. (2011)	Brisbane River in flood at Gardens Point Road	Mettler Viscosimeter	Cylindrical (0.59 mm between cylinders)		0	1,045	25	14 Jan. 2011	1.46	35.5	8.1	0.34

APPENDIX F - EXPERIMENTAL DATA: ACOUSTIC BACKSCATTER INTENSITY VERSUS SUSPENDED SEDIMENT CONCENTRATION

F.1 PRESENTATION

Some Garonne River bed materials were collected at low tide on 7 June 2012 afternoon and on 8 June 2012 afternoon at mid ebb tide, next to the right bank at Arcins (App. D & E). The soil samples consisted of fine mud and silt materials collected on the stream bed just above the water surface mark. The mud samples were soft and could be considered somehow as a form of mud cream (*crème de vase*). A series of laboratory tests were conducted with the Sontek™ microADV (16 MHz, serial number A1036F) system using the same settings as for the field observations on 7 June 2012 (App. C). The ADV was calibrated by measuring the signal amplitude of known, artificially produced concentrations of material obtained from the bed material sample, diluted in a water solution and thoroughly mixed. Both de-ionised (permutted) water and tap water solutions were used.

For each test, a known mass of sediment was introduced in the water tank which was stirred continuously with two propeller mixers (Fig. F-1). The blades of the mixers are shown in Figure F-1B. The ADV sampling volume was located 0.11 m above the tank bottom corresponding to a relative water elevation z/d = 0.32. The tank was strongly agitated by the two mixers (Fig. F1-B). Typically the standard deviations of the velocity components were: $v_x' \approx 0.05$-0.51 m/s, $v_y' \approx 0.06$-0.48 m/s, and $v_z' \approx 0.04$-0.15 m/s depending upon the experimental conditions.

The mass of wet sediment was measured with a Mettler™ Type PM200 (Serial 86.1.06.627.9.2) balance and the error was less than 0.01 g. The mass concentration was deduced from the measured mass of wet sediment and the measured water tank volume. The acoustic backscatter amplitude measurements were conducted with the microADV (16 MHz) system using the configuration employed in the field (scan rate, velocity range). The ADV signal outputs were scanned at 50 Hz for 3 minutes during each test. The average amplitude measurements represented the average signal strength of the three ADV receivers. They were measured in counts, with one count being equal 0.43 dB (Sontek 2006, Person. Comm.). Most ADV data were post-processed with the removal of average signal to noise ratio data less than 15 dB, average correlation values less than 60%, and communication errors. For SSC > 60 kg/m^3, unfiltered data were used since both the SNRs and correlations dropped drastically because of signal attenuation.

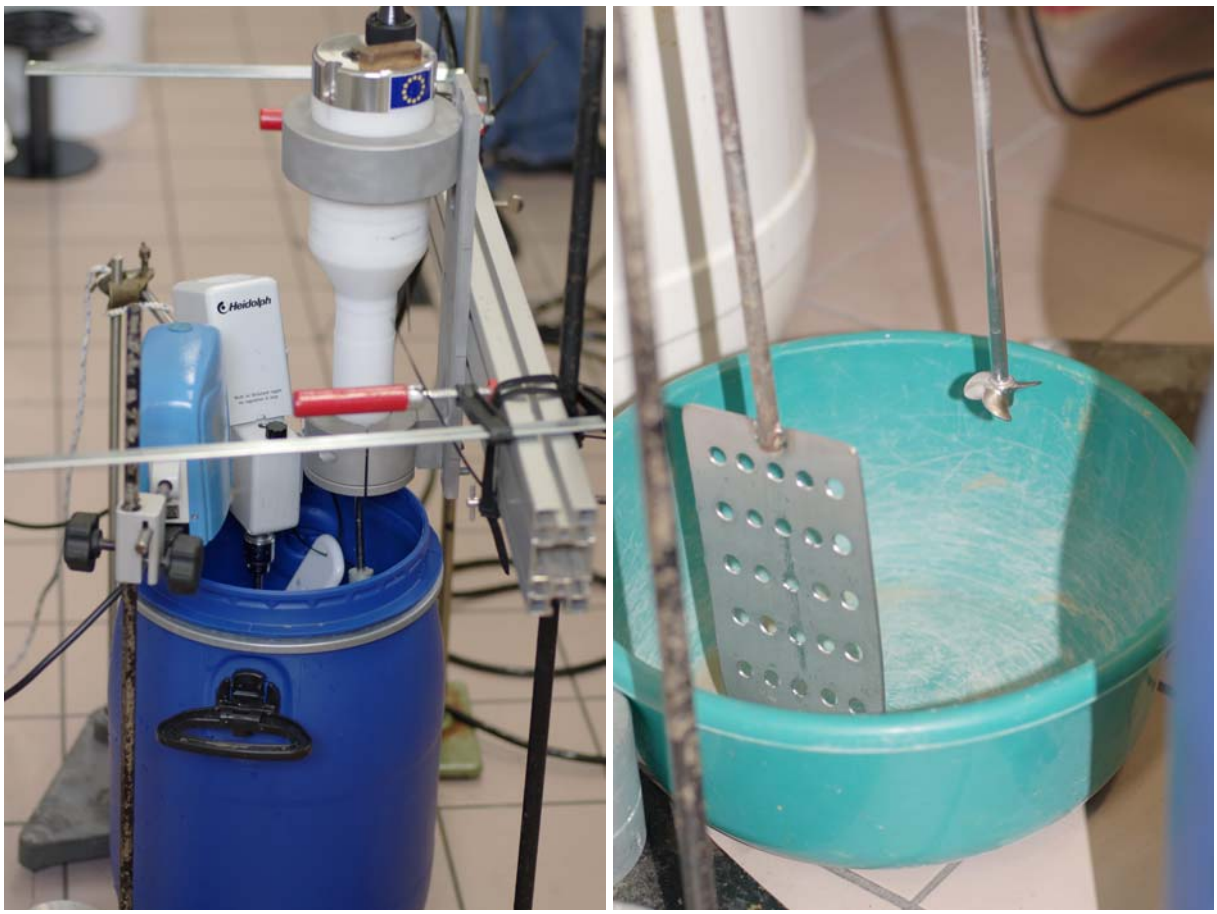

(A, Left) General view - The ADV system is on the right with two water mixers on the left

(B, Right) Details of the mixer blade and propeller

Fig. F-1 - Photograph of the laboratory experiment with the ADV and two mixers

F.2 EXPERIMENTAL RESULTS

Laboratory tests - MicroADV system measurements - Configuration Friday 8 June 2012

Location :	The University of Bordeaux (France)
Dates :	8 June 2012
Experiments by :	Alexandre IDARO
Data processing by:	Hubert CHANSON and Alexandre IDARO
Soil and water samples :	**De-ionised water**. Mud samples collected in the Arcins channel (Garonne River, France) next to the right bank just above the low water line on **7 June 2012** at about 18:36 before the tidal bore passage.
Instrumentation :	Sontek™ microADV (serial number A1036F) with a three-dimensional side-looking head scanned at 50 Hz for 3 minutes for each test. ADV settings: 7 June 2012 (App. C). Velocity range: 2.5 m/s.

Comments :	Soil sample collection on a sunny day. All the samples were kept in sealed, water tight containers until testing. Water temperature: 20 to 21 C. *It is likely that the water-sediment solution was not thoroughly mixed at high suspended sediment concentrations.*

Filename	SSC	Percent. good samples	Avg V_x	Avg V_y	Avg V_z	Std V_x	Std V_y	Std V_z	Avg Ampl	Avg Correl	Avg SNR
	kg/m^3	%	cm/s	cm/s	cm/s	cm/s	cm/s	cm/s	counts	%	dB
default 4.adv	0	86.3	-6.86	1.01	1.71	11.32	10.73	9.61	84.16	29.31	98.5
default 5.adv	0.25	99.6	-4.70	1.34	2.83	8.81	9.36	8.89	93	55.73	162.94
default 6.adv	0.5	99.7	-4.60	1.16	3.34	9.51	9.67	9.20	92.93	57.19	166.33
default 7.adv	0.75	99.7	-4.77	1.41	3.79	9.57	10.06	9.22	92.72	58.05	168
default 8.adv	1	99.4	-4.78	1.07	3.72	9.87	10.27	9.81	92.19	58.95	170.09
default 9.adv	1.25	99.3	-3.88	1.36	3.50	9.10	10.07	9.66	92.51	60.25	173.11
default 10.adv	1.5	99.3	-3.67	1.38	3.26	9.46	10.43	9.43	92.48	60.5	173.69
default 47.adv	1.75	99.4	-5.33	1.19	4.27	9.92	10.63	9.55	91.74	61.37	175.72
default 48.adv	2	99.2	-3.71	0.93	3.04	9.62	10.28	9.55	92.26	61.72	176.52
default 49.adv	4	99.2	-4.38	1.39	3.14	9.55	10.28	9.58	92.42	63.25	179.75
default 50.adv	6	99.2	-4.45	0.98	2.44	9.84	10.27	9.16	91.91	64.53	182.4
default 51.adv	8	100.0	-0.09	5.43	4.94	5.94	7.01	5.16	96.47	65.52	184.05
default 52.adv	10	100.0	0.16	6.23	4.95	5.90	6.35	4.93	96.68	65.81	184.38
default 53.adv	15	100.0	0.19	6.55	5.70	5.98	6.71	5.10	96.41	65.91	184.94
default 54.adv	20	100.0	0.62	3.85	2.46	5.77	6.79	4.97	96.2	63.99	180.81
default 55.adv	30	100.0	5.22	0.82	8.86	5.29	6.61	5.18	93.97	60.68	172.79
default 56.adv	40	100.0	4.72	2.19	7.70	6.12	6.54	5.14	89.5	56.19	162.68
default 57.adv	50	98.7	5.66	2.00	8.65	6.77	7.12	4.73	80.35	51.63	151.39
default 58.adv	60	73.1	0.82	4.75	3.10	8.08	7.93	4.20	74.83	48.02	143.35
default 59.adv	70	N/A	5.62	2.59	8.75	10.99	10.51	4.60	59.18	44.28	134.65
default 60.adv	80	N/A	4.77	2.65	8.08	15.73	14.63	4.90	48.66	42	129.01
default 61.adv	90	N/A	4.03	2.62	9.04	20.81	18.64	5.55	42.73	40.15	124.71
default 62.adv	100	N/A	3.89	2.61	8.23	25.95	23.79	5.79	38.64	38.13	119.68

Notes: MicroADV data scanned at 50 Hz for 3 minutes; Ampl: acoustic backscatter amplitude (counts); Avg: time-averaged; Correl: correlation; Percent. good samples: percentage of good ADV samples after post-processing; SNR: signal to noise ratio; Std: standard deviation; Shaded data: unfiltered data.

Laboratory tests - MicroADV system measurements - Configuration 11 June 2012

Location :	The University of Bordeaux (France)
Dates :	11 June 2012
Experiments by :	Alexandre IDARO and Hubert CHANSON
Data processing by:	Hubert CHANSON and Alexandre IDARO
Soil and water samples :	**De-ionised water**. Mud samples collected in the Arcins channel (Garonne River, France) next to the right bank just above the low water line on **8 June 2012** at about 16:00 at mid ebb tide.

Instrumentation :	Sontek™ microADV (serial number A1036F) with a three-dimensional side-looking head scanned at 50 Hz for 3 minutes for each test. ADV settings: 7 June 2012 (App. C). Velocity range: 2.5 m/s.
Comments :	Soil sample collection on a sunny day. All the samples were kept in sealed, water tight containers until testing. Water temperature: 21 to 21.5 C.

Filename	SSC	Percent. good samples	Avg V_x	Avg V_y	Avg V_z	Std V_x	Std V_y	Std V_z	Avg Ampl	Avg Correl	Avg SNR
	kg/m^3	%	cm/s	cm/s	cm/s	cm/s	cm/s	cm/s	counts	%	dB
Default 001	0.00	N/A	-0.63	-5.41	-3.90	8.99	9.99	6.94	82.35	11.8	57.44
Default 002	0.06	100.0	-0.23	-5.64	-4.65	7.26	8.37	8.20	94.26	47.17	140.36
Default 003	0.15	100.0	-0.24	-5.50	-4.07	7.83	8.59	8.02	93.92	52.19	152.04
Default 004	0.24	100.0	-0.82	-6.14	-3.66	7.32	8.75	8.29	93.95	54.84	158.2
Default 005	0.38	100.0	-0.62	-5.97	-3.99	7.44	8.53	8.09	93.96	57.19	163.68
Default 006	0.60	100.0	-0.10	-6.37	-4.13	7.59	8.45	7.90	94.15	59.38	168.42
Default 007	0.89	100.0	-0.31	-5.55	-4.71	7.33	9.01	8.02	94	60.65	171.7
Default 008	1.12	100.0	-0.95	-5.34	-3.85	7.83	8.90	8.25	93.72	61.75	173.93
Default 010	1.43	100.0	0.02	-6.31	-4.40	7.46	8.44	7.92	94.1	62.57	175.84
Default 011	1.96	99.9	-0.47	-5.50	-5.12	7.58	8.53	7.90	94.02	63.54	178.11
Default 012	2.55	99.9	-0.20	-5.25	-5.62	7.28	8.26	7.59	94.08	64.27	179.79
Default 013	3.38	100.0	0.07	-5.68	-5.07	7.63	8.41	8.06	94.04	64.98	181.45
Default 014	4.89	99.9	0.26	-4.80	-3.22	7.75	8.55	8.59	93.63	66.09	183.69
Default 015	7.09	99.9	-0.32	-5.13	-4.13	7.67	9.04	8.08	93.48	66.41	184.76
Default 016	9.17	99.9	0.06	-5.68	-3.53	7.78	9.21	8.34	93.53	66.66	185.35
Default 017	11.59	100.0	-3.66	-0.62	-12.81	6.16	6.95	6.07	94.9	66.7	185.12
Default 018	14.30	100.0	-3.39	-0.03	-12.89	6.31	6.74	5.84	94.82	66.06	183.96
Default 019	18.01	99.9	1.17	-5.39	-12.10	8.53	9.81	9.86	90.91	64.37	180.04
Default 020	22.65	99.4	3.20	-1.58	-8.00	10.84	14.07	11.89	88.25	62.68	176.1
Default 021	30.50	98.9	6.51	5.41	-5.26	10.94	11.73	12.25	85.64	59.15	167.9
Default 022	39.09	95.3	6.63	3.10	-5.15	11.83	13.27	13.07	78.63	54.72	157.58
Default 023	47.52	88.9	10.77	11.12	-7.92	12.02	13.11	12.10	69.85	50.22	147.12
Default 024	56.90	N/A	4.90	2.64	-3.70	20.09	19.70	15.41	47.93	45.28	135.64
Default 025	65.47	N/A	7.73	6.60	-6.78	24.30	22.77	12.442	40.66	42.25	128.25
Default 026	75.38	N/A	1.73	3.20	-3.27	34.52	31.62	12.4886	35.29	39.13	121.01
Default 027	85.10	N/A	6.64	11.18	-5.13	43.58	39.99	10.5538	31.16	36.17	114.45
Default 028	94.89	N/A	3.00	5.26	-4.99	50.67	47.86	10.373	28.12	33.7	108.38

Notes: MicroADV data scanned at 50 Hz for 3 minutes; Ampl: acoustic backscatter amplitude (counts); Avg: time-averaged; Correl: correlation; Percent. good samples: percentage of good ADV samples after post-processing; SNR: signal to noise ratio; Std: standard deviation; Shaded data: unfiltered data.

Laboratory tests - MicroADV system measurements - Configuration 12 June 2012

Location :	The University of Bordeaux (France)
Dates :	12 June 2012
Experiments by :	Alexandre IDARO
Data processing by:	Hubert CHANSON and Alexandre IDARO

Soil and water samples :	**Tap water**. Mud samples collected in the Arcins channel (Garonne River, France) next to the right bank just above the low water line on **7 June 2012** at about 18:36 before the tidal bore passage.
Instrumentation :	Sontek™ microADV (serial number A1036F) with a three-dimensional side-looking head scanned at 50 Hz for 3 minutes for each test. ADV settings: 7 June 2012 (App. C). Velocity range: 2.5 m/s.
Comments :	Soil sample collection on a sunny day. All the samples were kept in sealed, water tight containers until testing. Water temperature: 22 to 22.5 C.

Filename	SSC	Percent. good samples	Avg V_x	Avg V_y	Avg V_z	Std V_x	Std V_y	Std V_z	Avg Ampl	Avg Correl	Avg SNR
	kg/m^3	%	cm/s	cm/s	cm/s	cm/s	cm/s	cm/s	counts	%	dB
Default 001	0.00	87.3	0.28	-5.04	-0.45	9.55	9.53	9.25	89.56	26.06	92.28
Default 002	0.06	99.9	0.85	-4.26	-1.72	8.62	8.85	9.29	92.88	39.80	124.23
Default 003	0.13	99.8	0.82	-4.36	-1.41	8.79	9.10	9.33	92.76	47.66	142.51
Default 004	0.24	99.8	0.74	-5.10	-0.22	9.37	8.91	9.94	92.45	52.78	154.08
Default 005	0.36	99.9	0.73	-4.75	-0.80	9.08	8.78	10.19	92.54	55.65	160.76
Default 006	0.52	99.9	1.11	-5.04	-2.27	8.88	8.91	9.57	92.64	57.39	164.46
Default 007	0.77	99.9	0.84	-4.20	-1.48	8.70	8.85	9.61	92.47	59.20	169.00
Default 008	0.99	99.9	0.82	-4.42	-1.63	9.00	9.26	9.51	92.60	60.25	171.12
Default 009	1.34	99.9	0.86	-3.92	-0.93	9.16	8.90	9.85	92.35	60.73	172.56
Default 010	1.70	99.9	0.78	-4.79	0.23	9.24	9.13	10.12	92.40	61.33	173.64
Default 011	2.22	100.0	1.10	-5.10	-3.05	8.07	8.45	8.62	93.42	61.96	175.09
Default 012	2.77	99.9	0.27	-5.15	-2.66	8.48	8.46	9.10	93.14	62.17	175.59
Default 013	3.65	99.9	-0.42	-4.76	0.59	9.41	9.25	10.94	92.03	63.22	177.35
Default 014	4.76	99.9	-1.10	-3.80	3.36	10.22	9.36	11.01	91.36	63.53	178.74
Default 015	6.43	99.7	-1.61	-3.39	3.89	10.86	9.43	10.76	90.91	64.78	181.32
Default 016	8.42	99.4	-3.57	-2.45	5.11	11.06	9.44	13.40	90.22	65.53	183.06
Default 017	10.83	99.9	-1.13	-2.44	4.91	9.66	9.09	10.41	91.26	65.55	183.12
Default 018	13.28	100.0	2.79	2.61	-14.23	6.40	6.66	5.78	94.76	65.80	183.70
Default 019	16.11	100.0	2.45	2.63	-14.35	6.18	6.22	5.52	94.92	65.43	183.16
Default 020	19.81	98.1	4.36	7.69	-3.68	11.88	12.01	15.09	86.70	63.78	178.99
Default 021	24.13	97.4	5.03	7.65	-10.77	11.68	13.16	14.87	85.90	62.10	174.76
Default 022	32.45	97.0	8.58	14.18	-6.60	12.58	15.05	13.44	84.65	59.16	168.24
Default 023	41.42	99.1	8.85	19.83	-17.74	12.73	12.80	13.64	83.52	55.55	159.85
Default 024	50.72	98.02	-2.96	-7.02	-9.59	10.19	11.33	10.64	79.83	50.78	148.43
Default 025	60.43	82.69	-4.58	-4.66	-16.61	11.53	12.95	12.27	69.29	45.87	137.02
Default 026	70.27	N/A	-0.19	-2.59	-10.60	12.53	12.27	9.32	56.85	41.26	126.28
Default 027	80.11	N/A	-4.44	-0.54	-11.98	14.97	14.15	9.92	50.54	39.27	122.00
Default 028	89.9	N/A	-4.89	-2.26	-11.54	23.40	21.92	12.09	39.01	35.62	113.51

Notes: MicroADV data scanned at 50 Hz for 3 minutes; Ampl: acoustic backscatter amplitude (counts); Avg: time-averaged; Correl: correlation; Percent. good samples: percentage of good ADV samples after post-processing; SNR: signal to noise ratio; Std: standard deviation; Shaded data: unfiltered data.

Laboratory tests - MicroADV system measurements - Configuration 13 June 2012

Location :	The University of Bordeaux (France)
Dates :	13 June 2012

Experiments by :	Alexandre IDARO
Data processing by:	Hubert CHANSON and Alexandre IDARO
Soil and water samples :	**Tap water**. Mud samples collected in the Arcins channel (Garonne River, France) next to the right bank just above the low water line on **8 June 2012** at about 16:00 at mid ebb tide.
Instrumentation :	Sontek™ microADV (serial number A1036F) with a three-dimensional side-looking head scanned at 50 Hz for 3 minutes for each test. ADV settings: 7 June 2012 (App. C). Velocity range: 2.5 m/s.
Comments :	Soil sample collection on a sunny day. All the samples were kept in sealed, water tight containers until testing. Water temperature: 22 to 22.5 C.

Filename	SSC	Percent. good samples	Avg V_x	Avg V_y	Avg V_z	Std V_x	Std V_y	Std V_z	Avg Ampl	Avg Correl	Avg SNR
	kg/m^3	%	cm/s	cm/s	cm/s	cm/s	cm/s	cm/s	counts	%	dB
Default 001	0.00	99.6	-4.39	-2.58	-8.70	7.29	6.98	6.91	92.48	32.25	106.66
Default 002	0.11	100.0	-4.64	-2.36	-8.23	6.66	6.55	6.78	94.74	49.10	145.86
Default 003	0.19	100.0	-4.76	-2.02	-8.58	6.67	6.52	7.03	94.85	52.63	154.05
Default 004	0.29	100.0	-3.95	-2.40	-9.49	6.58	6.38	6.67	94.93	54.68	158.17
Default 005	0.41	100.0	-4.07	-3.06	-8.89	6.71	6.43	6.84	94.91	55.60	160.31
Default 006	0.56	100.0	-3.99	-2.78	-9.51	6.69	6.41	6.73	94.97	56.83	163.50
Default 007	0.78	100.0	-4.65	-2.90	-9.10	6.63	6.47	6.82	94.76	58.65	167.39
Default 008	1.02	100.0	-3.84	-2.64	-9.32	6.66	6.46	6.43	94.99	59.70	169.83
Default 009	1.44	100.0	-4.35	-2.80	-9.05	6.71	6.48	6.84	94.81	61.73	174.55
Default 010	1.81	100.0	-4.37	-2.63	-8.71	6.62	6.63	7.00	94.93	62.39	175.75
Default 011	2.30	100.0	-4.46	-2.99	-8.82	7.01	6.72	7.28	94.69	62.89	177.25
Default 012	2.93	100.0	-4.29	-1.83	-8.60	6.90	6.69	7.36	94.81	63.57	178.85
Default 013	3.74	100.0	-4.85	-1.59	-8.26	6.70	6.81	7.28	94.77	64.09	180.05
Default 014	4.98	100.0	-4.16	-2.04	-9.08	6.91	6.72	6.97	94.74	64.99	181.80
Default 015	6.65	100.0	-5.48	-2.69	-7.37	7.23	7.27	7.81	94.44	65.49	182.97
Default 016	8.61	100.0	-4.69	-2.16	-8.45	6.97	7.23	7.42	94.53	66.05	184.60
Default 017	11.08	100.0	-5.11	-3.11	-7.46	7.28	7.35	7.59	94.31	66.38	185.37
Default 018	13.52	100.0	-3.74	0.66	-11.88	6.87	6.29	7.08	94.28	66.23	184.35
Default 019	16.40	100.0	-4.21	0.84	-11.48	6.87	6.21	7.13	94.16	65.23	182.36
Default 020	19.93	99.8	0.95	7.51	-5.56	9.18	9.75	14.67	89.98	62.62	176.31
Default 021	24.50	100.0	2.42	-1.40	-14.34	6.71	7.46	7.42	91.16	60.94	172.72
Default 022	32.88	100.0	1.01	-5.84	-7.57	6.62	6.67	6.56	89.54	57.62	165.00
Default 023	41.82	99.9	0.85	-5.43	-7.77	7.64	7.39	6.76	81.38	52.21	152.42
Default 024	50.64	92.59	1.22	-5.45	-7.79	9.33	8.45	6.57	69.21	47.45	141.35
Default 025	60.37	N/A	0.89	-4.75	-8.45	15.92	12.87	6.84	51.99	43.22	131.52
Default 026	70.17	N/A	0.16	-4.20	-7.56	23.53	20.80	6.61	41.19	40.08	124.20
Default 027	79.81	N/A	-0.60	-2.26	-6.01	32.35	29.92	7.34	35.69	37.40	117.98
Default 028	89.5	N/A	-1.43	-3.34	-7.09	39.63	36.88	7.88	32.43	35.25	112.31

Notes: MicroADV data scanned at 50 Hz for 3 minutes; Ampl: acoustic backscatter amplitude (counts); Avg: time-averaged; Correl: correlation; Percent. good samples: percentage of good ADV samples after post-processing; SNR: signal to noise ratio; Std: standard deviation; Shaded data: unfiltered data.

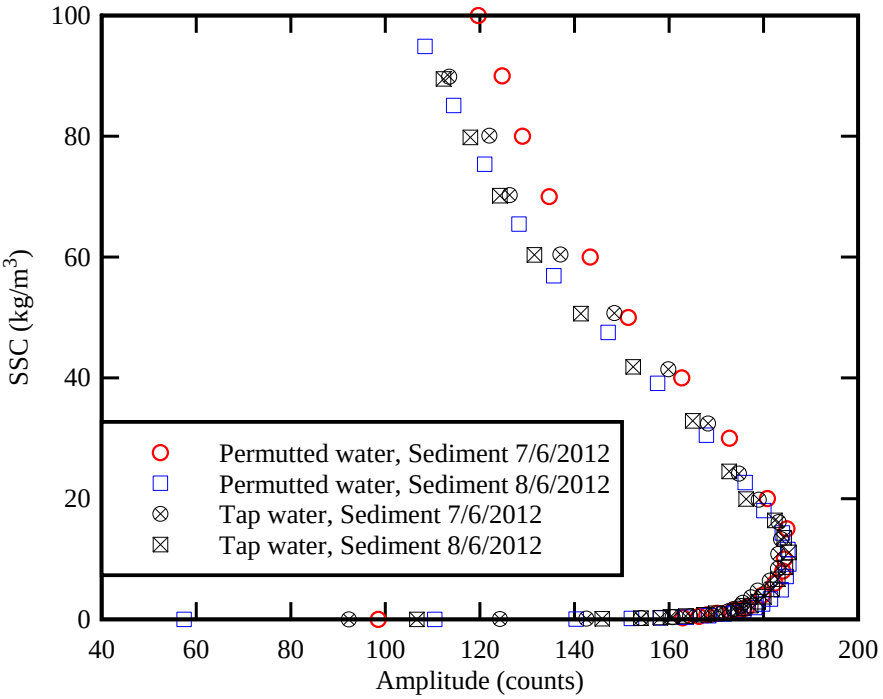

Fig. F-2 - Relationship between suspended sediment concentration (SSC) and acoustic signal amplitude (Ampl) with the sediment samples collected in the Garonne River at Arcins on 7 and 8 June 2012

F.3 DISCUSSION

The data showed a monotonic increase in ADV amplitude counts with increasing SSC up to 8 to 10 kg/m^3 (Fig. F-2). The trend was consistent with earlier results with cohesive sediments including CHANSON et al. (2008), HA et al. (2009), BROWN et al. (2011) and CHANSON et al. (2011). For larger suspended sediment concentrations (SSC > 8 to 10 kg/m^3), some signal amplitude attenuation was observed and believed to be linked multiple scattering and associated sound absorption. The ADV backscatter intensity was saturated and decreased with increasing SSC as previously reported by HA et al. (2008), CHANSON et al. (2011) and BROWN et al. (2011).

The experimental data showed that the results were basically independent of the water solution for the two selected solutions (i.e. de-ionised and tap water), but for zero sediment concentration. With a sediment laden solution, the finding was consistent with the earlier finding of CHANSON et al. (2008). Similarly the results were close for both types of sediments collected at low tide (7 June 2012) and mid-ebb tide (8 June 2012).

The present results indicated a maximum backscatter amplitude for a characteristic suspended sediment concentration $(SSC)_c \approx$ 8-10 kg/m^3. For comparison, BROWN et al. (2011) observed a maximum signal amplitude for $(SSC)_c \approx$ 3.2 kg/m^3 using a Sontek^{TM} microADV unit in the flood waters of the Brisbane River. CHANSON et al. (2011) obtained $(SSC)_c \approx$ 0.48 kg/m^3 with a

Nortek^{TM} Vector system in the Garonne River, while HA et al. (2009) reported $(SSC)_c \approx$ 1-10 kg/m^3 depending upon the type of sediments. The differences tended to illustrate that the calibration of an ADV system is specific to the instrument itself and to the type of sediment materials of the natural system.

Some researchers argued that the signal-to-noise ratio (SNR) might be a suitable surrogate measure for SSC (SALEHI and STROM 2011). In the present study, the relationship between SSC and SNR is shown in Figure F-3, illustrating similar features to the relationship between SSC and signal amplitude shown in Figure F-2. Although the SNR may be used as a SSC surrogate, the backscatter amplitude is with a physical measure of the number of particles in the sampling volume (Sontek 2008). That is, the backscatter signal amplitude might be deemed a more physical surrogate measure of SSC.

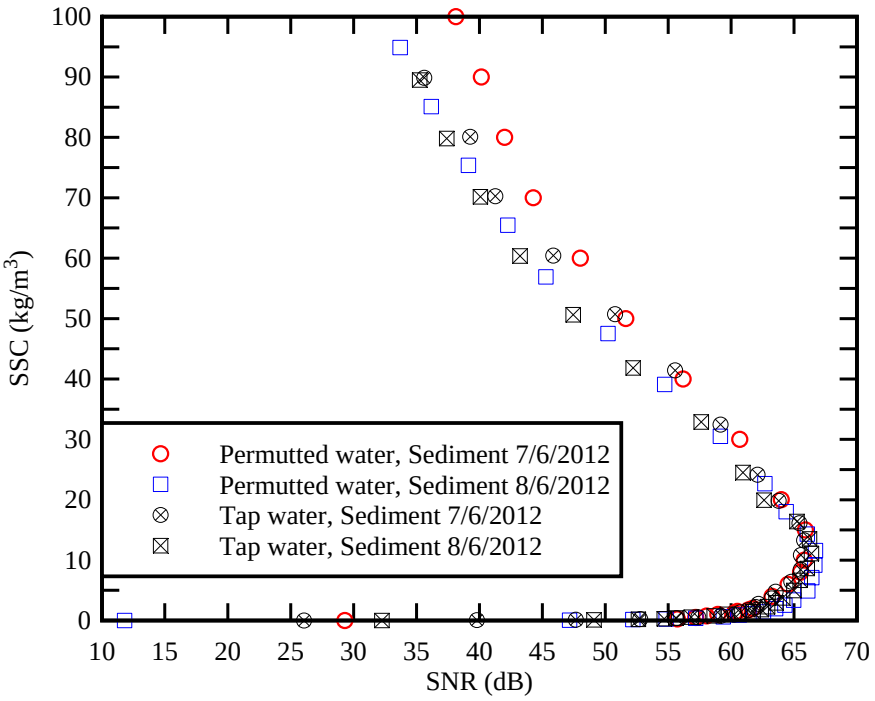

Fig. F-3 - Relationship between suspended sediment concentration (SSC) and signal-to-noise ratio (SNR) with the sediment samples collected in the Garonne River at Arcins on 7 and 8 June 2012

APPENDIX G - UNSTEADY TURBULENT REYNOLDS STRESSES DURING THE TIDAL BORE (FIELD STUDY G12, 7 JUNE 2012)

G.1 PRESENTATION

In the present study, detailed velocity measurements were performed at a relatively high frequency (50 Hz) prior to, during and after the tidal bore of the Garonne River on 7 June 2012 morning. The acoustic Doppler velocimeter (ADV) was installed at the downstream end of a large pontoon and the instrument sampled the turbulent velocity components about 1.03 m beneath the free-surface (Fig. G-1). The ADV velocity data underwent some post-processing to eliminate any erroneous and corrupted samples. The post processing was conducted with the software WinADV^{TM} version 2.028; it encompassed the removal of communication errors, the removal of average signal to noise ratio data less than 15 dB and the removal of average correlation values less than 60% (App. C).

A Reynolds stress are proportional to the product of two velocity fluctuations, where the turbulent velocity fluctuation is the deviation of the instantaneous velocity from a low-pass filtered velocity component, also called the variable interval time average VITA (PIQUET 1999, CHANSON and DOCHERTY 2012). The low-pass filtering was based upon a cut-off frequency F_{cutoff} which was derived based upon a sensitivity analysis conducted between an upper limit of the filtered signal (herein 25 Hz, the Nyquist frequency) and a lower limit corresponding to a period of about 4-6 s of the bore undulations ([1]). Figure G-2 illustrates the effect of the cutoff-frequency on the low-pass filtered longitudinal velocity component.

The results yielded an optimum threshold of F_{cutoff} = 0.5 Hz, and the filtering was applied to all velocity components. Note that KOCH and CHANSON (2009), CHANSON et al. (2011) and CHANSON and DOCHERTY (2012) selected a cutoff period $1/F_{cutoff}$ that was between the undulation period and half the undulation period of the tidal bore, as selected in the present study. Prior to the filtering, the erroneous data points were replaced by linear interpolation between the end points of the removed data interval. The filtering was applied to all velocity components, and the turbulent Reynolds stresses were calculated from the high-pass filtered signals.

The experimental results are presented in the next section.

[1] On 7 June 2012 morning, the oscillations of the free-surface had a period of about 4 to 6 s. The period of the undulations of the tidal bore on 7 June 212 afternoon was about 2 s.

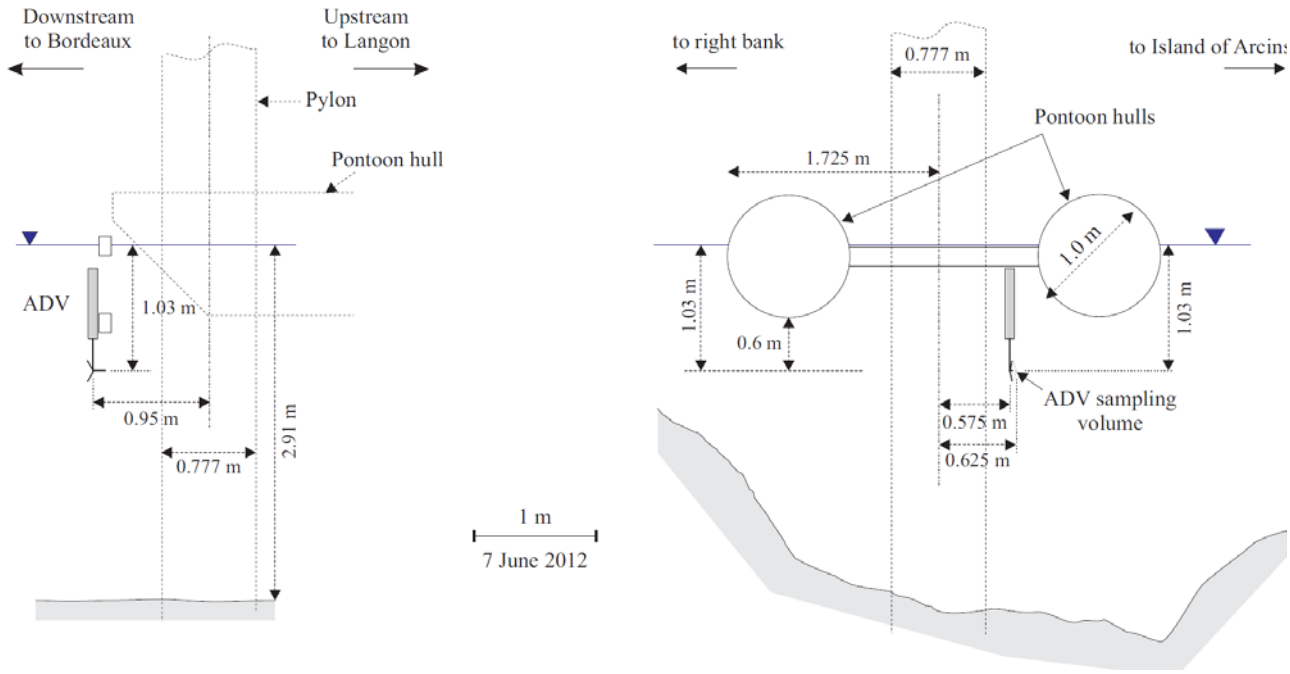

Fig. G-1 - Un-distorted sketch of the ADV mounting, sampling volume location and water surface 20 minutes prior to the tidal bore of the Garonne River at Arcins on 7 June 2012 morning - Left: view from Arcins Island - Right: looking upstream

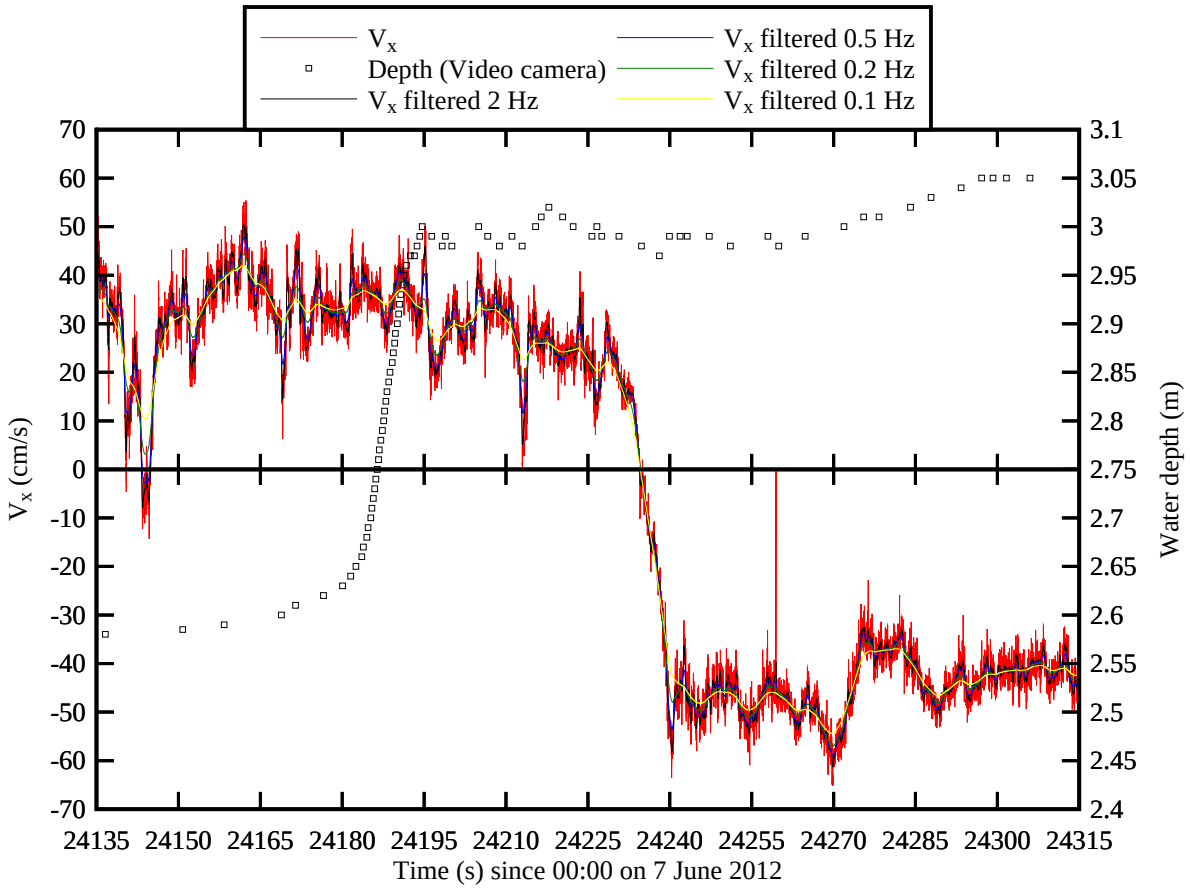

Fig. G-2 - Instantaneous water depth d and longitudinal velocity components as functions of time during the Garonne River tidal bore on 7 June 2012 morning - Comparison with low-pass filtered

velocity signals (cutoff frequencies: 2, 0.5, 0.2, 0.1 Hz)

G.2 EXPERIMENTAL RESULTS

G.2.1 Normal Reynolds stresses

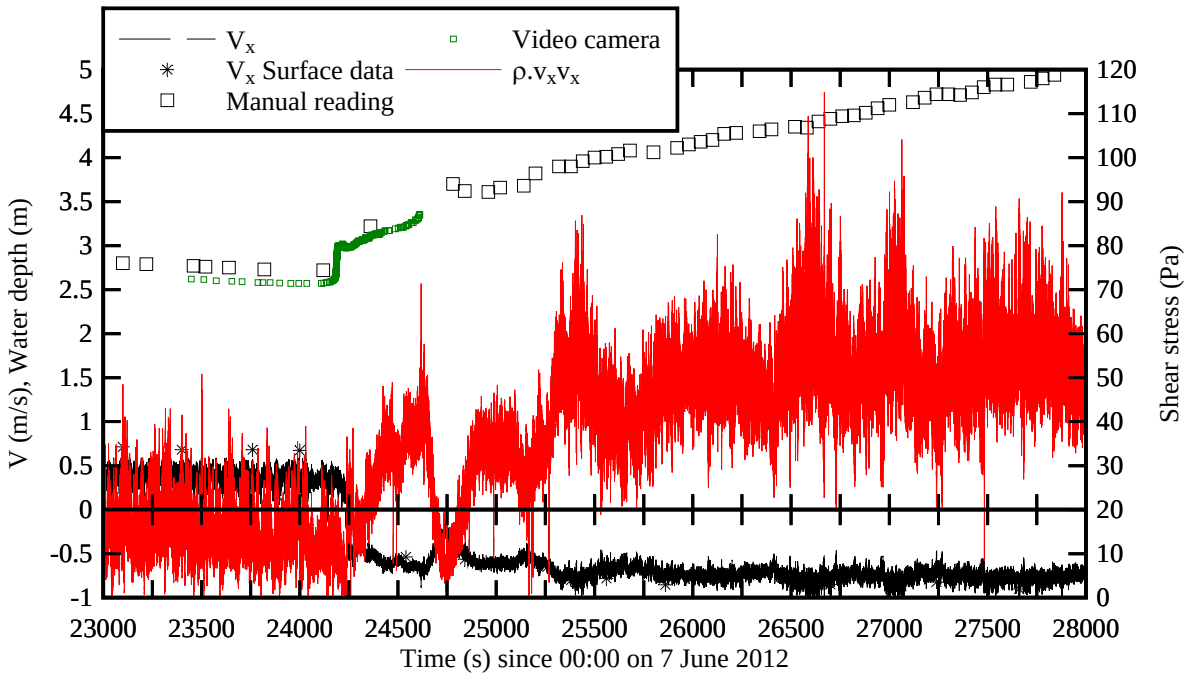

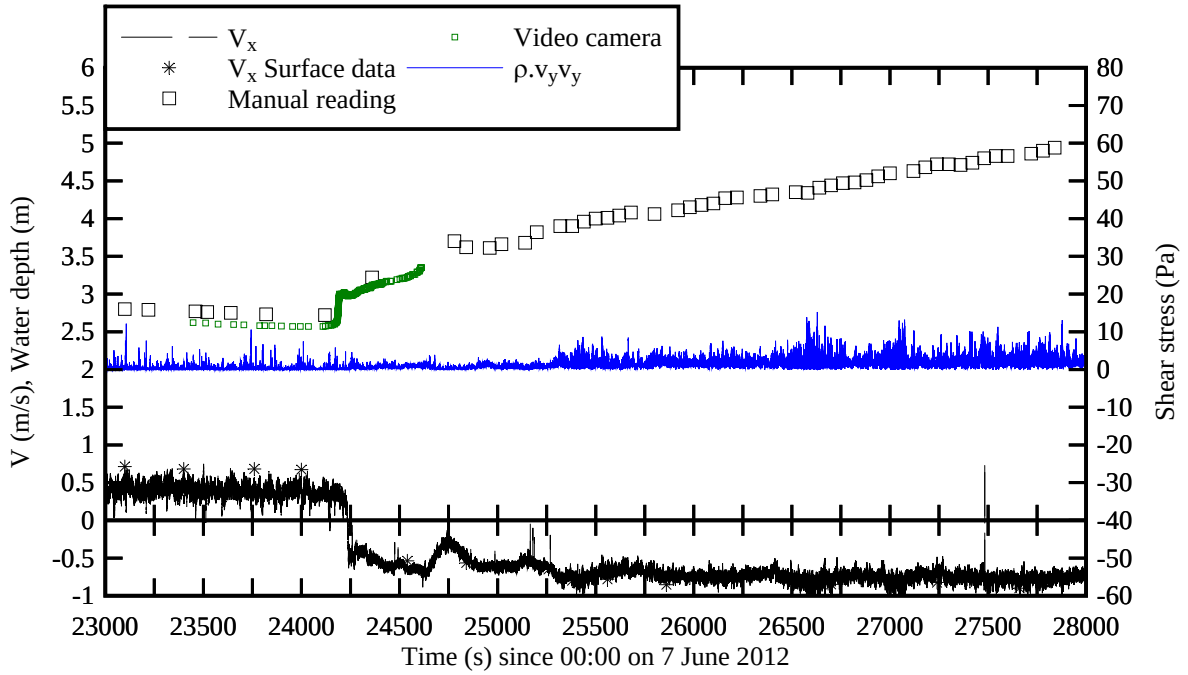

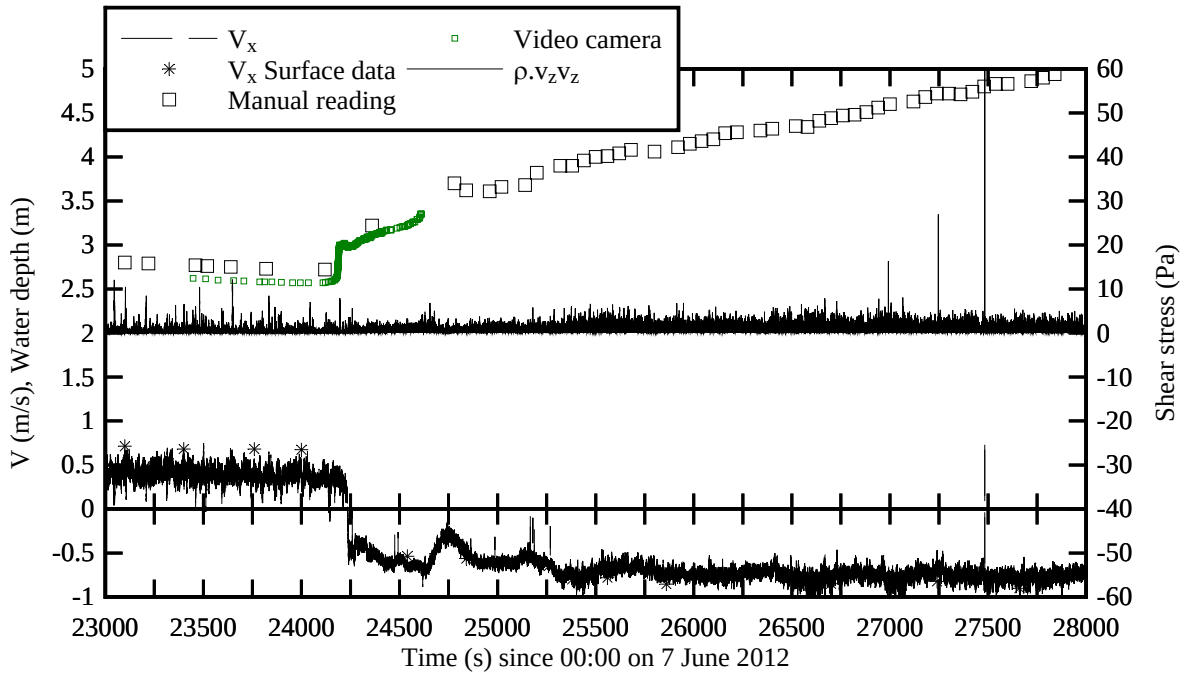

G.2 Tangential Reynolds stresses

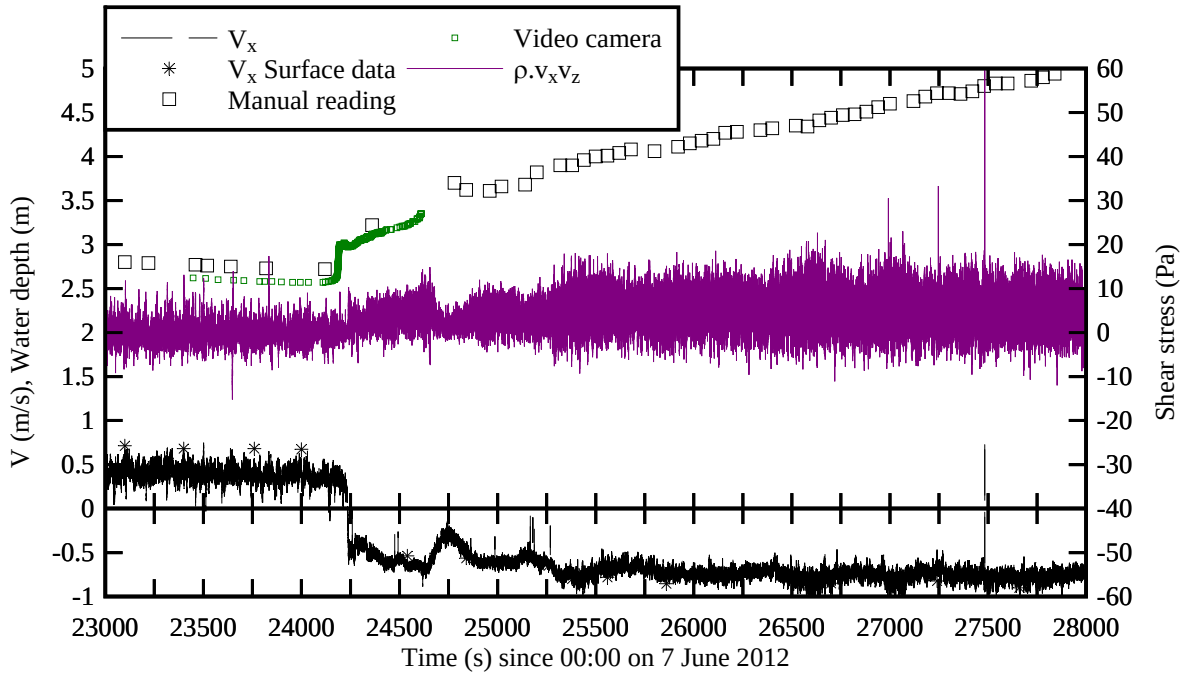

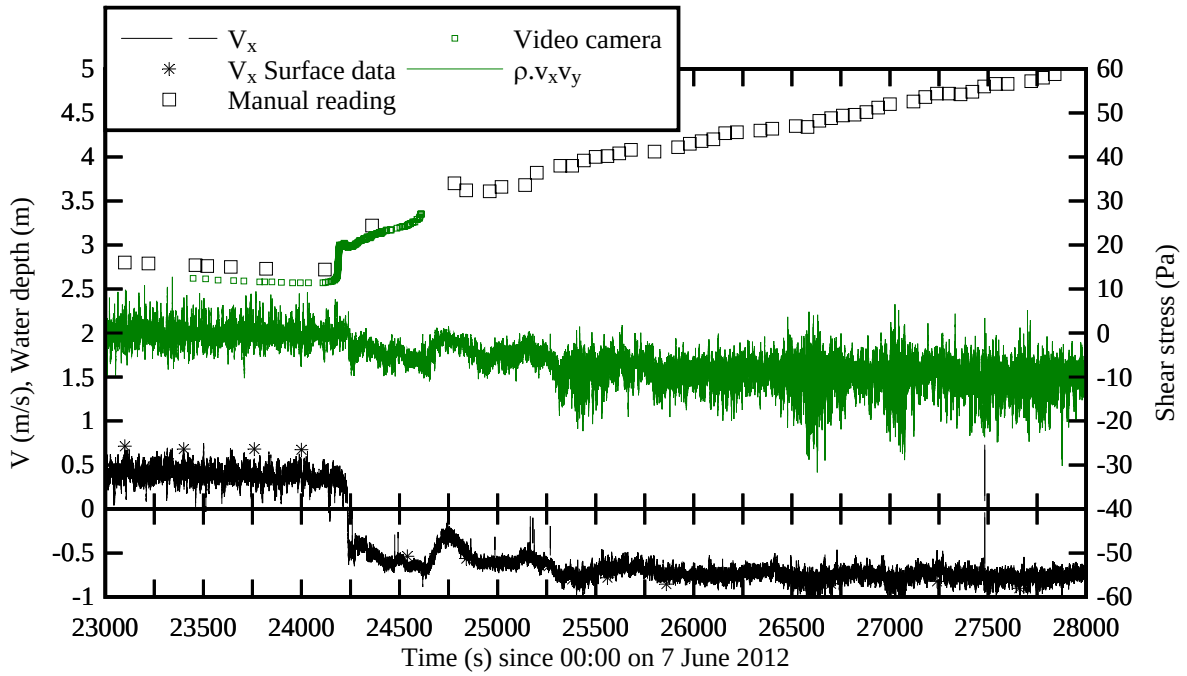
Vx
Vx Surface data
Manual reading
Video camera
ρ.vxvy
V (m/s), Water depth (m)
Shear stress (Pa)
Time (s) since 00:00 on 7 June 2012

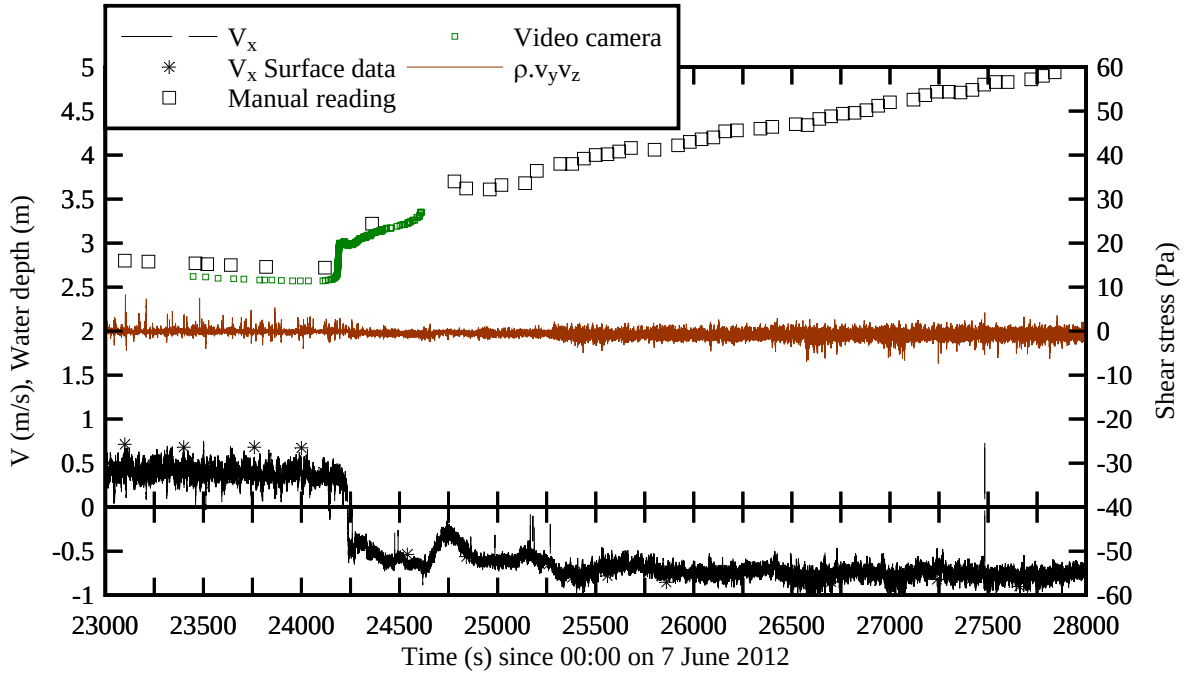
Vx
Vx Surface data
Manual reading
Video camera
ρ.vyvz
V (m/s), Water depth (m)
Shear stress (Pa)
Time (s) since 00:00 on 7 June 2012

REFERENCES

AKALI, S. (2002). "Water Temperature Effect on Sand Transport by Size fraction in the Lower Mississippi." *Ph.D. thesis*, Colorado State University, Fort Collins, USA, 243 pages.

ANTOINE, P., GIRAUD, A., MEUNIER, M., and VAN ASCH, T. (1995). "Geological and Geotechnical Properties of the "Terres Noires" in Southeastern France: Weathering, Erosion, Solid Transport and Instability." *Engineering Geology*, Vol. 40, pp. 223-234.

BAZIN, H. (1865). "Recherches Expérimentales sur la Propagation des Ondes." *Mémoires présentés par divers savants à l'Académie des Sciences*, Paris, France, Vol. 19, pp. 495-644 (in French).

BOUCHEZ, J., METIVIER, F., LIPKER, M., MAURICE, L., PEREZ, M., GAILLARDET, J., and FRANCE-LANORD, C. (2011). "Prediction of Depth-integrated Fluxes of suspended Sediment in the Amazon River: Particle Aggregation as a Complicating Factor." *Hydrological processes*, Vol. 25, pp. 778-794 (DOI 10.1002/hyp.7968).

BROWN, R., CHANSON, H., McINTOSH, D., and MADHANI, J. (2011). "Turbulent Velocity and Suspended Sediment Concentration Measurements in an Urban Environment of the Brisbane River Flood Plain at Gardens Point on 12-13 January 2011." *Hydraulic Model Report No. CH83/11*, School of Civil Engineering, The University of Queensland, Brisbane, Australia, 120 pages (ISBN 9781742720272).

BUCKLEY, A.B., (1921). "The influence of silt on the velocity of flowing water in open channels." *Minutes of Proceedings, Inst. Civ. Eng.*, UK, Vol. 216, 1922-1923, pp. 183-211

BURGESS, J. (1978). "Metal Ions in Solution." *Ellis Horwood*, New York, USA.

CHANSON, H. (2004). "The Hydraulics of Open Channel Flow: An Introduction." *Butterworth-Heinemann*, 2nd edition, Oxford, UK, 630 pages (ISBN 978 0 7506 5978 9).

CHANSON, H. (2008). "Photographic Observations of Tidal Bores (Mascarets) in France." *Hydraulic Model Report No. CH71/08*, Div. of Civil Engineering, The University of Queensland, Brisbane, Australia, 104 pages, 1 movie and 2 audio files (ISBN 9781864999303).

CHANSON, H. (2010). "Unsteady Turbulence in Tidal Bores: Effects of Bed Roughness." *Journal of Waterway, Port, Coastal, and Ocean Engineering*, ASCE, Vol. 136, No. 5, pp. 247-256 (DOI: 10.1061/(ASCE)WW.1943-5460.0000048).

CHANSON, H. (2011). "Tidal Bores, Aegir, Eagre, Mascaret, Pororoca: Theory and Observations." *World Scientific*, Singapore, 220 pages (ISBN 9789814335416).

CHANSON, H. (2012). "Momentum Considerations in Hydraulic Jumps and Bores." *Journal of Irrigation and Drainage Engineering*, ASCE, Vol. 138, No. 4, pp. 382-385 (DOI 10.1061/(ASCE)IR.1943-4774.0000409).

CHANSON, H., and DOCHERTY, N.J. (2012). "Turbulent Velocity Measurements in Open Channel Bores." *European Journal of Mechanics B/Fluids*, Vol. 32, pp. 52-58 (DOI 10.1016/j.euromechflu.2011.10.001).

CHANSON, H., JARNY, S., and COUSSOT, P. (2006). "Dam Break Wave of Thixotropic Fluid." *Journal of Hydraulic Engineering*, ASCE, Vol. 132, No. 3, pp. 280-293 (DOI: 10.1061/(ASCE)0733-9429(2006)132:3(280)).

CHANSON, H., REUNGOAT, D., SIMON, B., and LUBIN, P. (2011). "High-Frequency Turbulence and Suspended Sediment Concentration Measurements in the Garonne River Tidal Bore." *Estuarine Coastal and Shelf Science*, Vol. 95, No. 2-3, pp. 298-306 (DOI 10.1016/j.ecss.2011.09.012).

CHANSON, H., TAKEUCHI, M., and TREVETHAN, M. (2006). "Using Turbidity and Acoustic Backscatter Intensity as Surrogate Measures of Suspended Sediment Concentration. Application to a Sub-Tropical Estuary (Eprapah Creek)." *Report No. CH60/06*, Div. of Civil Engineering, The University of Queensland, Brisbane, Australia, Aug, 44 pages (ISBN 1864998628).

CHANSON, H., TAKEUCHI, M., and TREVETHAN, M. (2007). "High-Frequency Suspended Sediment Flux Measurements in a Small Estuary." *Proc. 6th International Conference on Multiphase Flow ICMF 2007*, Leipzig, Germany, July 9-13, M. SOMMERFIELD Editor, Session 7, Paper No. S7_Mon_C_S7_Mon_C_5, 12 pages (CD-ROM) (ISBN 978-3-86010-913-7).

CHANSON, H., TAKEUCHI, M., and TREVETHAN, M. (2008). "Using Turbidity and Acoustic Backscatter Intensity as Surrogate Measures of Suspended Sediment Concentration in a Small Sub-Tropical Estuary." *Journal of Environmental Management*, Vol. 86, No. 4, pp. 1406-1416 (DOI: 10.1016/j.jenvman.2007.07.009).

CHANSON, H., and TREVETHAN, M. (2011). "Vertical Mixing in the Fully Developed Turbulent Layer of Sediment-Laden Open-Channel Flow. Discussion." *Journal of Hydraulic Engineering*, ASCE, Vol. 137, No. 9, pp. 1095-1097 (DOI: 10.1061/(ASCE)HY.1943-7900.0000218).

CHEN, Jiyu, LIU, Cangzi, ZHANG, Chongle, and WALKER, H.J. (1990). "Geomorphological Development and Sedimentation in Qiantang Estuary and Hangzhou Bay." *Jl of Coastal Res.*, Vol. 6, No. 3, pp. 559-572.

CHEN, S. (2003). "Tidal Bore in the North Branch of the Changjiang Estuary." *Proc. Intl Conf. on Estuaries & Coasts ICEC-2003*, Hangzhou, China, Nov. 8-11, Intl Research & Training Center on Erosion & Sedimentation Ed., Vol. 1, pp. 233-239.

COATES, R. (2007). "The Genealogy of *Eagre* 'Tidal Surge in the River Trent'." *English Language and Linguistics*, Vol. 11, No. 3, pp. 507-523.

DOCHERTY, N.J., and CHANSON, H. (2012). "Physical Modelling of Unsteady Turbulence in Breaking Tidal Bores." *Journal of Hydraulic Engineering*, ASCE, Vol. 138, No. 5, pp. 412-419 (DOI: 10.1061/(ASCE)HY.1943-7900.0000542).

DOXARAN, D., FROIDEFOND, J.M., CASTAING, P., and BABIN, M. (2009). "Dynamics of the Turbidity in a Macrotidal Estuary (the Gironde, France): Observations from Field and MODIS Satellite Data." *Estuarine, Coastal and Shelf Science*, Vol. 81, pp. 321-332.

FUGATE, D.C., and FRIEDRICHS, C.T. (2002). "Determining Concentration and Fall Velocity of Estuarine Particle Populations using ADV, OBS and LISST." *Continental Shelf Research*, Vol. 22, pp. 1867-1886.

GORING, D.G., and NIKORA, V.I. (2002). "Despiking Acoustic Doppler Velocimeter Data." *Jl of Hyd. Engrg.*, ASCE, Vol. 128, No. 1, pp. 117-126. Discussion: Vol. 129, No. 6, pp. 484-489.

GRAF, W.H. (1971). "Hydraulics of Sediment Transport." *McGraw-Hill*, New York, USA.

GREB, S.F., and ARCHER, A.W. (2007). "Soft-Sediment Deformation Produced by Tides in a Meizoseismic Area, Turnagain Arm, Alaska." *Geology*, Vol. 35, No. 5, pp. 435-438.

HA, H.K., HSU, W.Y., MAA, J.P.Y., SHAO, Y.Y., and HOLLAND, C.W. (2009). "Using ADV Backscatter Strength for Measuring Suspended Cohesive Sediment Concentration." *Continental Shelf Research*, Vol. 29, pp. 1310-1316.

HENDERSON, F.M. (1966). "Open Channel Flow." *MacMillan Company*, New York, USA.

HORN, A., JOO, M., and POPLAWSKI, W. (1998). "Queensland Riverine Sediment Transport Rates. A Progress Report." *Water Quality Group Report No. 2/98*, Queensland Department of Natural Resources, Brisbane, Australia, 48 pages.

HORNUNG, H.G., WILLERT, C., and TURNER, S. (1995). "The Flow Field Downstream of a Hydraulic Jump." *Jl of Fluid Mech.*, Vol. 287, pp. 299-316.

HUANG, X., and GARCIA, M. (1998). "A Herschel-Bulkley Model for Mud Flow Down a Slope." *Jl of Fluid Mech.*, Vo. 374, pp. 305-333.

JORDAN, P.R. (1965). "Fluvial Sediment of the Mississippi River at St. Louis, Missouri." *Geological Survey Water-Supply Paper 1802*, USGS, Washington DC, USA, 98 pages.

JULIEN, P.Y. (1995). "Erosion and Sedimentation." *Cambridge University Press*, Cambridge, UK, 280 pages.

KAWANISI, K., and YOKOSI, S. (1997). "Characteristics of Suspended Sediment and Turbulence in a Tidal Boundary Layer." *Estuarine, Coastal and Shelf Science*, Vol. 38, pp. 447-469.

KHEZRI, N., and CHANSON, H. (2012). "Inception of Bed Load Motion beneath a Bore." *Geomorphology*, Vol. 153-154, pp. 39-47 (DOI: 10.1016/j.geomorph.2012.02.006).

KJERFVE, B., and FERREIRA, H.O. (1993). "Tidal Bores: First Ever Measurements." *Ciência e Cultura (Jl of the Brazilian Assoc. for the Advancement of Science)*, Vol. 45, No. 2, March/April, pp. 135-138.

KOCH, C., and CHANSON, H. (2008). "Turbulent Mixing beneath an Undular Bore Front." *Journal of Coastal Research*, Vol. 24, No. 4, pp. 999-1007 (DOI: 10.2112/06-0688.1).

KOCH, C., and CHANSON, H. (2009). "Turbulence Measurements in Positive Surges and Bores." *Journal of Hydraulic Research*, IAHR, Vol. 47, No. 1, pp. 29-40 (DOI: 10.3826/jhr.2009.2954).

LEWIS, A.W. (1972). "Field Studies of a Tidal Bore in the River Dee." *M.Sc. thesis*, Marine Science Laboratories, University College of North Wales, Bangor, UK.

LI, G., WEI, H., HAN, T., and CHEN, Y. (1998). "Sedimentation in the Yellow River delta, part I: flow and suspended sediment structure in the upper distributary and the estuary." *Marine Geology*, Vol. 149, pp. 93–111.

LIGGETT, J.A. (1994). "Fluid Mechanics." *McGraw-Hill*, New York, USA.

LIGHTHILL, J. (1978). "Waves in Fluids." *Cambridge University Press*, cambridge, UK, 504 pages.

McLELLAND, S.J., and NICHOLAS, A.P. (2000). "A New Method for Evaluating Errors in High-Frequency ADV Measurements." *Hydrological Processes*, Vol. 14, pp. 351-366.

MORRIS, P.H., and LOCKINGTON, D.A. (2002). "Geotechnical Compressibility and Consolidation Parameters and Correlations for Remoulded Fine-Grained Marine and Riverine Sediments." *Research Report*, CRC Sustainable Tourism, 51 pages.

MOUAZE, D., CHANSON, H., and SIMON, B. (2010). "Field Measurements in the Tidal Bore of the Sélune River in the Bay of Mont Saint Michel (September 2010)." *Hydraulic Model Report No. CH81/10*, School of Civil Engineering, The University of Queensland, Brisbane, Australia, 72 pages (ISBN 9781742720210).

NAVARRE, P. (1995). "Aspects Physiques du Caractère Ondulatoire du Macaret en Dordogne." ('Physical Features of the Undulations of the Dordogne River Tidal Bore.') *D.E.A. thesis*, Univ. of Bordeaux, France, 72 pages (in French).

Petit Robert (1996). "Dictionnaire de la Langue Française." ('Dictionary of the French Language.') *Dictionnaire Le Robert*, Paris, France (in French).

PIQUET, J. (1999). "Turbulent Flows. Models and Physics." *Springer*, Berlin, Germany, 761 pages.

PITLICK, J. (1992). "Flow Resistance under Conditions of Intense Gravel Transport." *Water Resources Research*, Vol. 28, No. 3, pp. 891-903.

RAYLEIGH, Lord (1908). "Note on Tidal Bores." *Proc. Royal Soc. of London, Series A containing Papers of a Mathematical and Physical Character*, Vol. 81, No. 541, pp. 448-449.

ROUSSEL, N., LE ROY, R., and COUSSOT, P. (2004). "Thixotropy Modelling at Local and Macroscopic Scales." *Jl of Non-Newtonian Fluid Mech.*, Vol. 117, No. 2-3, pp. 85-95.

ROWBOTHAM, F. (1983). "The Severn Bore." *David & Charles*, Newton Abbot, UK, 3rd edition, 104 pages.

SIMPSON, J.H., FISHER, N.R., and WILES, P. (2004). "Reynolds Stress and TKE Production in an Estuary with a Tidal Bore." *Estuarine, Coastal and Shelf Science*, Vol. 60, No. 4, pp. 619-627.

TESSIER, B., and TERWINDT, J.H.J. (1994). "An Example of Soft-Sediment Deformations in an intertidal Environment - The Effect of a Tidal Bore". *Comptes-Rendus de l'Académie des Sciences*, Série II, Vol. 319, No. 2, Part 2, pp. 217-233 (in French).

TOORMAN, E.A. (2008). "Vertical Mixing in the Fully Developed Turbulent Layer of Sediment-Laden Open-Channel Flow." *Journal of Hydraulic Engineering*, ASCE, Vol. 134, No. 9, pp. 1225-1235 DOl: 10.1 061/(ASCE)0733-9429(2008) 134:9(1225).

TREVETHAN, M., CHANSON, H., and TAKEUCHI, M. (2007). "Continuous High-Frequency Turbulence and Sediment Concentration Measurements in an Upper Estuary." *Estuarine Coastal and Shelf Science*, Vol. 73, No. 1-2, pp. 341-350 (DOI:10.1016/j.ecss.2007.01.014).

VAN DEN BERG, J.H., and VAN GELDER, A. (1993). "Prediction of suspended bed material transport in flows over silt and very fine sand." *Water Resources Research*, Vol. 29, No. 5, pp. 1393-1404.

VANONI, V. (1975). "Sedimentation Engineering." *ASCE*, New York, USA.

VOULGARIS, G., and MEYERS, S.T. (2004). "Temporal Variability of Hydrodynamics, Sediment Concentration and Sediment Settling in a Tidal Creek." *Continental Shelf Research*, Vol. 24, pp. 1659-1683.

WAHL, T.L. (2003). "Despiking Acoustic Doppler Velocimeter Data. Discussion." *Jl of Hyd. Engrg.*, ASCE, Vol. 129, No. 6, pp. 484-487.

WANG, Z.Y., LARSEN, P., and XIANG, W. (1994). "Rheological Properties of Sediment Suspensions and their Implications." *Jl of Hyd. Res.*, IAHR, Vol. 32, No. 4, pp. 495-516.

WILSON, S.D.R., and BURGESS, S.L. (1998). "The Steady, Speading Flow of a Rivulet of Mud." *Jl Non-Newtonian Fluid Mech.*, Vol. 79, pp. 77-85.

WOLANSKI, E., MOORE, K., SPAGNOL, S., D'ADAMO, N., and PATTIERATCHI, C. (2001). "Rapid, Human-Induced Siltation of the Macro-Tidal Ord River Estuary, Western Australia." *Estuarine, Coastal and Shelf Science*, Vol. 53, pp. 717-732.

WOLANSKI, E., WILLIAMS, D., SPAGNOL, S., and CHANSON, H. (2004). "Undular Tidal Bore Dynamics in the Daly Estuary, Northern Australia." *Estuarine, Coastal and Shelf Science*, Vol. 60, No. 4, pp. 629-636.

Bibliography

CHANSON, H. (2009). "Development of the Bélanger Equation and Backwater Equation by Jean-Baptiste Bélanger (1828)." *Journal of Hydraulic Engineering*, ASCE, Vol. 135, No. 3, pp. 159-163 (DOI: 10.1061/(ASCE)0733-9429(2009)135:3(159)).

CHANSON, H. (2009). "The Rumble Sound Generated by a Tidal Bore Event in the Baie du Mont Saint Michel." *Journal of Acoustical Society of America*, Vol. 125, No. 6, pp. 3561-3568 (DOI: 10.1121/1.3124781).

CHANSON, H., and TAN, K.K. (2010). "Turbulent Mixing of Particles under Tidal Bores: an Experimental Analysis." *Journal of Hydraulic Research*, IAHR, Vol. 48, No. 5, pp. 641-649 (DOI: 10.1080/00221686.2010.512779).

KHEZRI, N., and CHANSON, H. (2012). "Undular and Breaking Tidal Bores on Fixed and Movable Gravel Beds." *Journal of Hydraulic Research*, IAHR, Vol. 50, No. 4, pp. 353-363 (DOI: 10.1080/00221686.2012.686200).

MALANDAIN, J.J. (1988). "La Seine au Temps du Mascaret." ('The Seine River at the Time of the Mascaret.') *Le Chasse-Marée*, No. 34, pp. 30-45 (in French).

REICHSTETTER, R. (2011). "Hydraulic Modelling of Unsteady Open Channel Flow: Physical and Analytical Validation of Numerical Models of Positive and Negative Surges." *MPhil thesis*, School of Civil Engineering, The University of Queensland, Brisbane, Australia, 112 pages.

RULIFSON, R.A., and TULL, K.A. (1999). "Striped Bass Spawning in a Tidal Bore River: the Shubenacadie Estuary, Atlantic Canada." *Trans. American Fisheries Soc.*, Vol. 128, pp. 613-624.

TRICKER, R.A.R. (1965). "Bores, Breakers, Waves and Wakes." *American Elsevier Publ. Co.*, New York, USA.

Internet bibliography

VigiCrue	{http://www.vigicrues.gouv.fr/}
VigiCrue Bordeaux	{http://www.vigicrues.gouv.fr/niveau3.php?idspc=13&idstation=1429}
SHOM	{http://www.shom/fr}
SHOM - Reference Altitudes	{http://www.shom.fr/fr_page/fr_act_oceano/RAM/RAM_P1.htm#Contexte%20et%20aspects%20r%C3%A9glementaires}
SHOM - Reference Altitude: Zone Sud Gascogne	{http://www.shom.fr/fr_page/fr_act_oceano/RAM/RAM_SG_2010.pdf}
The tidal bore of the Seine River	{http://www.uq.edu.au/~e2hchans/mascaret.html}
Tidal bores, Mascaret, Pororoca. Myths, Fables and Reality!!!	{http://www.uq.edu.au/~e2hchans/tid_bore.html}
Mascaret, Aegir, Pororoca, Tidal Bore. Quid? Où? Quand? Comment? Pourquoi?	{http://espace.library.uq.edu.au/view.php?pid=UQ:9447}
The Rumble Sound Generated by a Tidal Bore Event in the Baie du Mont Saint Michel	{http://espace.library.uq.edu.au/view/UQ:178445}
Tidal river bores, National Oceanography Centre	{http://www.pol.ac.uk/home/insight/riverbores.html}

Open Access Repositories

OAIster	{http://www.oaister.org/}
UQeSpace	{http://espace.library.uq.edu.au/}

Bibliographic reference of the Report CH89/12

The Hydraulic Model research report series CH is a refereed publication published by the School of Civil Engineering at the University of Queensland, Brisbane, Australia.

The bibliographic reference of the present report is:

REUNGOAT, D., CHANSON, H., and CAPLAIN, B. (2012). "Field Measurements in the Tidal Bore of the Garonne River at Arcins (June 2012)." *Hydraulic Model Report No. CH89/12*, School of Civil Engineering, The University of Queensland, Brisbane, Australia, 121 pages (ISBN 9781742720616).

The Report CH89/12 is available, in the present form, as a PDF file on the Internet at UQeSpace:

http://espace.library.uq.edu.au/

It is listed at:

http://espace.library.uq.edu.au/list/author_id/193/

HYDRAULIC MODEL RESEARCH REPORT CH

The Hydraulic Model Report CH series is published by the School of Civil Engineering at the University of Queensland. Orders of any reprint(s) of the Hydraulic Model Reports should be addressed to the School Secretary.

School Secretary, School of Civil Engineering, The University of Queensland
Brisbane 4072, Australia - Tel.: (61 7) 3365 3619 - Fax : (61 7) 3365 4599
Url: http://www.eng.uq.edu.au/civil/ Email: enquiries@civil.uq.edu.au

Report CH	**Unit price**	Quantity	**Total price**
REUNGOAT, D., CHANSON, H., and CAPLAIN, B. (2012). "Field Measurements in the Tidal Bore of the Garonne River at Arcins (June 2012)." Hydraulic Model Report No. CH89/12, School of Civil Engineering, The University of Queensland, Brisbane, Australia, 121 pages (ISBN 9781742720616).	AUD$60.00		
CHANSON, H., and WANG, H. (2012). "Unsteady Discharge Calibration of a Large V-Notch Weir." *Hydraulic Model Report No. CH88/12*, School of Civil Engineering, The University of Queensland, Brisbane, Australia, 50 pages & 4 movies (ISBN 9781742720579).	AUD$60.00		
FELDER, S., FROMM, C., and CHANSON, H. (2012). "Air Entrainment and Energy Dissipation on a 8.9° Slope Stepped Spillway with Flat and Pooled Steps." *Hydraulic Model Report No. CH86/12*, School of Civil Engineering, The University of Queensland, Brisbane, Australia, 80 pages (ISBN 9781742720531).	AUD$60.00		
FELDER, S., and CHANSON, H. (2012). "Air-Water Flow Measurements in Instationary Free-Surface Flows: a Triple Decomposition Technique." *Hydraulic Model Report No. CH85/12*, School of Civil Engineering, The University of Queensland, Brisbane, Australia, 161 pages (ISBN 9781742720494).	AUD$60.00		
REICHSTETTER, M., and CHANSON, H. (2011). "Physical and Numerical Modelling of Negative Surges in Open Channels." *Hydraulic Model Report No. CH84/11*, School of Civil Engineering, The University of Queensland, Brisbane, Australia, 82 pages (ISBN 9781742720388).	AUD$60.00		
BROWN, R., CHANSON, H., McINTOSH, D., and MADHANI, J. (2011). "Turbulent Velocity and Suspended Sediment Concentration Measurements in an Urban Environment of the Brisbane River Flood Plain at Gardens Point on 12-13 January 2011." *Hydraulic Model Report No. CH83/11*, School of Civil Engineering, The University of Queensland, Brisbane, Australia, 120 pages (ISBN 9781742720272).	AUD$60.00		
CHANSON, H. "The 2010-2011 Floods in Queensland (Australia): Photographic Observations, Comments and Personal Experience." *Hydraulic Model Report No. CH82/11*, School of Civil Engineering, The University of Queensland, Brisbane, Australia, 127 pages (ISBN 9781742720234).	AUD$60.00		
MOUAZE, D., CHANSON, H., and SIMON, B. (2010). "Field Measurements in the Tidal Bore of the Sélune River in the Bay of Mont Saint Michel (September 2010)." *Hydraulic Model Report No. CH81/10*, School of Civil Engineering, The University of Queensland, Brisbane, Australia, 72 pages (ISBN 9781742720210).	AUD$60.00		

JANSSEN, R., and CHANSON, H. (2010). "Hydraulic Structures: Useful Water Harvesting Systems or Relics." *Proceedings of the Third International Junior Researcher and Engineer Workshop on Hydraulic Structures (IJREWHS'10)*, 2-3 May 2010, Edinburgh, Scotland, R. JANSSEN and H. CHANSON (Eds), Hydraulic Model Report CH80/10, School of Civil Engineering, The University of Queensland, Brisbane, Australia, 211 pages (ISBN 9781742720159).	AUD$60.00		
CHANSON, H., LUBIN, P., SIMON, B., and REUNGOAT, D. (2010). "Turbulence and Sediment Processes in the Tidal Bore of the Garonne River: First Observations." *Hydraulic Model Report No. CH79/10*, School of Civil Engineering, The University of Queensland, Brisbane, Australia, 97 pages (ISBN 9781742720104).	AUD$60.00		
CHACHEREAU, Y., and CHANSON, H., (2010). "Free-Surface Turbulent Fluctuations and Air-Water Flow Measurements in Hydraulics Jumps with Small Inflow Froude Numbers." *Hydraulic Model Report No. CH78/10*, School of Civil Engineering, The University of Queensland, Brisbane, Australia, 133 pages (ISBN 9781742720036).	AUD$60.00		
CHANSON, H., BROWN, R., and TREVETHAN, M. (2010). " Turbulence Measurements in a Small Subtropical Estuary under King Tide Conditions." *Hydraulic Model Report No. CH77/10*, School of Civil Engineering, The University of Queensland, Brisbane, Australia, 82 pages (ISBN 9781864999969).	AUD$60.00		
DOCHERTY, N.J., and CHANSON, H. (2010). "Characterisation of Unsteady Turbulence in Breaking Tidal Bores including the Effects of Bed Roughness." *Hydraulic Model Report No. CH76/10*, School of Civil Engineering, The University of Queensland, Brisbane, Australia, 112 pages (ISBN 9781864999884).	AUD$60.00		
CHANSON, H. (2009). "Advective Diffusion of Air Bubbles in Hydraulic Jumps with Large Froude Numbers: an Experimental Study." *Hydraulic Model Report No. CH75/09*, School of Civil Engineering, The University of Queensland, Brisbane, Australia, 89 pages & 3 videos (ISBN 9781864999730).	AUD$60.00		
CHANSON, H. (2009). "An Experimental Study of Tidal Bore Propagation: the Impact of Bridge Piers and Channel Constriction." *Hydraulic Model Report No. CH74/09*, School of Civil Engineering, The University of Queensland, Brisbane, Australia, 110 pages and 5 movies (ISBN 9781864999600).	AUD$60.00		
CHANSON, H. (2008). "Jean-Baptiste Charles Joseph BÉLANGER (1790-1874), the Backwater Equation and the Bélanger Equation." *Hydraulic Model Report No. CH69/08*, Div. of Civil Engineering, The University of Queensland, Brisbane, Australia, 40 pages (ISBN 9781864999211).	AUD$60.00		
GOURLAY, M.R., and HACKER, J. (2008). "Reef-Top Currents in Vicinity of Heron Island Boat Harbour, Great Barrier Reef, Australia: 2. Specific Influences of Tides Meteorological Events and Waves." *Hydraulic Model Report No. CH73/08*, Div. of Civil Engineering, The University of Queensland, Brisbane, Australia, 331 pages (ISBN 9781864999365).	AUD$60.00		
GOURLAY, M.R., and HACKER, J. (2008). "Reef Top Currents in Vicinity of Heron Island Boat Harbour Great Barrier Reef, Australia: 1. Overall influence of Tides, Winds, and Waves." *Hydraulic Model Report CH72/08*, Div. of Civil Engineering, The University of Queensland, Brisbane, Australia, 201 pages (ISBN 9781864999358).	AUD$60.00		
LARRARTE, F., and CHANSON, H. (2008). "Experiences and Challenges in Sewers: Measurements and Hydrodynamics." *Proceedings of the International Meeting on Measurements and Hydraulics of Sewers*, Summer School GEMCEA/LCPC, 19-21 Aug. 2008, Bouguenais, Hydraulic Model Report No. CH70/08, Div. of Civil Engineering, The University of Queensland, Brisbane, Australia (ISBN 9781864999280).	AUD$60.00		

CHANSON, H. (2008). "Photographic Observations of Tidal Bores (Mascarets) in France." *Hydraulic Model Report No. CH71/08*, Div. of Civil Engineering, The University of Queensland, Brisbane, Australia, 104 pages, 1 movie and 2 audio files (ISBN 9781864999303).	AUD$60.00		
CHANSON, H. (2008). "Turbulence in Positive Surges and Tidal Bores. Effects of Bed Roughness and Adverse Bed Slopes." *Hydraulic Model Report No. CH68/08*, Div. of Civil Engineering, The University of Queensland, Brisbane, Australia, 121 pages & 5 movie files (ISBN 9781864999198)	AUD$70.00		
FURUYAMA, S., and CHANSON, H. (2008). "A Numerical Study of Open Channel Flow Hydrodynamics and Turbulence of the Tidal Bore and Dam-Break Flows." *Report No. CH66/08*, Div. of Civil Engineering, The University of Queensland, Brisbane, Australia, May, 88 pages (ISBN 9781864999068).	AUD$60.00		
GUARD, P., MACPHERSON, K., and MOHOUPT, J. (2008). "A Field Investigation into the Groundwater Dynamics of Raine Island." *Report No. CH67/08*, Div. of Civil Engineering, The University of Queensland, Brisbane, Australia, February, 21 pages (ISBN 9781864999075).	AUD$40.00		
FELDER, S., and CHANSON, H. (2008). "Turbulence and Turbulent Length and Time Scales in Skimming Flows on a Stepped Spillway. Dynamic Similarity, Physical Modelling and Scale Effects." *Report No. CH64/07*, Div. of Civil Engineering, The University of Queensland, Brisbane, Australia, March, 217 pages (ISBN 9781864998870).	AUD$60.00		
TREVETHAN, M., CHANSON, H., and BROWN, R.J. (2007). "Turbulence and Turbulent Flux Events in a Small Subtropical Estuary." Report No. CH65/07, Div. of Civil Engineering, The University of Queensland, Brisbane, Australia, November, 67 pages (ISBN 9781864998993)	AUD$60.00		
MURZYN, F., and CHANSON, H. (2007). "Free Surface, Bubbly flow and Turbulence Measurements in Hydraulic Jumps." *Report CH63/07*, Div. of Civil Engineering, The University of Queensland, Brisbane, Australia, August, 116 pages (ISBN 9781864998917).	AUD$60.00		
KUCUKALI, S., and CHANSON, H. (2007). "Turbulence in Hydraulic Jumps: Experimental Measurements." *Report No. CH62/07*, Div. of Civil Engineering, The University of Queensland, Brisbane, Australia, July, 96 pages (ISBN 9781864998825).	AUD$60.00		
CHANSON, H., TAKEUCHI, M, and TREVETHAN, M. (2006). "Using Turbidity and Acoustic Backscatter Intensity as Surrogate Measures of Suspended Sediment Concentration. Application to a Sub-Tropical Estuary (Eprapah Creek)." *Report No. CH60/06*, Div. of Civil Engineering, The University of Queensland, Brisbane, Australia, July, 142 pages (ISBN 1864998628).	AUD$60.00		
CAROSI, G., and CHANSON, H. (2006). "Air-Water Time and Length Scales in Skimming Flows on a Stepped Spillway. Application to the Spray Characterisation." *Report No. CH59/06*, Div. of Civil Engineering, The University of Queensland, Brisbane, Australia, July (ISBN 1864998601).	AUD$60.00		
TREVETHAN, M., CHANSON, H., and BROWN, R. (2006). "Two Series of Detailed Turbulence Measurements in a Small Sub-Tropical Estuarine System." *Report No. CH58/06*, Div. of Civil Engineering, The University of Queensland, Brisbane, Australia, Mar. (ISBN 1864998520).	AUD$60.00		
KOCH, C., and CHANSON, H. (2005). "An Experimental Study of Tidal Bores and Positive Surges: Hydrodynamics and Turbulence of the Bore Front." *Report No. CH56/05*, Dept. of Civil Engineering, The University of Queensland, Brisbane, Australia, July (ISBN 1864998245).	AUD$60.00		
CHANSON, H. (2005). "Applications of the Saint-Venant Equations and Method of Characteristics to the Dam Break Wave Problem." *Report No. CH55/05*, Dept. of Civil Engineering, The University of Queensland, Brisbane, Australia, May (ISBN 1864997966).	AUD$60.00		

CHANSON, H., COUSSOT, P., JARNY, S., and TOQUER, L. (2004). "A Study of Dam Break Wave of Thixotropic Fluid: Bentonite Surges down an Inclined plane." *Report No. CH54/04*, Dept. of Civil Engineering, The University of Queensland, Brisbane, Australia, June, 90 pages (ISBN 1864997710).	AUD$60.00		
CHANSON, H. (2003). "A Hydraulic, Environmental and Ecological Assessment of a Sub-tropical Stream in Eastern Australia: Eprapah Creek, Victoria Point QLD on 4 April 2003." *Report No. CH52/03*, Dept. of Civil Engineering, The University of Queensland, Brisbane, Australia, June, 189 pages (ISBN 1864997044).	AUD$90.00		
CHANSON, H. (2003). "Sudden Flood Release down a Stepped Cascade. Unsteady Air-Water Flow Measurements. Applications to Wave Run-up, Flash Flood and Dam Break Wave." *Report CH51/03*, Dept of Civil Eng., Univ. of Queensland, Brisbane, Australia, 142 pages (ISBN 1864996552).	AUD$60.00		
CHANSON, H,. (2002). "An Experimental Study of Roman Dropshaft Operation : Hydraulics, Two-Phase Flow, Acoustics." *Report CH50/02*, Dept of Civil Eng., Univ. of Queensland, Brisbane, Australia, 99 pages (ISBN 1864996544).	AUD$60.00		
CHANSON, H., and BRATTBERG, T. (1997). "Experimental Investigations of Air Bubble Entrainment in Developing Shear Layers." *Report CH48/97*, Dept. of Civil Engineering, University of Queensland, Australia, Oct., 309 pages (ISBN 0 86776 748 0).	AUD$90.00		
CHANSON, H. (1996). "Some Hydraulic Aspects during Overflow above Inflatable Flexible Membrane Dam." *Report CH47/96*, Dept. of Civil Engineering, University of Queensland, Australia, May, 60 pages (ISBN 0 86776 644 1).	AUD$60.00		
CHANSON, H. (1995). "Flow Characteristics of Undular Hydraulic Jumps. Comparison with Near-Critical Flows." *Report CH45/95*, Dept. of Civil Engineering, University of Queensland, Australia, June, 202 pages (ISBN 0 86776 612 3).	AUD$60.00		
CHANSON, H. (1995). "Air Bubble Entrainment in Free-surface Turbulent Flows. Experimental Investigations." *Report CH46/95*, Dept. of Civil Engineering, University of Queensland, Australia, June, 368 pages (ISBN 0 86776 611 5).	AUD$80.00		
CHANSON, H. (1994). "Hydraulic Design of Stepped Channels and Spillways." *Report CH43/94*, Dept. of Civil Engineering, University of Queensland, Australia, Feb., 169 pages (ISBN 0 86776 560 7).	AUD$60.00		
POSTAGE & HANDLING (per report)	AUD$10.00		
GRAND TOTAL			

OTHER HYDRAULIC RESEARCH REPORTS

Reports/Theses	Unit price	Quantity	Total price
TREVETHAN, M. (2008). "A Fundamental Study of Turbulence and Turbulent Mixing in a Small Subtropical Estuary." Ph.D. thesis, Div. of Civil Engineering, The University of Queensland, 342 pages.	AUD$100.00		
GONZALEZ, C.A. (2005). "An Experimental Study of Free-Surface Aeration on Embankment Stepped Chutes." *Ph.D. thesis*, Dept of Civil Engineering, The University of Queensland, Brisbane, Australia, 240 pages.	AUD$80.00		

TOOMBES, L. (2002). "Experimental Study of Air-Water Flow Properties on Low-Gradient Stepped Cascades." *Ph.D. thesis*, Dept of Civil Engineering, The University of Queensland, Brisbane, Australia.	AUD$100.00		
CHANSON, H. (1988). "A Study of Air Entrainment and Aeration Devices on a Spillway Model." *Ph.D. thesis*, University of Canterbury, New Zealand.	AUD$60.00		
POSTAGE & HANDLING (per report)	AUD$10.00		
GRAND TOTAL			

CIVIL ENGINEERING RESEARCH REPORT CE

The Civil Engineering Research Report CE series is published by the School of Civil Engineering at the University of Queensland. Orders of any of the Civil Engineering Research Report CE should be addressed to the School Secretary.

School Secretary, School of Civil Engineering, The University of Queensland
Brisbane 4072, Australia
Tel.: (61 7) 3365 3619 Fax : (61 7) 3365 4599
Url: http://www.eng.uq.edu.au/civil/ Email: hodciveng@uq.edu.au

Recent Research Report CE	Unit price	Quantity	Total price
CALLAGHAN, D.P., NIELSEN, P., and CARTWRIGHT, N. (2006). "Data and Analysis Report: Manihiki and Rakahanga, Northern Cook Islands - For February and October/November 2004 Research Trips." *Research Report CE161*, Division of Civil Engineering, The University of Queensland (ISBN No. 1864998318).	AUD$10.00		
GONZALEZ, C.A., TAKAHASHI, M., and CHANSON, H. (2005). "Effects of Step Roughness in Skimming Flows: an Experimental Study." *Research Report No. CE160*, Dept. of Civil Engineering, The University of Queensland, Brisbane, Australia, July (ISBN 1864998105).	AUD$10.00		
CHANSON, H., and TOOMBES, L. (2001). "Experimental Investigations of Air Entrainment in Transition and Skimming Flows down a Stepped Chute. Application to Embankment Overflow Stepped Spillways." *Research Report No. CE158*, Dept. of Civil Engineering, The University of Queensland, Brisbane, Australia, July, 74 pages (ISBN 1 864995297).	AUD$10.00		
HANDLING (per order)	AUD$10.00		
GRAND TOTAL			

Note: Prices include postages and processing.

PAYMENT INFORMATION

1- VISA Card

Name on the card :	
Visa card number :	
Expiry date :	
Amount :	AUD$ .....

2- Cheque/remittance payable to: THE UNIVERSITY OF QUEENSLAND and crossed "Not Negotiable".

N.B. For overseas buyers, cheque payable in Australian Dollars drawn on an office in Australia of a bank operating in Australia, payable to: THE UNIVERSITY OF QUEENSLAND and crossed "Not Negotiable".

Orders of any Research Report should be addressed to the School Secretary.

School Secretary, School of Civil Engineering, The University of Queensland
Brisbane 4072, Australia - Tel.: (61 7) 3365 3619 - Fax : (61 7) 3365 4599
Url: http://www.eng.uq.edu.au/civil/ Email: hodciveng@uq.edu.au